# THE ROLE OF MINERAL COMPOSITION, ROCK PERMEABILITY, AND CONNATE-WATER COMPOSITION ON THE PERFORMANCE OF LOW-SALINITY WATERFLOODING IN SANDSTONE RESERVOIRS

A Dissertation

By

AHMED MAHMOUD SHEHATA AHMED HUSSEIN

Submitted to the Office of Graduate and Professional Studies of
Texas A&M University
In partial fulfillment of the requirements for the degree of

DOCTOR OF PHILOSOPHY

Chair of Committee, Hisham A. Nasr-El-Din
Committee Members, Stephen A. Holditch
Zoya Heidari
Mahmoud El-Halwagi
Head of Department, A. Daniel Hill

May 2016

Major Subject: Petroleum Engineering

## ABSTRACT

Extensive experimental work has indicated that low-salinity waterflooding is an enhanced oil recovery technique that improves oil recovery by lowering and optimizing the salinity of the injected water. Recent field applications and laboratory studies have recognized that low-salinity waterflooding is a potentially effective technique to achieve sufficient recovery in sandstone reservoirs. It was noted that the impact of clay content, rock permeability, rock quality, and the salinity of the reservoir connate water on the performance of low-salinity waterflooding are still questionable.

The main objectives of this work were to: (1) examine the performance of low-salinity waterflooding using four outcrop sandstone rocks, (2) investigate the role of clay content, rock permeability, and average pore throat radius on the performance of low-salinity waterflooding, (3) evaluate the effects of mineral type, brine salinity, cation type, and pH on the zeta-potential measurements, (4) investigate the role of the salinity and composition ($Na^+$, $Ca^{2+}$, and $Mg^{2+}$) of the reservoir connate water on the performance of low-salinity waterflooding, and (5) study the effect of the initial water saturation on the performance of low-salinity waterflooding.

Four sandstone types (Buff Berea, Grey Berea, Bandera, and Parker) with different mineralogy compositions were used. The mineralogy of the rock samples was assessed by X-ray powder diffraction, scanning electron microscopy, and X-ray fluorescence. Nuclear magnetic resonance, high pressure mercury injection, and Winland's empirical equation were used in order to characterize the pore geometry and provide capillary pressure curves.

Zeta-potential measurements were conducted for rock/brine and crude oil/brine interfaces to determine the suitable injection brine for the sandstone rocks used. In addition, several minerals such as quartz, carbonate (calcite and dolomite), clays (kaolinite, chlorite, and montmorillonite), micas (muscovite, biotite, and illite), feldspars (microcline and anorthoclase), and ilmenite were selected to perform this work. Various brines were tested including: seawater, 20% diluted-seawater, 0.5 wt% NaCl, 0.5 wt% $MgCl_2$, and 0.5 wt% $CaCl_2$.

Next, a set of comprehensive coreflood tests were conducted using Bandera, Parker, Grey Berea, and Buff Berea outcrop sandstone cores. The coreflood experiments were conducted using 6 and 20 in. lengths and 1.5 in. diameter outcrop cores at 185°F. The oil recovery, pressure drop across the core, pore volume injected, and core effluent samples were analyzed for each coreflood experiment. In addition, experimental studies of the spontaneous imbibition of oil by low-salinity and high-salinity brines used 20-in-long outcrop samples. The volume of produced oil was monitored and recorded against time on a daily basis. Imbibition brine samples were analyzed at the end of each experiment.

## DEDICATION

This dissertation is dedicated to my parents, sister, and brothers.

My ex fiancée Dena Hegab: Thank you

## ACKNOWLEDGEMENTS

I would like to take this opportunity to express my appreciation to my advisor and committee chair, Dr. Hisham A. Nasr-El-Din, for his continuous encouragement, support, trust, and academic guidance.

Appreciation is extended to the members of my committee, Dr. Stephen A. Holditch, Dr. Zoya Heidari, and Dr. Mahmoud El-Halwagi, for their help.

I also would like thank my colleagues.

Finally, I would like to acknowledge the financial support of the Texas A&M University, the Texas Engineering Experiment Station of Texas A&M University and Crisman Institute for Petroleum Research.

## NOMENCLATURE

CT = computed tomography

CW = connate water

EOR = enhanced oil recovery

FW = formation water

HSW = high-salinity waterflooding

ICP-OES = inductively coupled plasma optical emission spectroscopy

LSW = low-salinity waterflooding

MICP = mercury injection capillary pressure

MIE = multi-charged cations

NMR = nuclear magnetic resonance

OOIP = original oil in place

$k_r$ = relative permeability

SW = seawater

$S_{wi}$ = initial water saturation

$S_{or}$ = residual oil saturation

SEM = scanning electron microscopy

SI = spontaneous imbibition

SWCTT = single well chemical tracer tests

TAN = total acid number

TBN = total base number

TDS = total dissolved solids

XRD = x-ray powder diffraction

XRF = x-ray fluorescence

PALS = phase-analysis light-scattering

Pc = capillary pressure

ppm = parts per million

## TABLE OF CONTENTS

Page

## LIST OF FIGURES

Page

## LIST OF TABLES

Page

# CHAPTER I

# INTRODUCTION

Petroleum reservoirs are broadly classified as oil or gas reservoirs. Hydrocarbon systems found in petroleum reservoirs are mixtures of organic compounds that exhibit multiphase behavior over wide ranges of pressures and temperatures. These hydrocarbon accumulations may occur in the gaseous, liquid, and solid state, or in various combination of gas, liquid, and solid. These differences in phase behavior, attached with the physical properties of reservoir rock that determine the relative ease with which gas and liquid are transmitted or retained.

The terms primary oil recovery, secondary oil recovery, and tertiary (enhanced) oil recovery are traditionally used to describe hydrocarbons recovered according to the method of production or the time at which they are obtained. Primary oil recovery describes the production of hydrocarbons under the natural driving mechanisms present in the reservoir without supplementary help from injected fluids. The source of the natural energy necessary for oil recovery; rock and liquid expansion drive, depletion drive, gas-cap drive, water drive, gravity drainage drive, and combination drive. The secondary oil recovery refers to the additional recovery that results from the conventional methods of water-injection and immiscible gas injection. Enhanced oil recovery is that additional recovery over and above what could be recovered by primary and secondary recovery methods (Ahmed, 2010).

Waterflooding is the most common type of supplementary recovery in which water is injected to displace oil towards the producing zone. This procedure has several beneficial effects which include: the pressure differential between the field and the production well is maintained, and oil is ‘‘swept’’ in front of the injected water (Archer and Wall 1986).

In conventional waterflooding, injection water may be taken from the nearest available source. These sources include: produced water, rivers, lakes, seawater, and aquifers. Historically, the physical mechanism behind this improvement in oil recovery was attributed to the pressure maintenance and displacement of oil by injected water. Based on the conventional view, the injected brine composition and salinity were believed to have no effect on the efficiency of oil recovery by waterflooding (Schumacher 1978).

Recently, the tuning of the salinity of the injected water in sandstone reservoirs has been used to enhance oil recovery at different injection modes. Several possible low-salinity waterflooding mechanisms in sandstone formations have been studied. Over the last decade, several laboratory and field studies have shown that a low-salinity waterflood (LSW) and smart waterflooding improved the oil recovery for sandstone and carbonate reservoirs. Previous laboratory and field tests indicated that the injected brine was in the range of 500–5,000 parts per million (ppm) of the total dissolved solids (TDS).

### 1.1. Low-Salinity Waterflooding Mechanisms

Many studies have investigated the different LSW mechanisms. For the macro-scale and Darcy scale, the studies agree on wettability alteration toward water-wet as a mechanism (Alotaibi et al. 2011). However on the micro-scale different mechanisms such as a double-layer expansion (Ligthelm et al. 2009; Lee et al. 2010; Nasralla and Nasr-El-Din 2014), fines migration (Tang and Morrow 1997), pH increase (Tang and Morrow 1999; Austad et al. 2010), and multi-component ion exchange (Lager et al. 2006) were reported.

### 1.2. Field Scale History of Low-Salinity Waterflooding

Several studies have been carried out at the field scale to test the potential of LSW to improve oil recovery compared to high-salinity waterflooding (HSW). Log/inject/log measurements indicated a reduction of 60% of residual oil within approximately four inches of a wellbore (Webb et al. 2004). Furthermore, single well chemical tracer tests (SWCTT) have been used to evaluate the performance of LSW. The SWCTT is a technique carried out by injecting and then producing back through the same well for measuring the residual oil saturation in reservoir intervals following displacement process. McGuire et al. (2005) presented the results of four sets of SWCTT within a radius of 13 to 14 ft around a wellbore in the Alaskan North Slope reservoir. Residual oil saturation was substantially reduced by 5 to 13% of OOIP by using LSW after HSW. The reductions in residual oil saturations were 4, 4, 8, and 9% in these four tests.

Seccombe et al. (2010) reported oil recovery of residual oil between wells separately by 1,000 ft. for an offshore oil field (Endicott field) located on the North Slope of Alaska. They observed that the reduced-salinity waterflooding reduced the water cut from 95 to 92%. Also, several fields in the Powder River basin in Wyoming have been waterflooded using low-salinity brine of nearly 1,000 ppm (Robertson 2007). The obtained data showed that the oil recovery tended to increase as the salinity ratio of waterflood decreased.

Veldder et al. (2010) observed from the reservoir scale that the change in wettability led to an associated incremental recovery of 10-15% of the stock tank oil initially in place. Mahani et al. (2011) used a combination of analytical and numerical modeling approaches to analyze low-salinity waterflooding responses in the Omar and Sijan fields in Syria. Skrettingland et al. (2011) carried out SWCTT in the Upper Statfjord formation. The average oil saturations after seawater injection, diluted seawater injection, and after a new seawater injection were determined; no significant change in the remaining oil saturation was shown.

Robbana et al. (2012) showed the process to implement low-salinity EOR in the Clair Ridge field. Clair has the largest oil accumulation in the United Kingdom continental shelf, and it contains over 6 billion barrels of oil in place. Farida et al. (2013) tested the LSW in the greater Burgan field for high-quality intervals with low clay contents using SWCTT. The Burgan field in Kuwait is the second largest field and the largest clastic field in the world. Two pairs of SWCTT tests were conducted on two different wells. The $S_{or}$ before and after LSW injection was measured. The LSW recovered 23.7% of the

remaining oil left after conventional waterflooding. Also, researchers observed no damage in the injectivity of the wells when reducing the salinity from 140,000 to 5,000 ppm for relatively low clay rock types (good quality rock).

Bedrikovetsky et al. (2015) analyzed the data from the Bastrykskoye and Zichebashskoe fields (Russia) which includes low-salinity waterflooding. Low-salinity water injection under field conditions results in low incremental recovery and a slight decrease in the produced water when compared with waterflooding by formation water with a 5-fold decrease in relative permeability for water due to induced fines migration.

### 1.3. Previous Laboratory Work of Low-Salinity Waterflooding

Hughes and Pfister (1947) pointed out that brines would keep the clay content of producing sands in a permanently flocculated condition, and, therefore, brines were recommended for use in secondary recovery of petroleum by water flooding.

Baptist and Sweeney (1955) discussed the effect of the type and amount of clays present in the cores on the water sensitivity in petroleum reservoir sands in Wyoming. They stated that the water sensitivity of the reservoir sands is related to the salinity of the water and to the permeability of the sand. Water sensitivity increases with decreasing salinity and with decreasing permeability. The sand containing kaolins, illites, and mixed-layer clay (illite-montmorillonite) was found to be the most sensitive to water, and the sand containing only small amounts of kaolins and illites was the least sensitive. The sand that contained the most kaolins and illites was intermediate in water sensitivity.

Bernard (1967) noticed that the water sensitive cores produced more oil with a freshwater flood than with a brine flood. However, the fresh-water flood was accompanied by a lowering of permeability and the development of a relatively high pressure drop. If the freshwater flood did not develop a high pressure drop, then no additional oil is produced. They attributed the improvement to improved microscopic sweep efficiency induced by clay swelling and plugging of pore throat by migrating fines.

Yildiz and Morrow (1996) introduced the idea that variation of the brine composition could be used to optimize the waterflooding recovery. In 1997, Tang and Morrow noticed that low-salinity waterflood (LSW) has a good potential to improve oil recovery more than high-salinity waterflood. They carried out various core flooding experiments for different oil compositions, temperatures, and salinities. They concluded that oil recovery can benefit from low-salinity waterflooding. Filoco and Sharma (1998) observed that there were recovery benefits by reducing the salinity of the injected water, but they reported an increase in the volume of recovered oil only when the connate-water salinity was reduced. They reported that the recovery benefits might have been as a result of wettability alteration to a mixed-wet state.

Tang and Morrow (1999) identified the necessary conditions to achieve the target recovery using low-salinity waterflooding. The conditions included: 1) significant clay fraction, 2) presence of connate water, and 3) exposure to crude oil to create mixed-wet conditions.

Sharma and Filoco (2000) found that the salinity of reservoir connate water was the primary factor controlling the oil recovery. They used different salinities of connate water: 0.3, 3, and 20% NaCl. The oil recovery was greater for lower connate brine salinities. They attributed this dependence to the alteration of the wettability to mixed-wet conditions from water-wet conditions during the drainage process.

Zhang and Morrow (2006) observed that there was no benefit from LSW if no connate water saturation was present.

Lager et al. (2006) discussed the responsible mechanism for improved oil recovery by low-salinity brine injection. They reported that multi-component ionic exchange between mineral surfaces and invading brine was the primary mechanism behind. They suggested that during aging, crude oil can be attracted or adsorbed onto the surface through specific interactions, and during a LSW it is possible the divalent cations are exchanged for monovalent cations which no longer hold the oil to the surface.

Webb et al. (2008) interpreted the water/oil relative permeability at reservoir condition for the same reservoir rock type. High- and low-salinity relative permeability data were compared from similar initial water saturation. They described the design, execution, analyses, and interpretation of full reservoir condition tests on reservoir rock/oil, comparing high and low-salinity waterflood tests with live oil and brine. They noted that the end point relative permeability to water appears to be similar after high and low salinity. Furthermore, the shape of the water relative permeability curve indicated that there is no damage to the sample due to fines migration or clay swelling for these samples.

Rivet et al. (2010) conducted linear laboratory coreflood to study the effect of low-salinity waterflooding on residual oil saturation and relative permeability. They observed that the end-point water relative permeability decreased, and the post-waterflood end-point relative permeability to oil increased during the low salinity injection.

Cissokho et al. (2010) observed an additional oil recovery of 10% when the salinity of brine decreased from 50 to 1 g/l. The mineral composition of these samples is similar to the mineral composition of Bandera sandstone cores. Their used samples contained clay of 9.2% and a high amount of albite (28-34%).

Austad et al. (2010) proposed a chemical mechanism for wettability alteration by the desorption of the adsorbed cations from the clay present in the sandstone that was caused by an injection of LSW. The $Ca^{2+}$ is substituted by $H^{+}$ on the clay surface and promotes desorption of organic material from the clay as a result of an ordinary acid-base reaction. Based on this suggested chemical mechanism, clay must be present in the sandstone. Polar components (acidic and/or basic material) must be present in the crude oil as well, and the connate water must contain active cations such as $Ca^{2+}$.

RezaeiDoust et al. (2010) examined the performance of LSW for the North Sea offshore field, Varg. The Varg Field had the following reservoir parameters: total clay content of 8-16 wt%, crude oil acid and base numbers of 0.13 and 0.85 mg KOH/g, respectively, FW salinity of 201,000 ppm, and a reservoir temperature of 266°F. They found that the low salinity effect decreased from 6 to 2% when the clay content of the core material decreased from 16 to 8 wt%.

Pu et al. (2010) performed coreflood studies to examine the effect of LSW using three types of sandstone cores. These cores contained interstitial anhydrite, calcite, and dolomite. All of the cores showed increased oil recovery ranging from 5 to 8% original oil in place (OOIP) through injection of low-salinity water. They noticed an increase in the sulfate ion content of the effluent brine, confirming the dissolution of anhydrite for all three rock types.

Nasralla et al. (2011) indicated that LSW does not work as tertiary method because the expansion of double-layer between rock and low-salinity water is the primary mechanism of improved oil recovery by low-salinity waterflooding. The expansion of the double layer may not help to recover more oil in tertiary mode because of the absence of continuous oil film, and the repulsive forces, caused by low-salinity water, are not strong enough for the trapped oil to be swept by the imposed flow. Nasralla and Nasr-El-Din (2011) investigated the relationship between the composition of injected brine cations and oil recovery improvement. They used solutions of NaCl, $CaCl_2$, and $MgCl_2$ at concentrations of 1 and 5 wt% for waterflooding. Results demonstrated that the existing cations in the injected water solution have a more dominant effect on oil recovery than the concentration of salts in water. Alotaibi et al. (2011) measured the zeta-potential of sandstone rocks and selected clay minerals (kaolinite, chlorite, illite, and montmorillonite) as a function of ionic strength. A three-phase test using crude oil, limestone particles, and water was carried out to investigate the effect of the salinity on the double layer thickness for limestone rock (Alotaibi and Nasr-El-Din 2011).

Suijkerbuijk et al. (2012) performed a series of SI experiments on sandstone Berea outcrop core plugs and some reservoir rock core plugs with properties of a 1.5 in. diameter and a 2 in. length. They examined the impact of FW composition and crude oil composition on wettability and on wettability modification by LSW. SI experiments with FW and low-salinity brine executed on Berea outcrop material aged with crude oil showed excellent reproducibility. These results suggested that improved oil recovery occurs after the exposure of aged plugs to NaCl brines when the imbibing phase was either higher or lower in salinity than the FW. An increasing concentration of divalent cations in the FW makes a crude oil/brine/rock system more oil-wet. Furthermore, the extent of wettability modification towards more oil-wet depends on the types of cations present in the FW.

Ingebret Fjelde et al. (2012) described the brine-rock interactions at high and low salinity for sandstone reservoir rock with high clay content. They used core plugs from a sandstone oil reservoir in the North Sea. The clay content in the rock was about 13% weight of the bulk sample. The cation exchange capacity for the rock was 2meq/100g. They prepared core plugs with formation water (FW) and aged with crude oil at initial water saturation ($S_{wi}$). They found that when low salinity water prepared by dilution of formation water (diluting FW 1000 times with distilled water) was injected to reservoir sandstone cores with high clay content, the wettability was altered to less water-wet and the oil was produced over a longer period than during the water flooding with the formation water (FW, high salinity) at more water-wet conditions. Analyses of the effluent samples for pH and cations, have shown that interactions between rock and

brines took place during the low salinity floods. Then they estimated the $k_r$ and Pc curves by history matching of production and differential pressure data from the unsteady-state flooding experiments. They found that the core flooded with formation water was more water-wet than the core flooded with diluted formation water. Also, they used a two-phase model to predict the release of divalent cations from the rock during LSW. Modelling of cation-exchange shows that the concentration of divalent cations on clay surfaces was higher during injection of the low salinity brine (diluted formation water) than during injection of the high salinity brine (formation water). The concentration of polar oil components bonded to the clay surfaces by the divalent cations can therefore be higher during the flood with the low salinity brine (diluted formation water) than during the flood with the high salinity brine (formation water). This is in accordance with the less water-wet conditions in the low salinity (diluted FW) flood than in the high salinity (FW) flood.

Fjelde et al. (2012) obtained relative permeability ($k_r$) and capillary pressure ($P_c$) curves by history matching of production and differential pressure data from the unsteady-state flooding experiments using a simulation tool.

Law et al. (2014) carried out work to compare the conventional approach of modeling LSW using high and low-salinity relative permeabilities with the latest MIE methods by numerical simulation.

Shojaei et al. (2015) evaluated the capillary pressure and relative permeability curves by history matching technique at three levels of high, medium, and low salinities. They performed a series of oil displacement by water on a sandstone rock aged with crude oil

in the presence of connate water. They observed that the capillary pressure as well as oil relative permeability curves is salinity dependent in LSW flooding process. The obtained parameters of relative permeability and capillary pressure models as well as the residual oil saturation follow a linear behavior with the salinity of the injected water. Their results showed that the mechanism of LSW is controlled by wettability alteration to a more water wet state, and also IFT reduction as a result of carbonate dissolution.

Xie et al. (2015) used low-permeability reservoir cores with high clay contents (more than 23% in total). Their coreflood experiments showed that a high potential in slight water-wet reservoirs can be achieved by low-salinity waterflooding due to the electrical double layer expansion.

Sorop et al. (2015) showed a significant change in relative permeability between the high-salinity and low-salinity brines. Their work confirmed the shift toward a more water-wet state and a reduction in $S_{or}$ due to low-salinity waterflooding by extracting the relative permeability curves for both oil and water for the whole saturation range. The modification was observed in both water and oil relative permeability curves; in other words water relative permeability decreased and oil relative permeability increased, including the end points. The water relative permeability curve experienced more change than oil relative permeability curve.

Shehata and Nasr-El-Din (2015a) used the phase-analysis light-scattering (PALS) technique to determine the zeta potential for rock/brine interface. The researcher examined the effect of salinity, cation type, and pH on zeta potential values for Buff Berea and Bandera sandstone. Seawater (54,680), 20% diluted-SW (10,936 mg/l), NaCl,

$CaCl_2$, and $MgCl_2$ (0.5 wt%) brines were tested. They observed that the zeta potential values became more negative as the salinity of the brine decreased. The 0.5 wt% NaCl brine showed stronger negatively charged surfaces on the Buff Berea and Bandera sandstones, more than those of 0.5 wt% $CaCl_2$ and $MgCl_2$ brines. A comparison between the measured values of zeta potential versus pH at 25 °C for Buff Berea and Bandera showed that the magnitude of the negative zeta potential increased as the pH of the solution increased. The zeta potential of Bandera is more negative than that of Buff Berea. Minerals such as quartz, carbonates (calcite and dolomite), clays (kaolinite, chlorite, and smectite), micas (muscovite and illite), feldspars (microcline), and ilmenite were tested in this previous work.

Shehata and Nasr-El-Din (2015b) combined the results of spontaneous imbibition and coreflood tests to understand the role of salinity and composition ($Na^+$, $Ca^{2+}$, and $Mg^{2+}$) of the connate water on the performance of low-salinity waterflooding recovery for sandstone rocks. Their study included two types of sandstone cores (Buff Berea and Bandera) and connate water compositions with wide ranges of salinity. They observed that the changes in the ion composition of reservoir connate water ($Ca^{2+}$, $Mg^{2+}$, and $Na^+$) showed a measurable change in the oil production trend. The reservoir cores saturated with connate water containing divalent cations of $Ca^{+2}$ and $Mg^{+2}$ showed a higher oil recovery than for cores saturated with monovalent cations ($Na^+$).

### 1.4. Objectives

The main objectives of this work are to: (1) evaluate the potential of LSW on the performance of oil recovery improvement four outcrop sandstone rocks (Buff Berea, Grey Berea, Bandera, and Parker, (2) investigate the role of clay content, rock permeability, and average pore throat radius on the performance of low-salinity waterflooding, (3) examine the effect of the salinity of the reservoir connate water, (4) investigate the role of the composition ($Na^+$, $Ca^{2+}$, and $Mg^{2+}$) of reservoir connate water, (5) test the effect of temperature and rock quality on the performance of the LSW performance, and (6) evaluate the effects of mineral type, brine salinity, cation type, and pH on the zeta-potential measurements.

This research reports coreflood, spontaneous imbibition, zeta potential, x-ray powder diffraction, x-ray fluorescence, scanning electron microscope, nuclear magnetic resonance, and high pressure mercury injection experimental investigations on these parameters. In order to achieve our objectives, several tasks will be required to build the methodology of this research. The experimental approaches to accomplish the objectives of this dissertation are stated as follows:

- Mineral Identification were determined for the sandstone samples using x-ray powder diffraction, x-ray fluorescence, and scanning electron microscopy.
- High-pressure mercury injection measurements were performed to characterize the pore geometry and provide capillary pressure curves.
- Nuclear magnetic resonance measurements were conducted on the four sandstones types saturated with formation water to characterize pore throat radius.

- The zeta potential at oil/brine and rock/brine interfaces were measured using the ZetaPALS technique (Phase Analysis Light Scattering).
- Coreflood experiments were conducted to determine the oil recovery performance in the secondary and tertiary recovery modes.
- Spontaneous imbibition experiments were conducted to examine the oil recovery and wettability in the secondary recovery mode.

# CHAPTER II

# EXPERIMENTAL PROCEDURE

## 2.1. Coreflood Experiments

### 2.1.1. Coreflood Setup

The coreflood setup consists of a stainless steel core holder, three accumulators, an ISCO syringe pump that was used to inject the fluids into the core at a constant rate, a hydraulic pump to apply overburden pressure on the core injection of hydraulic oil in an oil bank between the core-holder internal surface, and a rubber sleeve that cased the core, regulators, and gauges to monitor the pressure drop across the core with time. A single pressure transducer was used in all experiments. The pressure transducer was connected to LabVIEW$^{Tm}$ software to record the pressure drop between the core inlet and outlet as a function of time. The core samples were placed in the core-holder, which was mounted vertically inside an electrical oven to simulate reservoir temperature (**Figure 1**). **Figure 2** shows the schematic of the coreflood setup.

### 2.1.2. Core Handling, Preparation, and Experimental Procedure

All of the sandstone cores were prepared using a similar procedure. Prior to drying, the individual weight of each core was measured. Then, the cores were dried at 250°F. After the first day of drying, the core was weighed, and drying continued until a constant weight was achieved for all of the cores. The core samples were saturated with the

synthetic connate water brine. The selected core plugs remained in the degassed synthetic connate water and were there for at least 10 days for ionic equilibrium to be established between the rock and the brine. At the end of this equilibration time, the absolute permeability of the brine was measured. The saturation, porosity, and permeability measurements of the cores were carried out at the ambient temperature.

The porosity of the cores was determined by using the weight method from the weight difference between the saturated and dried cores. The brine permeability was determined at 77°F using various injection rates of 0.25, 0.5, 1, and 2.0 $cm^3$/min. Continuous values of the pressure drop across each core were monitored (using connate water) until steady state conditions were achieved. The permeability's of the cores were calculated using Darcy's law. The overburden and back pressures were maintained constantly for all tests at 2,000 and 500 psi, respectively. Then, the brine saturated cores were flooded with oil until the core stopped producing water to establish the initial water saturation. To establish an initial water saturation, the brine-saturated cores were flooded with crude oil at the rates of 0.1, 0.2, 0.5, 1, 2, and 3 $cm^3$/min until the core stopped producing water by observing the collected samples. For each injection rate, the amount of injected oil varied from 5 to 7 PV to make sure that there was no more produced water at each rate.

The cores were then aged for 20 to 30 days in a sealed steel pipe filled with crude oil and stored in an oven. The aging temperature was 185°F, simulating a Middle East reservoir condition, while the pressure was at atmospheric condition. The core was reloaded again in the core holder for waterflooding tests. All experiments were

conducted at 185°F. The pressure drop across the core was monitored. Aging time was chosen to be 20 days due to the following observations in the literature: Jadhunandan and Morrow (1995) conducted the studies on Berea sandstone rock. They observed the effect of aging time on the wettability for crude-oil/Brine/Rock systems. No significant differences in wettability was found when the aging period was extended beyond 20 days. Jia et al. (1991) studied the effect of aging time from 0 to 20 days on the rock wettability using sandstone core plugs. They observed that at a high temperature (140$^{o}$F) the effect of aging time is more pronounced. The water wettability index decreased from 0.65 at the first day to around 0.1 after 20 days. Also, several studies have been investigated the effect of aging for less than 20 days (Morrow et al. 1998; Yildiz et al. 1999; Zhou et al. 2000).

The produced oil and water were collected throughout the experiment with 15 cm$^3$ tube samples using an automatic fraction collector. The oil recovery was estimated using the volume of oil recovered over the original oil in the core. The incremental oil recovery due to the LSW compared to HSW was estimated at a water cut of 100%.

To minimize the effect of sample variety on the recovery performance results, the following work flow was carried out: (a) the (CT) scan showed that the Buff Berea and Bandera sandstone cores were homogenous, (b) the selected cores had a consistent rock type based on the routine core analysis property (permeability and porosity), (c) long sandstone cores (20 and 6 in.) were used to minimize uncertainty in oil volume to reduce the impact of the capillary end effects that are common in short plugs, (d) the sandstone cores were prepared and saturated using the same procedure, (e) oil and water

saturations were determined using the produced volumes method, (f) the selected cores had similar values of initial water saturation for each set of experiments.

**Figure 1—Coreflood and oven system.**

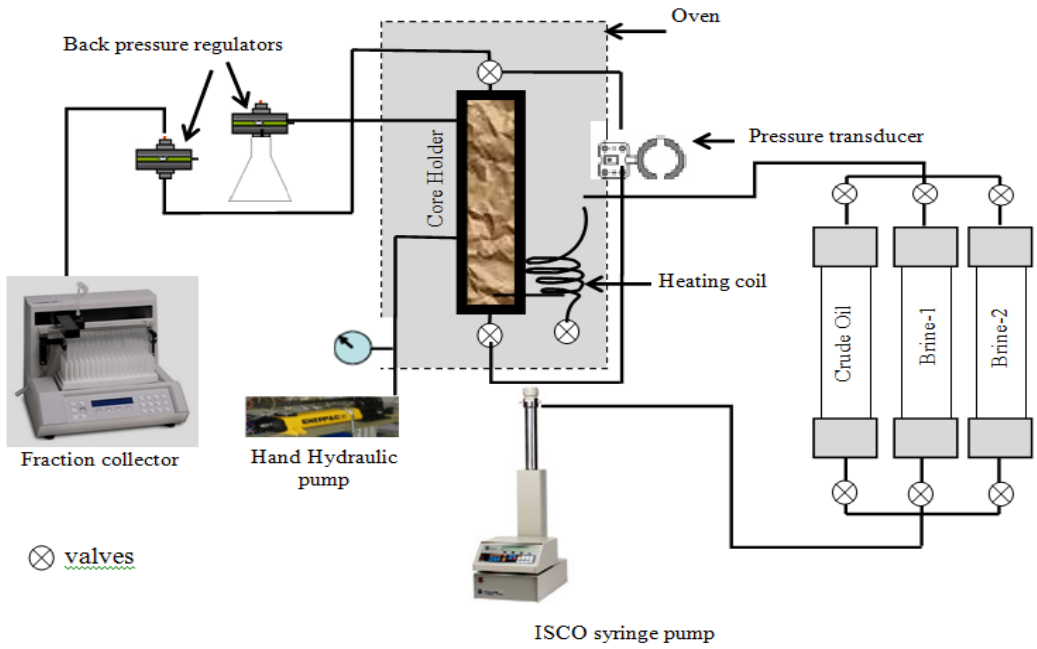


**Figure 2—A schematic diagram of the coreflood apparatus.**

### 2.2. Spontaneous Imbibition Tests

Spontaneous (or capillary) imbibition (SI) is an alternative enhanced oil production strategy. Capillary pressure causes water to invade into water-wet and mixed-wet rock containing oil (Tavassoli et al. 2005). Measurements of oil production by SI were made in order to aid in identifying the wetting state of the cores. Oil production by water imbibition displacement has concentrated on evaluating the relationship between time and oil production rate. The effectiveness of this process depends on several parameters: matrix block size, rock porosity and permeability, fluid viscosities, interfacial tensions, and rock wettability.

In this work, the procedure of Cuiec (1984) using an Amott-wettability cell was followed. After the aging stage, the cores were loaded into the cells for the SI test as

shown in **Figure 3**. All SI experiments were conducted using core samples with 1.5 in. diameter and 20 in. length. The cores were placed vertically inside the cell and surrounded by the imbibing brine with all sides subjected to imbibition. The displaced oil accumulated in the graduated tube by gravity segregation. During the experiment, the volume of the produced oil was recorded against time. Before taking the oil volume reading, the glass container was gently shaken to expel oil drops adhering to the core surface and the lower part of the cap, so that all of the oil produced accumulated in the graduated portion of the glass cap. SI tests were conducted at temperatures of 77 and 150°F. The amount of oil recovery versus time as a percentage of original oil in place (%OOIP) was determined. Imbibition brine samples were analyzed after each experiment using ICP-OES to determine the concentrations of different cations. The pH of the imbibition fluids was measured before and after the experiments.

**Figure 3—Amott wettability cell for 1.5 in. diameter and 20 in. length cores for Bandera sandstone (R-1, R-2, R-3 and R-4) at the beginning of the test.**

### 2.3. Zeta Potential Experiments Apparatus and Procedure

A phase-analysis light-scattering (PALS) technique was used to determine the zeta potential for rock/brine or oil/brine interface. The instrument's electrodes were coated with palladium, and a He-Ne laser was used as a light source to measure the electrophoretic mobility of charged colloidal suspensions. The zeta potential range for this instrument is -220 to 220 mV. The instrument has an accuracy of ±2%.

The procedure of Nasralla and Nasr-El-Din (2014) was followed to prepare the rock/mineral suspension. The minerals were crushed to very fine particles of less than 75 µm using an Allen-Bradley sonic sifter. The solid/brine samples were prepared by adding 1 wt% of solids powder to the brine. A solution of 0.2 g of powdered particles of minerals with 20 $cm^3$ of aqueous solutions. In addition, the crude oil-brine suspension samples were prepared by adding crude oil to brine with a weight ratio of 1:10 (Nasralla and Nasr-El-Din 2014 and Alotaibi and Nasr-El-Din 2011). Each solution was mixed by the sonication method using the Ultrasonic Homogenizer-model 150VT at ambient conditions. The probe tip was placed approximately 0.5 in. into the solution and set at a constant rate for one minute. The pH of the solution was adjusted using either acetic acid or NaOH buffer solutions. The solution was shaken and remained still for about 15 minutes. The pH was measured directly before running the test. Then, a sample of the solution was transferred slowly to a cuvette. A polystyrene cuvette was used to hold 1.5 $cm^3$ of the sample. A plastic pipette (1 $cm^3$) was inserted at a 45° angle and placed all the way in the bottom corner of the cuvette. The needle was submerged all of the time to prevent the air bubbles. A parallel-plate electrode was placed into the cuvette to run the

zeta potential measurements. At least five runs were conducted for each sample, and the average was taken. In all of the reported results, the standard errors of the five different runs were less than 2%. **Figure 4** shows an image of the ZetaPals setup used in this study.


**Figure 4—A photo of the ZetaPals setup used to measure the zeta potential.**

### 2.4. Rock Characterization

Porous media consists of pores and smaller channels (pore-throats) connecting the pores. The pore-throats control the movement of fluid in the reservoir. In this work, high pressure mercury injection and nuclear magnetic resonance techniques were performed. The main objective of these tests are to characterize the capillary pressure curves, the

distribution of pore-throat sizes, and understand the structure of pore system in the reservoir.

### 2.4.1. Mercury Injection Capillary Pressure Apparatus and Procedure (MICP)

During the mercury injection test, each clean dry sample was immersed in mercury in a pressure-sealed chamber. The pressure of the surrounding mercury was gradually increased from 0 psia up to 60,000 psia. The increasing pressure gradually forced the mercury to intrude into the sample pore spaces and the amount of mercury injected, expressed as a fraction of the sample pore volume, was determined. The relationship of injection pressure to mercury saturation was used to calculate several parameters, including pore throat size distribution, and capillary pressure for various fluid systems. **Figure 5** shows the mercury injection capillary pressure setup.

**Figure 5—An image of the mercury injection capillary pressure setup.**

Here are the steps that we followed during preparation and running the test

- Drying the samples in a vacuum oven, the samples were placed into a desiccator to prevent adsorption of moisture from the atmosphere, as the samples cooled.
- Dry weights were measured on a three-place (±0.001 gm) analytical balance.
- The samples were each placed into a chamber into which helium was allowed to expand from reference cells of known volume and pressure. Grain volumes were calculated using Boyle's law of gas expansion. Sample dry weight of was divided by grain volume, to calculate the grain density.

- An ambient, mercury immersion bulk volume was determined. Pore volume was calculated as the difference between the bulk volume and the grain volume. The pore volume was divided by the bulk volume, to calculate the porosity fraction.
- The samples were placed into a stainless steel cylinder and evacuated overnight, prior to pressure saturation with toluene, a strongly wetting fluid. Saturated pore volume data were then obtained and compared to the previously determined (mercury bulk – grain volume) pore volumes. The saturated pore volumes are generally the preferred values used.
- The samples were re-dried in a vacuum oven to remove the toluene.
- Testing was performed using the Micrometrics Autopore, an automated, high-pressure mercury injection device, which operates at injection pressures of 0 to 60,000 psia. For this project, the maximum injection pressure of 60,000 psia was used.
- Each test sample was weighed, and then loaded into a glass penetrometer consisting of a sample chamber attached to a capillary stem with a cylindrical coaxial capacitor. Each penetrometer used, was selected on the basis of how well its volumetric capacity matched the sample pore volume, to maximize accuracy and resolution.
- The sample/penetrometer assembly was weighed, and then placed into the low-pressure system.
- The sample chamber was evacuated and filled with mercury, and then the pressure was increased incrementally to slightly above atmospheric pressure. At the

conclusion of the low-pressure phase, the assembly was temporarily removed and re-weighed, then placed into the high-pressure side of the apparatus.

- Pressures were increased incrementally to a maximum of 60,000 psia.
- Time was allowed at each incremental pressure for saturation equilibrium. The volume of mercury injected at each pressure was determined by the change in the capacitance of the capillary stem.
- The pressure was decreased to ambient and a final reading was obtained. After the sample was unloaded a final weight was recorded to calculate the drained, gravimetric residual mercury saturation.
- Micrometrics data were processed and the mercury volumes were calculated. Apparent injected mercury volumes were corrected using a conformance value determined for each sample from an evaluation of a plot of the apparent injected volume versus injection pressure. The conformance value is the volume of mercury pressed into surface roughness and around sample edges after the penetrometer chamber is initially filled with mercury, volume corrections made, and the saturations calculated.
- Pore throat size, fluid system pressure conversions, and height data were calculated using the "typical" parameters that are reported at the end of this discussion.
- The mercury injection data are presented in tabular and graphical formats. The tabular data include: injection pressure, mercury saturation, pore throat radius, conversions of pressure to other laboratory systems, and estimated height above free water level.

- The relationship of injection pressure to mercury saturation was used to calculate the pore-throat radius (**Eq. 1**).

$$R_i = \frac{2 * C * \sigma * \cos\theta}{P_c} \quad \text{..... (1)}$$

where:

- $R_i$ = pore entry radius, microns
- σ = Interfacial tension between mercury and air in dynes/cm (typically 480 dynes/cm)
- Θ =Contact angle between mercury and air in degrees (typically 140 degrees)
- C = unit conversion constant to microns (0.145)
- Pc = Capillary pressure between the mercury and air phases in psia

### 2.4.2. Nuclear Magnetic Resonance (NMR)

The NMR measurements were conducted using a 2 MHz NMR benchtop spectrometer (GeoSpec2 Core Analyzer). NMR measurements were conducted on the sandstone cores saturated with FW. Core plugs with dimensions of 1.5 in. diameter and 2 in. length were used. The distribution of transverse relaxation times, *T2s*, was determined. The proton (hydrogen nuclei) in the fluid within pore space are manipulated by magnetic field and their relaxation is measured. The initial amplitude of the NMR relaxation signal is related to number of hydrogen protons within the pore space. The time it takes for hydrogen protons to relax from their motion is also measured and called transvers relaxation time ($T_2$).

## 2.5. Mineral Identification

The sandstone samples were evaluated using x-ray powder diffraction (XRD), x-ray fluorescence (XRF), and scanning electron microscopy (SEM).

### 2.5.1. X-ray Fluorescence Apparatus and Procedure (XRF)

X-ray fluorescence (XRF) spectrometry is an elemental analysis technique with broad application in science and industry. XRF is based on the principle that individual atoms, when excited by an external energy source, emit X-ray photons of a characteristic energy or wavelength. By counting the number of photons of each energy emitted from a sample, the elements present may be identified and quantitated. In this study, S2 Ranger XRF apparatus from Bruker was used for the analysis (**Figure 6).**

X-ray fluorescence (XRF) test was performed to determine the elemental composition of the different sandstone samples in my own lab using. We performed this test especially to quantify the iron oxides in each type of sandstone samples. Two runs were performed to determine the average of the oxides percentage. The average $Fe_2O_3$ represents almost 1.45, 1.46, 3.02, and 2.45% of the total oxides in the samples for Buff Berea, Grey Berea, Bandera, and Parker, respectively. We found that the iron oxides present in the Bandera sample is higher than the other sandstone samples. **Table 1** through **4** present the percentages of the main oxides present in the different sandstone samples.

Before running the experiment, the core plug at particular depth was crushed (**Figure 7**). After that the sample was put on the sieve size of 75 microns. The samples which

were larger than 75 microns were collected in the plastic tube. These samples were used for the XRF analysis. The procedure for the analysis are described below;

1. Wait the machine to warm up (20 minutes)
2. Run the copper disk calibration
    a. If it is good, it will show 2 green lights
3. Run the QC (quality check) sample using BAXS-S2 glass standard
    a. If it is good, it will show 6 green lights
4. Loading sample (crushed core sample > 75 microns)
    a. Sample should be kept clean and dry
    b. Insert sample carefully inside the sample ring (Do not overfill sample)
    c. On the touchscreen, press the shutter control picture on the loader screen to open the shutter
    d. Check the sample plate is located on the pin and will not rotate
    e. Insert the sample ring into chamber
    f. Ensure the located ring inside the recess


**Figure 6—An S2 ranger XRF apparatus.**

Fig.1-a – Core sample crushing

Fig.1-b – Mylar thin film

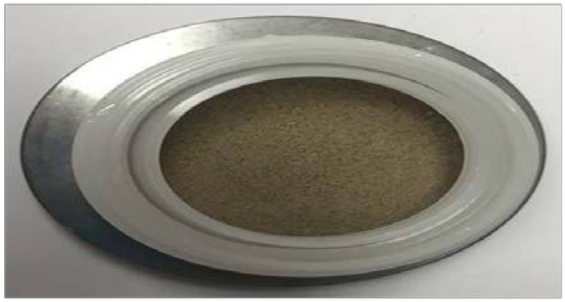

Fig.1-c—Crushed sample in the sample ring

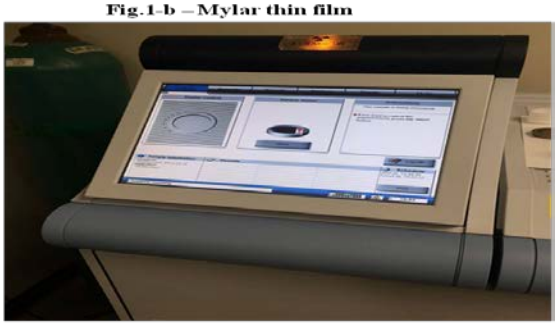

Fig. 1-d—Touchscreen controller

**Figure 7—XRF preparation procedure.**

**Table 1—XRF Analysis of Buff Berea Sandstone.**

| Run-1 | | Run-2 | | Average, % |
|---|---|---|---|---|
| **Formula** | **Concentration, %** | **Formula** | **Concentration, %** | |
| $SiO_2$ | 85.3 | $SiO_2$ | 83.9 | 84.6 |
| $Al_2O_3$ | 7.9 | $Al_2O_3$ | 8.51 | 8.205 |
| $K_2O$ | 1.58 | $K_2O$ | 1.66 | 1.62 |
| $Fe_2O_3$ | 1.49 | $Fe_2O_3$ | 1.40 | 1.45 |
| MgO | 1.01 | MgO | 1.19 | 1.1 |
| CaO | 0.896 | CaO | 1.13 | 1.013 |
| $TiO_2$ | 0.707 | $TiO_2$ | 0.695 | 0.701 |
| $Na_2O$ | 0.656 | $Na_2O$ | 1.06 | 0.858 |
| Cl | 0.0968 | Cl | 0.109 | 0.1029 |
| $ZrO_2$ | 0.0957 | $ZrO_2$ | 0.0707 | 0.0832 |
| CuO | 0.0608 | CuO | 0.0397 | 0.05025 |
| $SO_3$ | 0.0401 | $SO_3$ | 0.0421 | 0.0411 |
| MnO | 0.0357 | MnO | 0.0365 | 0.0361 |
| $CeO_2$ | 0.0274 | $CeO_2$ | 0.0284 | 0.0279 |
| BaO | 0.0234 | BaO | 0.0187 | 0.02105 |
| CoO | 0.0169 | CoO | 0.0138 | 0.01535 |
| $SnO_2$ | 0.0152 | $SnO_2$ | 0.0149 | 0.01505 |
| $Nd_2O_3$ | 0.0142 | $Nd_2O_3$ | 0 | 0.0071 |
| $Cr_2O_3$ | 0.0134 | $Cr_2O_3$ | 0 | 0.0067 |
| $La_2O_3$ | 0 | $La_2O_3$ | 0.033 | 0.0165 |
| $Pr_6O_{11}$ | 0 | $Pr_6O_{11}$ | 0 | 0 |
| $V_2O_5$ | 0 | $V_2O_5$ | 0 | 0 |
| Sum | 100 | Sum | 100 | 100 |

**Table 2—XRF Analysis of Grey Berea Sandstone.**

| Run-1 | | Run-2 | | Average, % |
|---|---|---|---|---|
| **Formula** | **Concentration, %** | **Formula** | **Concentration, %** | |
| $SiO_2$ | 84.6 | $SiO_2$ | 84.5 | 84.55 |
| $Al_2O_3$ | 8.51 | $Al_2O_3$ | 8.79 | 8.65 |
| $K_2O$ | 1.99 | $K_2O$ | 1.83 | 1.91 |
| $Fe_2O_3$ | 1.52 | $Fe_2O_3$ | 1.39 | 1.46 |
| MgO | 1.08 | MgO | 1.13 | 1.105 |
| CaO | 0.457 | CaO | 0.319 | 0.388 |
| $TiO_2$ | 0.614 | $TiO_2$ | 0.594 | 0.604 |
| $Na_2O$ | 0.677 | $Na_2O$ | 1.01 | 0.8435 |
| Cl | 0.231 | Cl | 0.104 | 0.1675 |
| $ZrO_2$ | 0.0746 | $ZrO_2$ | 0.0844 | 0.0795 |
| CuO | 0 | CuO | 0.0137 | 0.00685 |
| $SO_3$ | 0.036 | $SO_3$ | 0.0527 | 0.04435 |
| MnO | 0.0275 | MnO | 0.0262 | 0.02685 |
| $CeO_2$ | 0.021 | $CeO_2$ | 0.0331 | 0.02705 |
| BaO | 0.0388 | BaO | 0.0222 | 0.0305 |
| CoO | 0 | CoO | 0 | 0 |
| $SnO_2$ | 0.0158 | $SnO_2$ | 0.0157 | 0.01575 |
| $Nd_2O_3$ | 0.0112 | $Nd_2O_3$ | 0 | 0.0056 |
| $Cr_2O_3$ | 0 | $Cr_2O_3$ | 0 | 0 |
| $La_2O_3$ | 0.045 | $La_2O_3$ | 0.0452 | 0.0451 |
| $Pr_6O_{11}$ | 0 | $Pr_6O_{11}$ | 0 | 0 |
| $V_2O_5$ | 0.0114 | $V_2O_5$ | 0 | 0.0057 |
| Sum | 100 | Sum | 100 | 100 |

**Table 3—XRF Analysis of Bandera Sandstone.**

| Run-1 | | Run-2 | | Average, % |
|---|---|---|---|---|
| **Formula** | **Concentration, %** | **Formula** | **Concentration, %** | |
| $SiO_2$ | 72.9 | $SiO_2$ | 71.3 | 72.1 |
| $Al_2O_3$ | 14.1 | $Al_2O_3$ | 14 | 14.05 |
| $K_2O$ | 1.91 | $K_2O$ | 1.38 | 1.645 |
| $Fe_2O_3$ | 3.34 | $Fe_2O_3$ | 2.69 | 3.02 |
| MgO | 2.86 | MgO | 2.11 | 2.485 |
| CaO | 1.92 | CaO | 1.94 | 1.93 |
| $TiO_2$ | 0.803 | $TiO_2$ | 1.89 | 1.3465 |
| $Na_2O$ | 1.62 | $Na_2O$ | 0.588 | 1.104 |
| Cl | 0.138 | Cl | 0.0359 | 0.08695 |
| $ZrO_2$ | 0.061 | $ZrO_2$ | 0.0636 | 0.0623 |
| CuO | 0.026 | CuO | 0.0181 | 0.02205 |
| $SO_3$ | 0.119 | $SO_3$ | 0.162 | 0.1405 |
| MnO | 0.0638 | MnO | 0.0353 | 0.04955 |
| $CeO_2$ | 0.0148 | $CeO_2$ | 0.0289 | 0.02185 |
| BaO | 0.036 | BaO | 0.0193 | 0.02765 |
| CoO | 0.0186 | CoO | 0.0161 | 0.01735 |
| $SnO_2$ | 0.014 | $SnO_2$ | 0 | 0.007 |
| $Nd_2O_3$ | 0.0271 | $Nd_2O_3$ | 0.0111 | 0.0191 |
| $Cr_2O_3$ | 0.0171 | $Cr_2O_3$ | 0.0144 | 0.01575 |
| $La_2O_3$ | 0 | $La_2O_3$ | 0.026 | 0.013 |
| $Pr_6O_{11}$ | 0 | $Pr_6O_{11}$ | 0 | 0 |
| SrO | 0.0105 | SrO | 0 | 0.00525 |
| Sum | 100 | Sum | 100 | 100 |

**Table 4—XRF Analysis of Parker Sandstone.**

| Run-1 | | Run-2 | | Average, % |
|---|---|---|---|---|
| **Formula** | **Concentration, %** | **Formula** | **Concentration, %** | |
| $SiO_2$ | 85.7 | $SiO_2$ | 84.9 | 85.3 |
| $Al_2O_3$ | 7.83 | $Al_2O_3$ | 8.06 | 7.945 |
| $K_2O$ | 0.997 | $K_2O$ | 1.05 | 1.0235 |
| $Fe_2O_3$ | 2.45 | $Fe_2O_3$ | 2.45 | 2.45 |
| MgO | 1.33 | MgO | 1.38 | 1.355 |
| CaO | 0.294 | CaO | 0.615 | 0.4545 |
| $TiO_2$ | 0.267 | $TiO_2$ | 0.281 | 0.274 |
| $Na_2O$ | 0.798 | $Na_2O$ | 0.756 | 0.777 |
| Cl | 0.0981 | Cl | 0.268 | 0.18305 |
| $ZrO_2$ | 0.0234 | $ZrO_2$ | 0.0231 | 0.02325 |
| CuO | 0 | CuO | 0 | 0 |
| $SO_3$ | 0 | $SO_3$ | 0 | 0 |
| MnO | 0.0205 | MnO | 0.0198 | 0.02015 |
| $CeO_2$ | 0.0232 | $CeO_2$ | 0.0146 | 0.0189 |
| BaO | 0.0347 | BaO | 0.0318 | 0.03325 |
| CoO | 0.0137 | CoO | 0.0141 | 0.0139 |
| $SnO_2$ | 0.0146 | $SnO_2$ | 0.0142 | 0.0144 |
| $Nd_2O_3$ | 0.0181 | $Nd_2O_3$ | 0.0238 | 0.02095 |
| $Cr_2O_3$ | 0 | $Cr_2O_3$ | 0 | 0 |
| $La_2O_3$ | 0.0302 | $La_2O_3$ | 0.015 | 0.0226 |
| $Pr_6O_{11}$ | 0.0165 | $Pr_6O_{11}$ | 0 | 0.00825 |
| $V_2O_5$ | 0 | $V_2O_5$ | 0.0132 | 0.0066 |
| Sum | 100 | Sum | 100 | 100 |

### 2.5.2. X-ray Diffraction of Minerals (XRD)

X-ray powder diffraction (XRD) is a rapid analytical technique primarily used for phase identification of a crystalline material and can provide information on unit cell dimensions. We performed XRD analysis on the bulk samples for the different sandstone types (Buff Berea, Grey Berea, Bandera, and Parker). A representative sample was taken, crushed, and passed through (140-180 mesh) to obtain uniform particle size of the mineral within the sample. Then we added the sample to fill cavity of the XRD mount. The sample was pressed using glass slide without orienting the grains to certain direction as shown in **Figure 8**. The samples were subsequently subjected to Cu Kα radiation with XRD patterns recorded for the 2°-70° 2θ range (**Figure 9). Table 5** presents the mineralogy composition of the sandstone core.


**Figure 8—Bulk Buff Berea sample onto a glass disc.**


**Figure 9—X-ray diffraction (XRD) D8 ADVANCE with DAVINCI design by Bruker.**

**Table 5—Mineralogy of Sandstone Cores.**

| Buff Berea | | Grey Berea | | Bandera | | Parker | |
|---|---|---|---|---|---|---|---|
| **Mineral** | **Concentration (wt%)** | **Mineral** | **Concentration (wt%)** | **Mineral** | **Concentration (wt%)** | **Mineral** | **Concentration (wt%)** |
| Quartz | 91 | Quartz | 87 | Quartz | 59 | Quartz | 87 |
| Kaolinite | 3 | Kaolinite | 6 | Kaolinite | 3 | Kaolinite | 2 |
| Microline | 4 | Albite | 3 | Albite | 12 | Albite | 5 |
| Muscovite | 1 | Illite | 2 | Chlorite | 1 | Illite | 4 |
| Smectite | 1 | Calcite | 2 | Illite | 10 | Mica | 2 |
| | | | | Dolomite | 15 | | |

### 2.5.3. Scanning Electron Microscope Apparatus and Procedure (SEM)

Scanning electron microscope is a microscope that uses focused beam of electrons to scan a sample and form a magnified image. The interaction of electrons with atoms of sample produces detectable signals which contain information about surface topography composition. X-rays are produced on interaction of electrons with sample which can be detected by EDS (Energy Dispersive X-ray Spectroscopy) equipped with SEM. A small portion of core sample was selected and taken in the form of a chip for SEM analysis. The chip was a better means for analysis than crushed form as the grain composition represented that of actual core sample. Chip was attached to the SEM sample holder by means of black tape and analyzed. Then, MSC-1000 mini-sputter coater was used to coat the gold to the samples for SEM (**Figure 10**). In this study, Evex Mini SEM was used

which has a magnification of up to x 30,000 (**Figure 11**). **Figure 12** presents SEM graphs and an EDS patterns of quartz (Q), kaolinite (K), muscovite (Mu), and microcline (Mi) particles in the silt fraction of Buff Berea sandstone. The operating principle for EDS consists of four steps:

- Incoming primary electron beam strikes an inner electron.
- Bound electron is ejected leaving the atom in excited state.
- Outer shell electron jumps to fill the vacancy emitting X-ray photon.
- X-rays emitted are characteristic of energy difference between orbitals for each element which can be used for analysis.

Working procedure for SEM are as follows:

- Electron gun generates a stream of accelerated electrons in vacuum.
- The stream passes through apertures and electronic lens system to control the flow of electron beam.
- The focused beam impinges on the specimen, secondary electrons are emitted and collected by secondary electron detector.
- Signal is amplified and sent to the monitor.
- Electron beam scans back and forth from sample building up an image from the number of electrons emitted from each spot on the sample.


**Figure 10—MSC-1000 mini-sputter coater.**

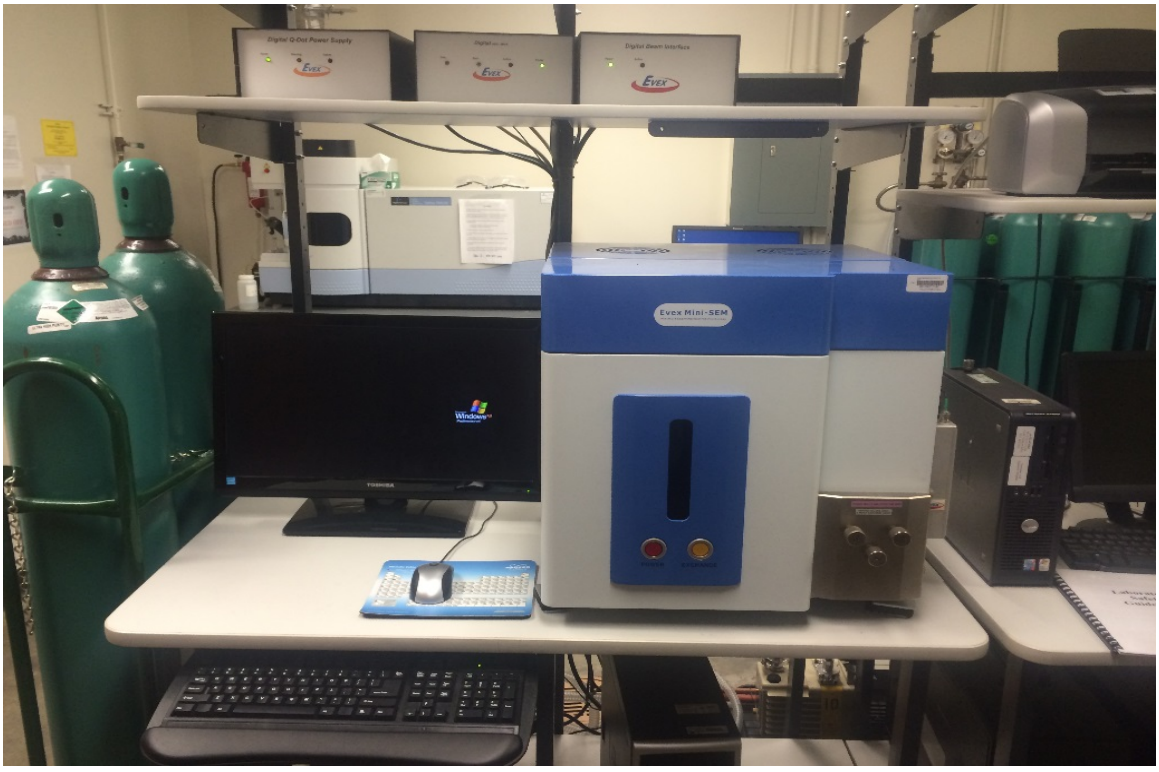


**Figure 11—Image of evex mini- scanning electron microscope (SEM).**

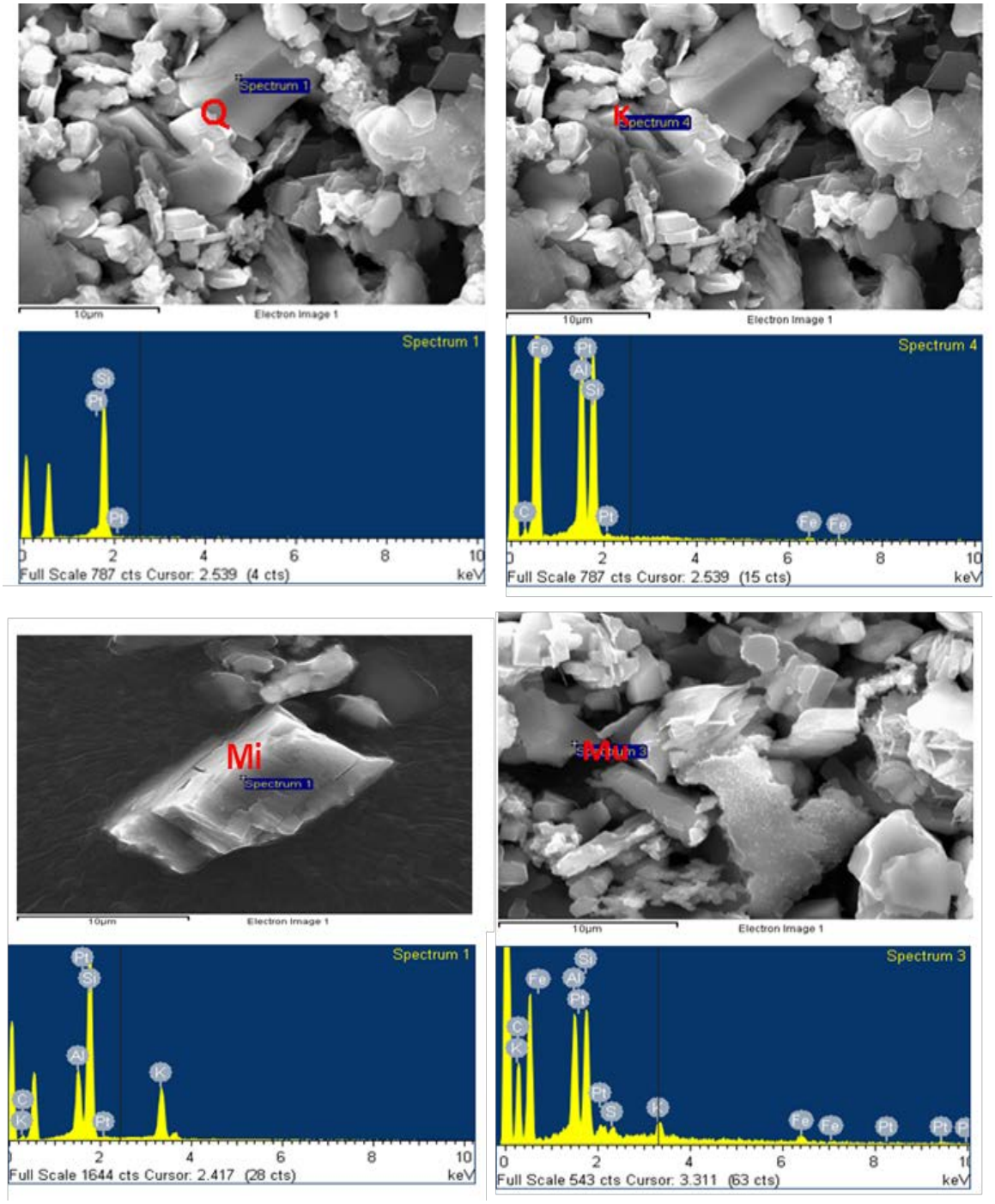


**Figure 12—SEM graphs and EDS pattern of Buff Berea rock samples in the silt fraction.**

# CHAPTER III

# MATERIALS

The purpose of this chapter is to illustrate the used materials in this work.

## 3.1. Cores

For the coreflood experiments, eight cylindrical cores from four sandstone outcrop rocks (Buff Berea, Grey Berea, Parker, and Bandera) of 1.5 in. diameter were cut with a core bit. Also, six core samples of approximately 1.5 in. diameter and 6 in. length of outcrop Buff Berea (average porosity of 19.57% and permeability of 98-129 md) were used. A total of eleven core samples of approximately 1.5 in. diameter and 20 in. length were used in the spontaneous imbibition study. Seven core samples were cut from the same block of outcrop Buff Berea (an average porosity of 18.7% and permeability of 164-207.7 md), and four core samples were cut from the same block of outcrop Bandera sandstone (an average porosity of 20.3% and permeability of 31.1-39.2 md).

To have a consistent permeability anisotropy range, the cores were only drilled in one direction. The porosity and permeability were measured using a coreflood apparatus. The petrophysical properties of each core sample along with important experimental parameters are reported in **Tables 6 through 9**.

**Table 6—Petrophysical Properties of Sandstone Cores Used for Coreflood Experiments.**

| | Buff Berea | | Grey Berea | | Parker | | Bandera | |
|---|---|---|---|---|---|---|---|---|
| Core ID | B-1 | B-2 | A-2 | A-4 | D-4 | D-7 | C-1 | C-4 |
| Length (in.) | 20 | 20 | 20 | 20 | 6 | 6 | 6 | 6 |
| Porosity (vol%) | 19.2 | 19.1 | 21.2 | 20.8 | 16.5 | 16.8 | 20.2 | 20.1 |
| Brine Permeability (md) | 165.4 | 164.5 | 63.6 | 66.4 | 6.0 | 5.7 | 25.6 | 24.8 |
| Connate Water Saturation (%) | 34.5 | 35.3 | 33.3 | 34.7 | 38.6 | 39.5 | 34.4 | 35.8 |
| Pore-Throat Radius at 35% Mercury Saturation (microns)* | 8.45 | 8.47 | 4.43 | 4.61 | 1.37 | 1.42 | 2.71 | 2.68 |

*The pore-throat radius was calculated using Eq. 1.

**Table 7—Petrophysical Properties of Buff Berea Sandstone Cores Used for Spontaneous Imbibition Experiments.**

| Core ID | O-1 | O-2 | O-3 | O-4 | O-5 | R-20 | R-40 |
|---|---|---|---|---|---|---|---|
| Porosity (vol%) | 18.6 | 19.0 | 19.3 | 17.9 | 18.8 | 18.7 | 18.5 |
| Brine Permeability (md) | 207.7 | 203.2 | 200.5 | 164.0 | 166.5 | 205.3 | 201.7 |
| Initial Water Saturation (%) | 38.5 | 39.5 | 37.3 | 39.3 | 38.6 | 37.6 | 38.2 |
| Average Pore-Throat Radius at 35% Mercury Saturation (micron)* | 10.0 | 9.6 | 9.4 | 9.0 | 8.8 | 9.8 | 9.8 |

*The average pore-throat radius was calculated using Eq. 1

**Table 8—Petrophysical Properties of Bandera Sandstone Cores Used for Spontaneous Imbibition Experiments.**

| Core ID | R-1 | R-2 | R-3 | R-4 |
|---|---|---|---|---|
| Porosity (vol%) | 20.5 | 20.4 | 20.3 | 19.9 |
| Brine Permeability (md) | 31.1 | 38.9 | 31.4 | 39.2 |
| Initial Water Saturation (%) | 42.0 | 39.5 | 43.4 | 46.8 |
| Average Pore-Throat Radius at 35% Mercury Saturation (micron)* | 3.0 | 3.4 | 3.0 | 3.5 |

*The average pore-throat radius was calculated using Eq. 1

**Table 9—Petrophysical Properties of Buff Berea Sandstone Cores Used for Coreflood Experiments.**

| Core ID | S-1 | S-2 | S-4 | S-5 | S-20 | S-21 |
|---|---|---|---|---|---|---|
| Porosity (vol%) | 19.4 | 18.7 | 19.2 | 19.7 | 19.4 | 19.5 |
| Brine Permeability (md) | 128.9 | 98.0 | 109.3 | 111.3 | 115.6 | 117.2 |
| Initial Water Saturation (%) | 30.6 | 35.9 | 29.0 | 29.9 | 31.1 | 30.8 |

### 3.2. Minerals

Several minerals such as quartz, carbonate (calcite and dolomite), clays (kaolinite, chlorite, and montmorillonite), micas (muscovite, biotite, and illite), feldspars (microcline and anorthoclase), and ilmenite are selected to study the zeta potential measurements. These minerals are purchased from Ward's Natural Science Establishment, NY. The classification of used minerals along with the chemical formula and physical description are reported in **Table 10**.

**Table 10—Common Sandstone Minerals (Schulze 2002; Kampf et al. 1999; Klein and Hurlbut 1993).**

| Mineral Class | Mineral | Chemical Formula |
|---|---|---|
| Phyllosilicates | Muscovite | $KAl_2(AlSi_3)\ O_{10}\ (OH)_2$ |
| | Biotite | $K(Mg,Fe^{2+})_3(AlSi_3)\ O_{10}\ (OH)_2$ |
| | Illite | $K_{0.75}\ (Al_{1.75}\ [MgFe]_{0.25})\ (Al_{0.5}Si_{3.5})\ O_{10}\ (OH)_2$ |
| | Chlorites | $(Mg,\ Fe)_3(Si,Al)_4O_{10}(OH)_2(Mg,Fe)_3(OH)_6$ |
| | Kaolinite | $Al_2Si_2O_5(OH)_4$ |
| | Montmorillonite | $M_{0.3}Al_2(Al_{0.3}Si_{3.7})O_{10}(OH)_2$<br>$M^+ = Ca^{2+}, Mg^{2+}, K^+$, etc. |
| Tectosilicates | Quartz | $SiO_2$ |
| | Anorthoclase | $(K,\ Na)\ AlSi_3O_8$ |
| | Microcline | $KAlSi_3O_8$ |
| Carbonates | Calcite | $CaCO_3$ |
| | Dolomite | $CaMg(CO_3)_2$ |
| Oxides | Ilmenite | $Fe^{2+}TiO_3$ |

### 3.3. Brines

Different synthetic connate water with different compositions of the monovalent and divalent cations were used to saturate the core samples. In this work, high-salinity reservoir connate water is defined as a brine having a salinity of 174,156 ppm while low-salinity connate water includes brines of 4,633 ppm salinity. High-salinity connate water

(CW (H-1), CW (H-2), and CW (H-3)) and low-salinity connate water (CW (L-1), CW (L-2), and CW (L-3)) were prepared by mixing reagent-grade salts with deionized water. The compositions of the different types of synthetic connate water are listed in **Table 11**. Low-salinity NaCl brine (500 and 5,000 ppm) was prepared with deionized water containing 0.05 wt% NaCl and 0.5 wt% NaCl, respectively. The density and viscosity of all brines used were measured at different temperatures (**Table 12**). The DMA 4100 densitometer was used to measure the density of the brines and crude oil, whereas a capillary viscometer was used to measure the viscosities.

**Table 11—Composition of Connate (Formation) Water.**

| | High-Salinity Connate Water | | | Low-Salinity Connate Water | | |
|---|---|---|---|---|---|---|
| **Ions** | **Connate Water (H-1)** [a] | **Connate Water (H-2)** | **Connate Water (H-3)** | **Connate Water (L-1)** [b] | **Connate Water (L-2)** | **Connate Water (L-3)** |
| $Na^+$ | 54,400 | 54,400 | - | 610 | 610 | - |
| $K^+$ | 56 | - | - | 79 | - | - |
| $Ca^{2+}$ | 10,600 | - | 10,600 | 630 | - | 630 |
| $Mg^{2+}$ | 1,610 | - | 1,610 | 133 | - | 133 |
| $Cl^-$ | 107,000 | 83,881 | 23,499 | 576 | 940 | 1,977 |
| $HCO_3^-$ | 176 | - | - | 495 | - | - |
| $SO_4^{2-}$ | 370 | - | - | 2,110 | - | - |
| Total dissolved solids | 174,156 | 138,281 | 35,659 | 4,633 | 1,550 | 2,686 |

a. Alotaibi et al. (2010)

b. Robertson (2007)

**Table 12—Density and Viscosity of Different Brines.**

| Brine | Density ($g/cm^3$) | Viscosity (cp) | Density ($g/cm^3$) | Viscosity (cp) |
|---|---|---|---|---|
| | AT T = 150°F AND P = 14.7 psi | | AT T = 77°F AND P = 14.7 psi | |
| Connate water (H-1) | 1.11 | 0.72 | 1.13 | 1.28 |
| Connate water (H-2) | 1.08 | 0.68 | 1.04 | 1.12 |
| Connate water (H-3) | 1.01 | 0.54 | 1.03 | 0.99 |
| Connate water (L-1) | 0.98 | 0.49 | 1.00 | 0.91 |
| Connate water (L-2) | 0.98 | 0.54 | 0.99 | 0.96 |
| Connate water (L-3) | 0.98 | 0.48 | 0.99 | 0.95 |
| NaCl (5,000 ppm) | 0.97 | 0.62 | 1.00 | 0.87 |
| NaCl (500 ppm) | 0.88 | 0.46 | 0.99 | 0.76 |
| Deionized water | 0.86 | 0.43 | 0.98 | 0.72 |

### 3.4. Crude Oil

In this work two crude oil types were used. A dead crude oil sample was centrifuged at 5,000 rpm for five minutes to remove suspended solids and to separate out the aqueous phase. Then, it was filtrated through the sandstone core to avoid any plugging from solids or emulsion. The properties and composition of the crudes oil used are listed in **Tables 13 through 15**. The density and viscosity of the crudes oil were measured at 77°F and at atmospheric pressure. The total acid number (TAN) and total base number (TBN) were measured by a Metrohm 907 Titrando in the lab.

**Table 13—Composition of the Crude Oil (A).**

| | Component | Concentration, wt% |
|---|---|---|
| 1 | Benzene, 1,3-dimethyl- | 10.54 |
| 2 | Octane, 2,6-dimethyl- | 7.05 |
| 3 | Benzene, 1,2,4-trimethyl- | 13.63 |
| 4 | Benzene, 1-ethyl-2,3-dimethyl- | 8.04 |
| 5 | Benzene, 1,2,4,5- tetramethyl- | 5.39 |
| 6 | Dodecane | 4.21 |
| 7 | Dodecane, 2,6,10-trimethyl- | 5.93 |
| 8 | Tetradecane | 2.66 |
| 9 | Dodecane, 2,6,11-trimethyl- | 4.00 |
| 10 | Pentadecane | 4.07 |
| 11 | Hexadecane | 3.93 |
| 12 | Pentadecane, 2,6,10,14-tetramethyl- | 6.18 |
| 13 | Hexadecane, 2,10,10-trimethyl- | 5.35 |
| 14 | Hexadecane, 2,6,10,14-tetramethyl- | 6.18 |
| 15 | Nonadecane | 2.13 |
| 16 | Eicosane | 2.96 |
| 17 | Heneicosane | 2.37 |
| 18 | Docosane | 1.86 |
| 19 | Tricosane | 1.58 |
| 20 | Tetracosane | 1.96 |

**Table 14—Composition of the Crude Oil (B).**

| | Component | Concentration, wt% |
|---|---|---|
| 1 | Hexane, 3-methyl | 4.38% |
| 2 | Cyclohexane, methyl- | 4.51% |
| 3 | Heptane, 2,3-dimethyl- | 5.69% |
| 4 | Nonane | 4.92% |
| 5 | Decane | 6.63% |
| 6 | Undecane | 5.77% |
| 7 | Dodecane | 5.90% |
| 8 | Tridecane | 5.77% |
| 9 | Tetradecane | 5.38% |
| 10 | Pentadecane | 6.36% |
| 11 | Hexadecane | 6.69% |
| 12 | Heptadecane | 5.37% |
| 13 | Octadecane | 4.82% |
| 14 | Nonadecane | 4.08% |
| 15 | Eicosane | 4.06% |
| 16 | Heneicosane | 3.86% |
| 17 | Docosane | 4.15% |
| 18 | Tricosane | 3.31% |
| 19 | Tetracosane | 3.11% |
| 20 | Pentacosane | 2.94% |
| 21 | Hexacosane | 2.30% |

**Table 15—Properties of Crude Oil at T = 77°F AND P = 14.7 psi.**

| Property | Density ($g/cm^3$) | Viscosity (cp) | $^oAPI$ | Acid number (mg KOH/g oil) | Base number (mg HCl/g oil) |
|---|---|---|---|---|---|
| Crude oil (A) | 0.83 | 14.03 | 39.0 | 0.92 | 0.68 |
| Crude Oil-B | 0.81 | 8.93 | 43.2 | 0.88 | 0.38 |

# CHAPTER IV

# IMPACT OF ROCK PERMEABILITY AND PORE-THROAT RADIUS ON LOW-SALINITY WATERFLOODING PERFORMANCE

Understanding the pore size and distribution of the sandstone cores can explain the different incremental values from each sandstone type. Pittman (1979) mentioned that the concept of pore geometry (size, shape, and distribution of pores) in a reservoir was important in understanding reservoir behavior. Lucia (1995) stated that the pore-size distribution was controlled by the grain size in the grain-dominated packstone and by the mud size in mud-dominated packstone. Chilingarian (1963) showed that the relationship between porosity and permeability depends on the granulometric composition of sandstones.

In this work, two-phase flow coreflood experiments were carried out to observe how LSW performed in the presence of different rock permeability and pore-throat radius. Four outcrop sandstone rock types were used. Eight coreflood tests were performed using Buff Berea, Grey Berea, Bandera, and Parker sandstone cores. The cores were saturated with FW at initial water saturation. These experiments were conducted at a temperature of 185°F, a backflow pressure of 500 psi, and an overburden pressure of 2,000 psi. In this work, the secondary and tertiary recovery modes in all experiments were conducted at injection rates of 0.5, 1, and 2 $cm^3$/min to ensure no further oil production from the cores. The secondary recovery mode was initiated at the initial oil

saturation ($S_{oi}$) from the beginning. The tertiary recovery mode was started when no extra oil was produced after introducing formation water brine using an injection rate of 2 $cm^3$/min. The tertiary recovery mode was subsequently applied using a low-salinity brine (5,000 ppm NaCl).

### 4.1. Buff Berea Sandstone Rock Experiments, Cores B-1 and B-2

Two core samples with designations B-1 and B-2 were cut from the same block of outcrop Buff Berea (average porosity of 19% and permeability of 165 md). XRD mineral analysis for the Buff Berea sandstone core indicated that the quartz content was in the range of 91 wt%. The dominating clay was kaolinite (3%) and small proportions of smectite (1%) and muscovite (1%). The sample contained significant proportions of K-feldspars of (microcline) 4%. Iron oxides and titanium oxides were also detected. Core B-1 was flooded with low-salinity NaCl brine (5,000 ppm) to simulate the secondary oil recovery mode. The obtained oil recovery and the monitored pressure drop across the core are presented in **Figure 13**. A constant injection flow rate of 0.5 $cm^3$/min was used; then, the injection rate was increased to 1 and 2 $cm^3$/min. Continuous injection of 5,000 ppm NaCl resulted in a final oil recovery of 60.91% OOIP. The oil recovery was 53.29% which occurred after 7.71 PV was injected using an injection rate of 0.5 $cm^3$/min. The additional oil recovery after injection of 3.29 PV was 7.6% of OOIP.

The observed increase in the pressure drop across the core in the beginning of the experiment at the injection rate of 0.5 $cm^3$/min was attributed to the two-phase flow. An

increase in the pressure drop was observed after breakthrough which indicate fines migration, or plugging occurred at this time. The average stabilized pressure was around 21.7 psi at a rate of 0.5 $cm^3$/min. Then, a stable pressure profile was noticed at different injection rates of 1 and 2 $cm^3$/min. The pressure drops were 40 and 80 psi at injection rates of 1 and 2 $cm^3$/min, respectively. A change in the injection rate induced a major increase in the pressure profile. The delay of the production was due to dead volumes in the coreflood setup and time of displacement in the core.

For core B-2, the continuous injection of FW (first step) resulted in a final recovery of 44.7% OOIP (**Figure 14**). Compared to experiment B-1, there is a significant decrease in the recovery of more than 17%. The experiment was extended with a continuous injection of low-salinity 5,000 ppm NaCl brine (second step) for 5.9 PV. The injection of low-salinity brine as a tertiary recovery mode resulted in no change in the residual oil saturation for Buff Berea sandstone. Some results have been reported by low salinity waterflooding, showing benefit reported in tertiary mode. In this work, the tertiary recovery mode indicated the injection of low-salinity brine after no benefits were shown from high-salinity brine. Results do not show there is movable oil in the plug after the high salinity injection. The secondary recovery mode was conducted at various injection rates of 0.5, 1, and 2 $cm^3$/min to ensure no further oil production from the cores during HSW. Nasralla and Nasr-El-Din (2014) indicated that LSW does not work as a tertiary method because the expansion of the double layer may not help to recover more oil in the tertiary-recovery mode. This could have been a result of the absence of a continuous

oil film which is a result of the repulsive forces caused by the LSW not being strong enough to sweep the residual oil.

Figure 14 shows the pressure profile for experiment B-2 for the different injection slugs. This experiment showed the attributed pressure profile behavior due to the two-phase flow similar to experiments B-1 at the beginning of the experiment. The average stabilized pressure was around 23 psi at a rate of 0.5 $cm^3$/min. The pressure profile was almost steady for the formation water at different injection rates (1 and 2 $cm^3$/min). The pressure drops were 43 and 85 psi at injection rates of 2 and 4 $cm^3$/min, respectively. No fine minerals or color changes were observed in the effluent samples by injecting brine of 5,000 ppm NaCl. The differential pressure is an indication that no clay swelling or plugging occurred during injection low-salinity brine after formation water. At the end of each slug, there was a major jump in the pressure profile induced by a change in the injection rate for the different experiments. Gradual decrease in pressure drop during low-salinity brine ceased due to the change of viscosity.

**Tables 16** and **17** summarize the oil recovery, the number of PV injected, and the injection rate for B-1 and B-2 experiments. The increase in the oil recovery after increasing the injection rate was most likely due to the response of fines migration plugging of smaller pore-throat radii or reduction in the capillary end effect at higher rates. The compared oil recovery obtained during experiment B-1 and B-2 during the secondary recovery mode. This indicates that decreasing the injected brine salinity from 174,156 to 5,000 ppm caused a significant increase in the total volume of the recovered oil, 17% of OOIP. The pH of the injected formation brine and low-salinity brine at the

beginning of the experiments were 6.34 and 6.86, respectively. The pH of the effluent samples were measured after the coreflood experiments. The pH for the B-2 experiment varied between 7.0 and 7.23, while the pH for the B-1 experiment varied between 7.9 and 8.1.

**Table 16—Summary of Coreflood Experiment (B-1) For Buff Berea Sandstone AT T = 185°F.**

| Slug Type | Recovery Mode | Injection Rate (ml/min) | Slug Size (PV) | Incremental Oil Recovery (% OOIP) | Total Oil Recovery (% OOIP) |
|---|---|---|---|---|---|
| 0.5 wt% NaCl | Secondary | 0.5 | 7.71 | 53.29 | 53.29 |
| | | 1 | 3.29 | 7.62 | 61.8 |
| | | 2 | 2.28 | 0.0 | 61.8 |

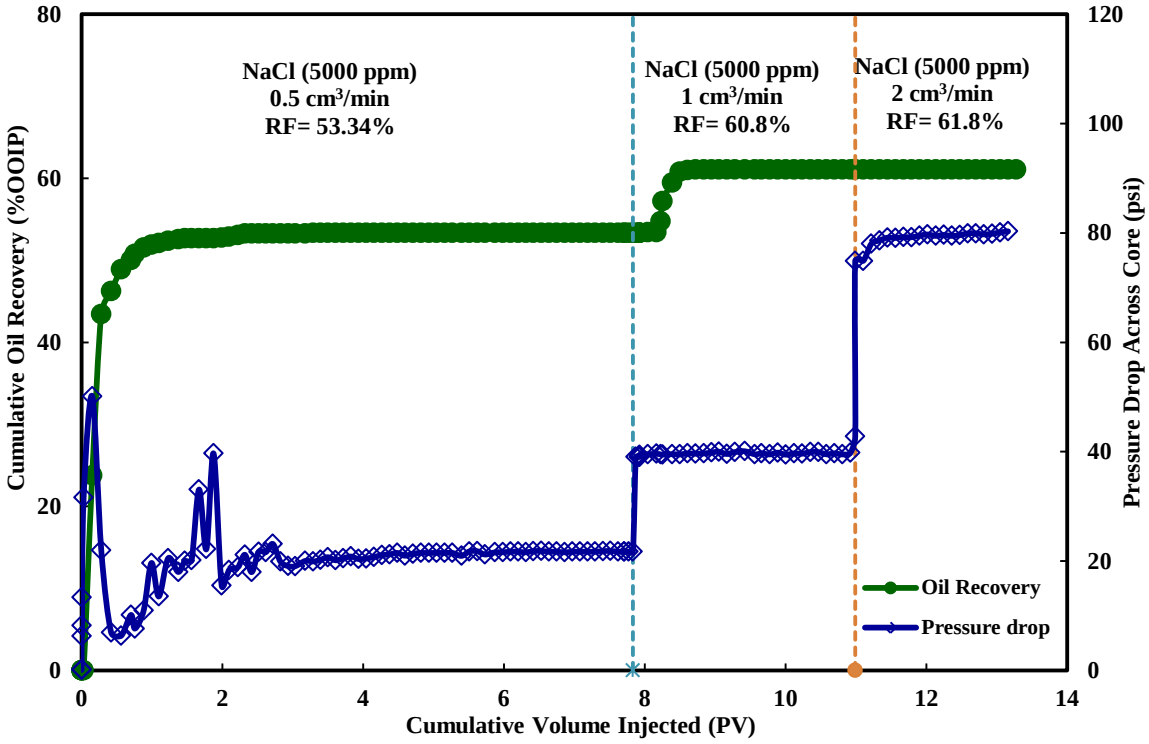


**Figure 13—Oil recovery and pressure drop across the core for experiment B-1 at 185°F and $S_{wc}$ = 34.5%. The injection was performed by NaCl brine (5,000 ppm) using injection rates of 0.5, 1, and 2 $cm^3$/min. The vertical dashed lines separate the different injected brine stages.**

**Table 17—Summary of Coreflood Experiment (B-2) For Buff Berea Sandstone AT T = 185°F.**

| Slug Type | Recovery Mode | Injection Rate (ml/min) | Slug Size (PV) | Incremental Oil Recovery (% OOIP) | Total Oil Recovery (% OOIP) |
|---|---|---|---|---|---|
| Formation Water (174,156 ppm) | Secondary | 0.5 | 7.73 | 39.64 | 39.64 |
| | | 1 | 3.67 | 5.07 | 44.71 |
| | | 2 | 2.45 | 0.0 | 44.71 |
| 0.5 wt% NaCl | Tertiary | 1 | 2.91 | 0.0 | 44.71 |
| | | 2 | 2.99 | 0.0 | 44.71 |

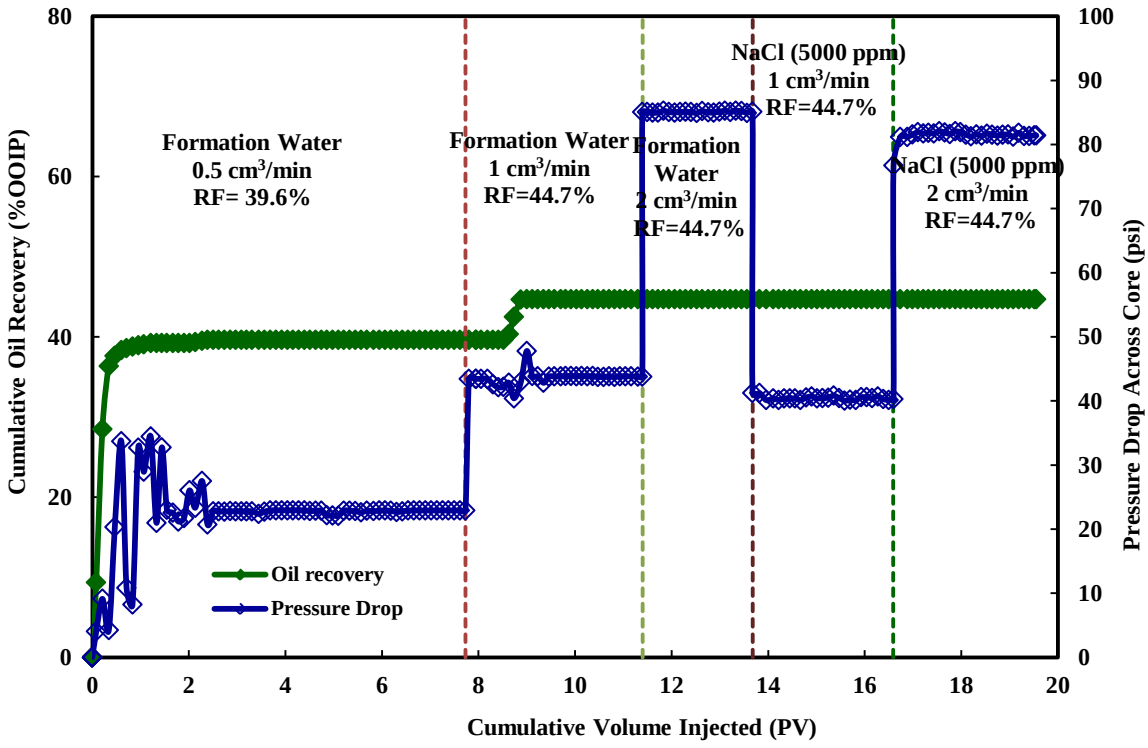


**Figure 14—Oil recovery and pressure drop across core for experiment B-2 at 185°F and $S_{wc}$ = 35.3%. The injection was performed by formation water (174,156 ppm) using injection rates of 0.5, 1, and 2 $cm^3$/min, followed by NaCl brine (5,000 ppm) using injection rates of 1 and 2 $cm^3$/min. The vertical dashed lines separate the different injected brine stages.**

### 4.2. Grey Berea Sandstone Rock Experiments, Cores A-2 and A-4

Two core samples with designations A-2 and A-4 were cut from the same block (average porosity of 20% and permeability of 65 md). XRD mineral analysis for Grey Berea sandstone detected quartz (87%), kaolinite (6%), albite (3%), illite (2%), and calcite (2%). The main objective of experiment A-2 was to test the effect of low-salinity brine injection. Injection began at a rate of 0.5 $cm^3$/min. Approximately 7.82 PV of 5,000 ppm NaCl brine had been injected, and the estimated incremental oil recovery was around 49.77% of OOIP. After oil production ceased, the rate was increased to 1 and 2 $cm^3$/min. The oil continued to be produced after increasing the injection rate to 1 $cm^3$/min. A small increase in oil recovery was observed after an injection of about 5.73 PV. The final oil recovery was 51.2% of OOIP. The oil recovery versus the injected pore volume is given in **Table 18**.

For core A-4, the injection was performed by FW (174,156 ppm) using injection rates of 0.5, 1, and 2 $cm^3$/min followed by NaCl brine (5,000 ppm) using injection rates of 1 and 2 $cm^3$/min. The ultimate oil recovery for FW was 37.42% of OOIP. The results in **Table 19** shows that no more oil could be produced during the tertiary recovery mode. These results confirmed the results of experiment B-2 during the injection of LSW in the tertiary recovery mode. Also, these results are consistent with previous observations that LSW does not work as a tertiary recovery mode for Grey Berea sandstone (Nasralla et al. 2011). As demonstrated in Tables 18 and 19, the oil recovery was improved by 13.32% of OOIP by using LSW instead of FW. Alotaibi et al. (2011) studied the effect

of brine salinity on contact-angle measurements and zeta potential by using Grey Berea rock surfaces and three different brines (174,156, 54,680, and 5,436 ppm). The injection of LSW altered the Berea sandstone wettability toward strongly water-wet. This could have been a result of the expansion of the double layer is not sufficient to improve oil recovery in the tertiary recovery mode. It was noticed that the LSW performance in the Grey Berea was lower than in Buff Berea cores. The incremental oil recovery decreased from 17.12 to 13.32% of OOIP. Grey Berea contains 2% of calcite as a cement material. The pH for the A-4 experiment varied between 6.6 and 7, while the pH for the A-2 experiment varied between 7.6 and 8. The pressure drop profile for experiment A-2 was similar to the previous experiment on Buff Berea using as shown in **Figure 15**. **Figure 16** show the pressure profiles for experiments A-4 for the different injection slugs.

**Table 18—Summary of Coreflood Experiment (A-2) For Grey Berea Sandstone AT T = 185°F.**

| Slug Type | Recovery Mode | Injection Rate (ml/min) | Slug Size (PV) | Incremental Oil Recovery (% OOIP) | Total Oil Recovery (% OOIP) |
|---|---|---|---|---|---|
| 0.5 wt% NaCl | Secondary | 0.5 | 7.82 | 49.77 | 49.77 |
| | | 1 | 5.73 | 1.54 | 51.22 |
| | | 2 | 3.62 | 0.0 | 51.22 |

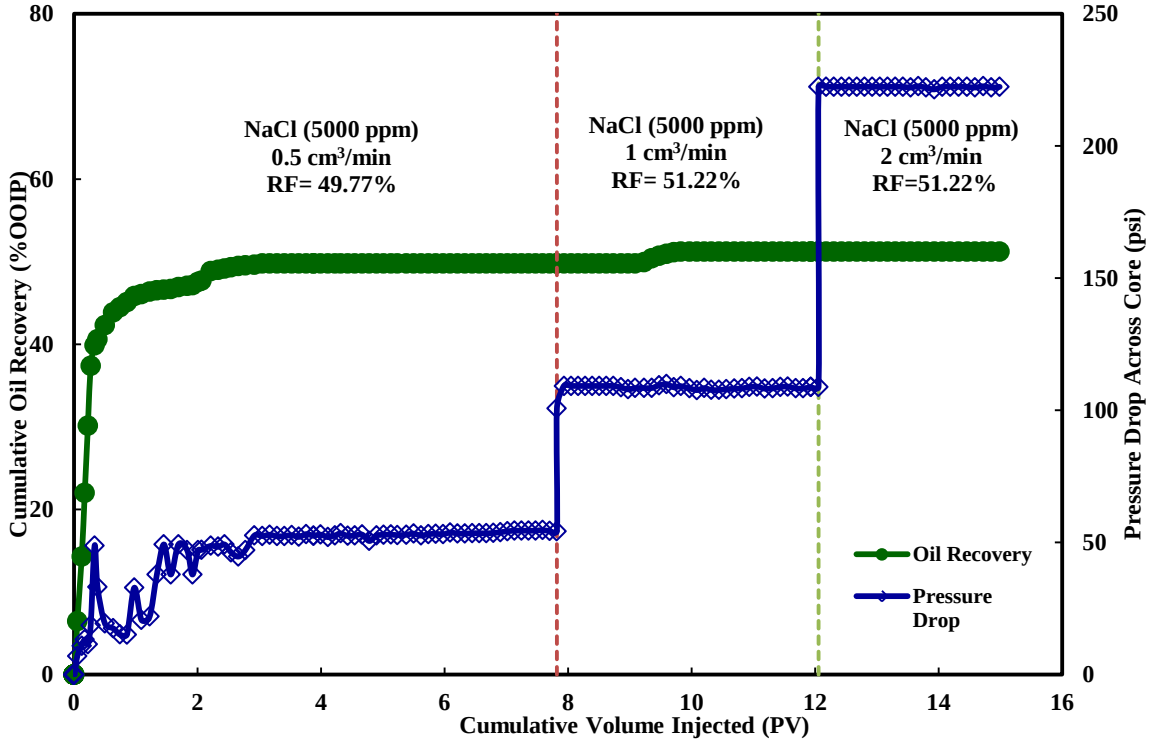


**Figure 15—Oil recovery and pressure drop across the core for experiment A-2 at 185°F and $S_{wc}$ = 33.3%. The injection was performed by NaCl brine (5,000 ppm) using injection rates of 0.5, 1, and 2 cm$^3$/min. The vertical dashed lines separate the different injected brine stages.**

**Table 19—Summary of Coreflood Experiment (A-4) For Grey Berea Sandstone AT T = 185°F.**

| Slug Type | Recovery Mode | Injection Rate (ml/min) | Slug Size (PV) | Incremental Oil Recovery (% OOIP) | Total Oil Recovery (% OOIP) |
|---|---|---|---|---|---|
| Formation Water (174,156 ppm) | Secondary | 0.5 | 7.63 | 35.64 | 35.64 |
| | | 1 | 4.23 | 1.78 | 37.42 |
| | | 2 | 3.55 | 0.0 | 37.42 |
| 0.5 wt% NaCl | Tertiary | 1 | 3.40 | 0.0 | 37.42 |
| | | 2 | 4.20 | 0.0 | 37.42 |

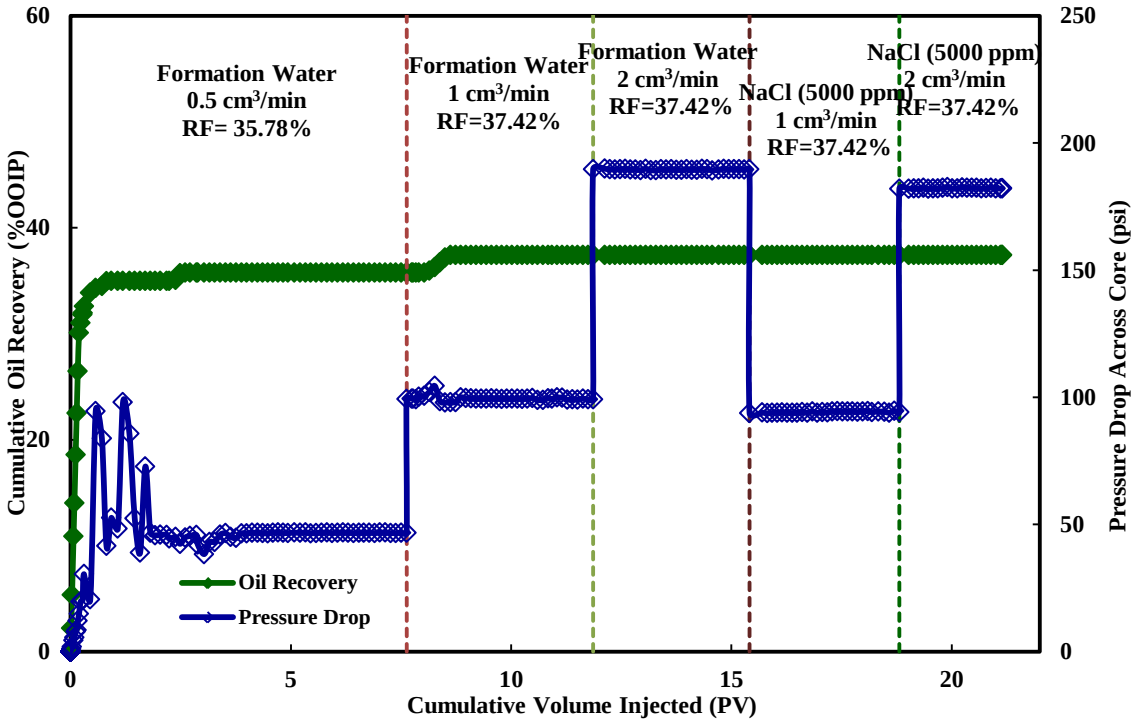


**Figure 16—Oil recovery and pressure drop across core for experiment A-4 at 185°F and $S_{wc}$ = 34.7%. The injection was performed by formation water (174,156 ppm) using injection rates of 0.5, 1, and 2 $cm^3$/min, followed by NaCl brine (5,000 ppm) using injection rates of 1 and 2 $cm^3$/min. The vertical dashed lines separate the different injected brine stages.**

### 4.3. Bandera Sandstone Rock Experiments, Cores C-1 and C-4

Two core samples were cut from the same block (average porosity of 20% and permeability of 25 md). From the XRD analyses, Bandera samples contain a higher amount of clay minerals than Buff and Grey Berea. Bandera contains a considerable amount of illite (10%), kaolinite (3%), and small proportions of chlorite clays (1%), as well as a large amount of albite minerals (12%). The Bandera cores are rich in dolomite minerals (15%), while quartz made up the remainder.

For core C-1, the continuous injection of NaCl (5,000 ppm) brine from the connate water saturation resulted in a total recovery of 42.44% of OOIP. **Table 20** summarizes the results of coreflood experiment C-1. For this experiment, no more oil was observed when the injection rate increased from 0.5 to 1 and 2 $cm^3$/min. The comparison between cores C-1, B-1, and A-2, showed that no relationship was noticed between the total clay contents and incremental oil recovery. The distribution of the clays and presence of other minerals, such as dolomite or feldspar, seem to be playing a significant role in the mechanisms of LSW.

In experiment C-4, 17.8 PVs of FW was injected as a secondary recovery mode and then followed by 9.87 PVs of 5,000 ppm NaCl brine as a tertiary recovery mode. A total of eight pore volumes at 0.5 $cm^3$/min were injected. After oil production ceased, the injection rate was increased to 1 and 2 $cm^3$/min. Oil recovery increased slightly to 33.2% after increasing the injection rate to 1 $cm^3$/min. Then, switching the injection brine from FW to NaCl brine resulted in an increase in the produced oil. The oil recovery that was obtained when using the 5,000 ppm NaCl brine was about 6.9% of the OOIP. Hence, this represented a significant contribution to the total volume of the recovered oil. It was noticed that the secondary mode experiments produced more oil than the tertiary mode. **Table 21** summarizes the results of coreflood experiment C-4.

The oil recovery from core C-1 reached approximately 42.44% of OOIP, while only 33.2% of the oil was recovered from core C-4. The most notable detail is that the incremental oil recovery from Bandera cores is lower than the Buff Berea and Grey Berea cores; however, Bandera had a clay content higher than Buff Berea sandstone.

These results indicated that the total clay content is not the main parameter to get a higher oil recovery using LSW. The composition of other minerals will affect the LSW performance. Also, the rock quality has a significant effect in the performance of LSW. The pH for the C-4 experiment varied between 6.9 and 7.1, while the pH for the C-1 experiment varied between 7.2 and 7.7. **Figures 17** and **18** depict the pressure drop profile for coreflood experiments C-1 and C-4 for the different injection slugs.

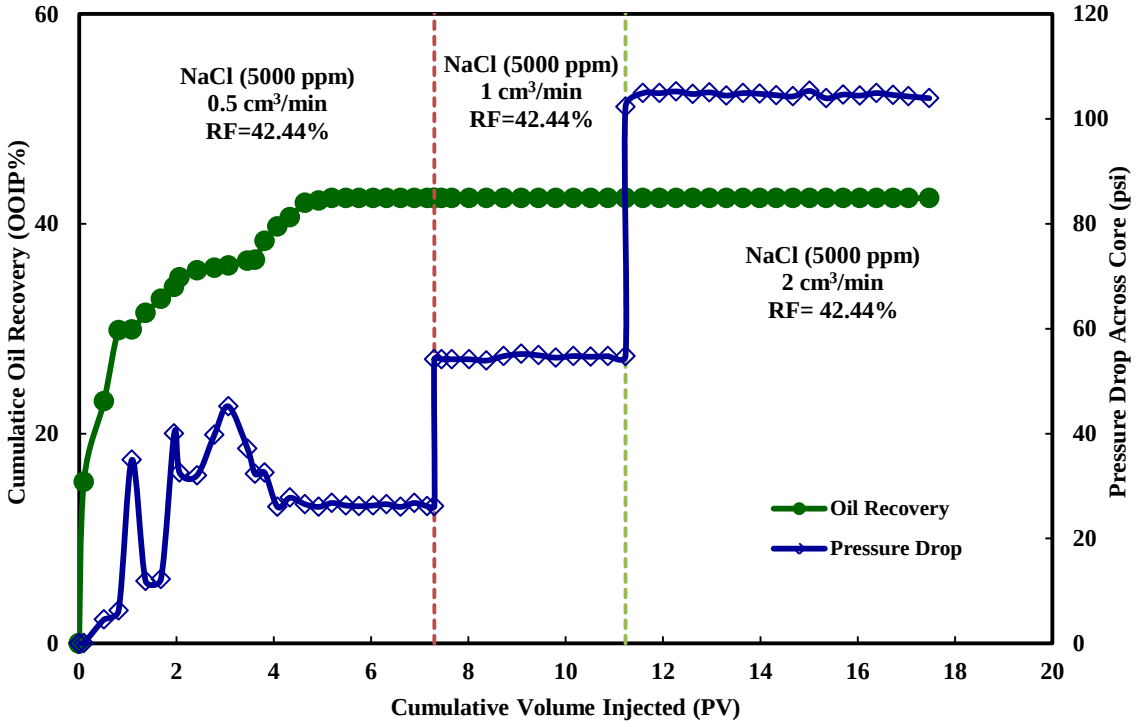


**Figure 17—Oil recovery and pressure drop across the core for experiment C-1 at 185°F and $S_{wc}$ = 34.4%. The injection was performed by NaCl brine (5,000 ppm) using injection rates of 0.5, 1, and 2 $cm^3$/min. The vertical dashed lines separate the different injected brine stages.**

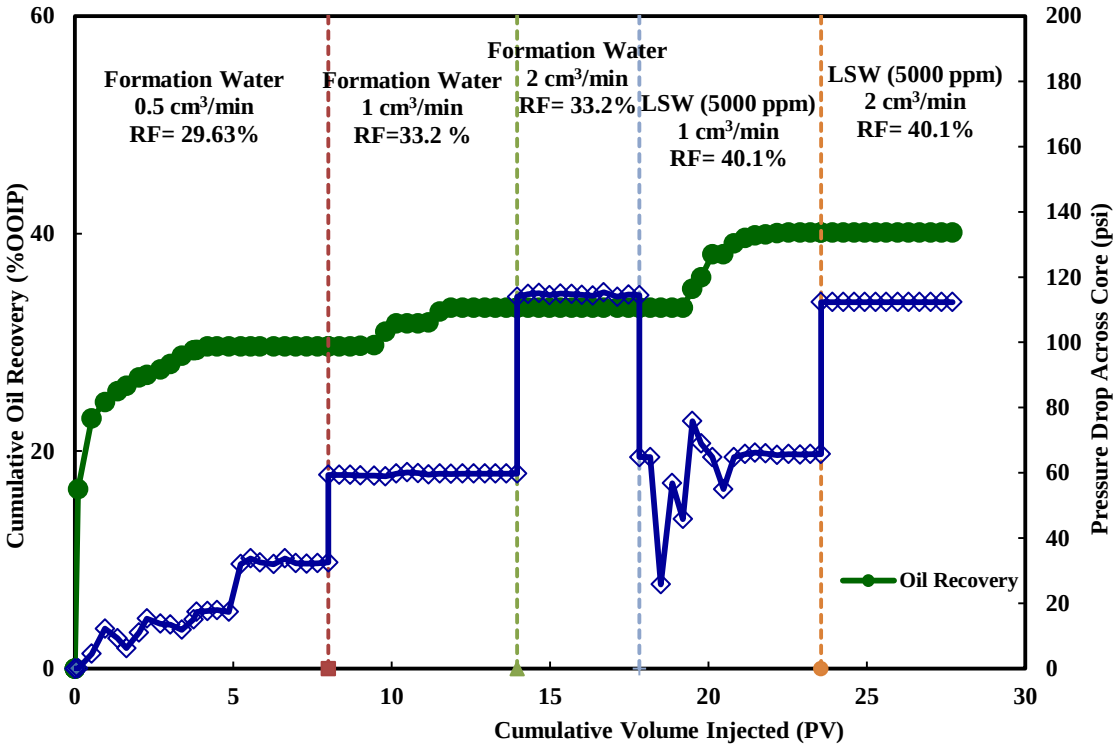


**Figure 18—Oil recovery and pressure drop across core for experiment C-4 at 185°F and $S_{wc}$ = 35.8%. The injection was performed by formation water (174,156 ppm) using injection rates of 0.5, 1, and 2 cm$^3$/min, followed by NaCl brine (5,000 ppm) using injection rates of 1 and 2 cm$^3$/min. The vertical dashed lines separate the different injected brine stages.**

**Table 20—Summary of Coreflood Experiment (C-1) For Bandera Sandstone AT T = 185°F.**

| Slug Type | Recovery Mode | Injection Rate (ml/min) | Slug Size (PV) | Incremental Oil Recovery (% OOIP) | Total Oil Recovery (% OOIP) |
|---|---|---|---|---|---|
| | | 0.5 | 7.3 | 42.44 | 42.44 |
| 0.5 wt% NaCl | Secondary | 1 | 3.93 | 0.0 | 42.44 |
| | | 2 | 6.24 | 0.0 | 42.44 |

**Table 21—Summary of Coreflood Experiment (C-4) For Bandera Sandstone AT T = 185°F.**

| Slug Type | Recovery Mode | Injection Rate (ml/min) | Slug Size (PV) | Incremental Oil Recovery (% OOIP) | Total Oil Recovery (% OOIP) |
|---|---|---|---|---|---|
| Formation Water (174,156 ppm) | Secondary | 0.5 | 8.0 | 29.65 | 29.65 |
| | | 1 | 5.95 | 3.55 | 33.20 |
| | | 2 | 3.85 | 0.0 | 33.20 |
| 0.5 wt% NaCl | Tertiary | 1 | 5.73 | 6.90 | 40.10 |
| | | 2 | 4.14 | 0.0 | 40.10 |

### 4.4. Parker Sandstone Rock Experiments, Cores D-4 and D-7

Two core samples with designations D-4 and D-7 were cut from the same block (average porosity of 16% and permeability of 6 md). Two coreflood experiments were conducted to investigate the effect of LSW on the sandstone rock with a low permeability. XRD mineral analysis for the Parker sandstone consists of quartz (87%), kaolinite (2%), albite (5%), illite (4%), and mica (2%). The total PVs, incremental oil recovery, and oil recovery for experiment D-4 are given in **Table 22**. The continuous injection of NaCl (5,000 ppm) brine from the connate water saturation resulted in a total recovery of 28.92% of OOIP. There was no incremental increase in oil recovery due to the increase in the injection rate to 1 and 2 $cm^3$/min.

On the other hand, the D-7 experiment was started with an injection of FW. The total oil recovery for experiment D-7 was about 24.64% lower than the total oil recovery of experiment D-4. The Parker cores showed no response to LSW as a tertiary recovery

performance. A summary of experiment D-7 is given in **Table 23**. Both oil recovery and differential pressure by high and low-salinity waterflooding are presented as shown in **Figures 19** and **20**. As can be noticed, low-salinity brine improve the displacement efficiency by 4.28% of OOIP compared to FW. The pH for the D-7 experiment varied between 6.7 and 6.95, while the pH for the D-4 experiment varied between 6.3 and 6.82.

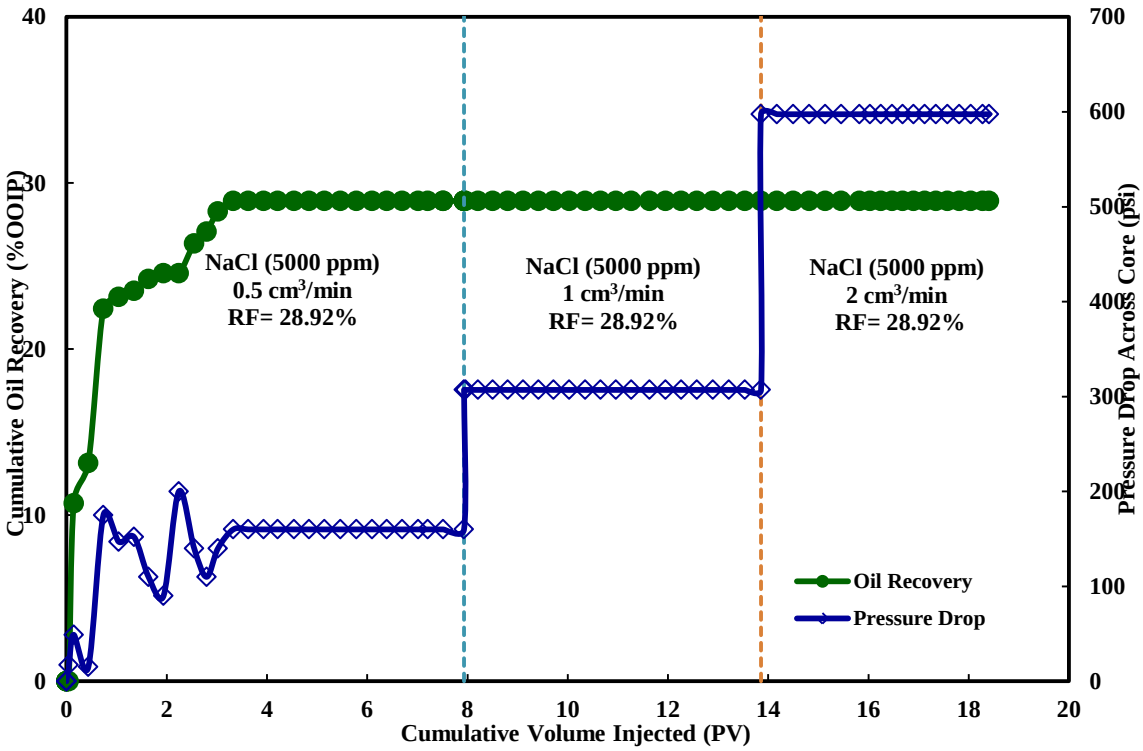


**Figure 19—Oil recovery and pressure drop across the core for experiment D-4 at 185°F and $S_{wc}$ = 38.6%. The injection was performed by NaCl brine (5,000 ppm) using injection rates of 0.5, 1, and 2 $cm^3$/min. The vertical dashed lines separate the different injected brine stages.**

**Table 22—Summary of Coreflood Experiment (D-4) For Parker Sandstone AT T = 185°F.**

| Slug Type | Recovery Mode | Injection Rate (ml/min) | Slug Size (PV) | Incremental Oil Recovery (% OOIP) | Total Oil Recovery (% OOIP) |
|---|---|---|---|---|---|
| 0.5 wt% NaCl | Secondary | 0.5 | 7.93 | 28.92 | 28.92 |
| | | 1 | 5.92 | 0.0 | 28.92 |
| | | 2 | 4.55 | 0.0 | 28.92 |

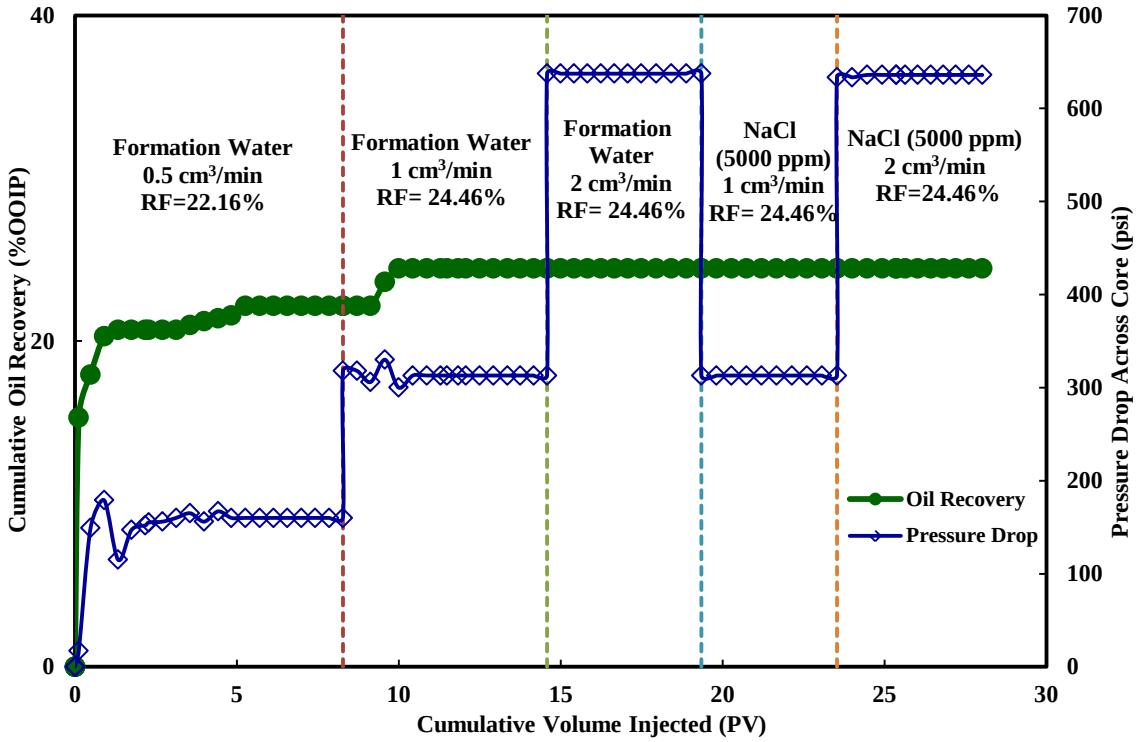


**Figure 20—Oil recovery and pressure drop across the core for experiment D-7 at 185°F and $S_{wc}$ = 39.5%. The injection was performed by formation water (174,156 ppm) using injection rates of 0.5, 1, and 2 $cm^3$/min, followed by NaCl brine (5,000 ppm) using injection rates of 1 and 2 $cm^3$/min. The vertical dashed lines separate the different injected brine stages.**

**Table 23—Summary of Coreflood Experiment (D-7) For Parker Sandstone AT T = 185°F.**

| Slug Type | Recovery Mode | Injection Rate (ml/min) | Slug Size (PV) | Incremental Oil Recovery (% OOIP) | Total Oil Recovery (% OOIP) |
|---|---|---|---|---|---|
| Formation Water (174,156 ppm) | Secondary | 0.5 | 8.28 | 22.14 | 22.14 |
| | | 1 | 6.30 | 2.50 | 24.64 |
| | | 2 | 4.76 | 0.0 | 24.64 |
| 0.5 wt% NaCl | Tertiary | 1 | 4.19 | 0.0 | 24.64 |
| | | 2 | 4.49 | 0.0 | 24.64 |

### 4.5. Effect of the Rock Permeability on the LSW

A variety of different sandstone cores were selected that covered a wide range of porosity and permeability. The results demonstrated that the effect of permeability is significant. As the permeability of the sandstone cores increased from 6 to 167 md, an additional oil recovery of up to 32.9% of OOIP was observed by low-salinity waterflooding as a secondary recovery mode. An additional oil recovery of up to 18% of OOIP was observed for high-salinity waterflooding as a secondary recovery mode. The additional oil recovery, using LSW instead of HSW, decreased from 17.12 to 4.28% of OOIP when the permeability decreased from 167 to 6 md. The decrease in recovery when the permeability decreased could be due to fines migration. This effect would be higher when the permeability of the rock decreased because the size of the pores are smaller compared to the high permeability rock samples. **Figure 21** shows the

incremental oil recovery (OOIP%) versus average horizontal permeability during the secondary recovery mode.

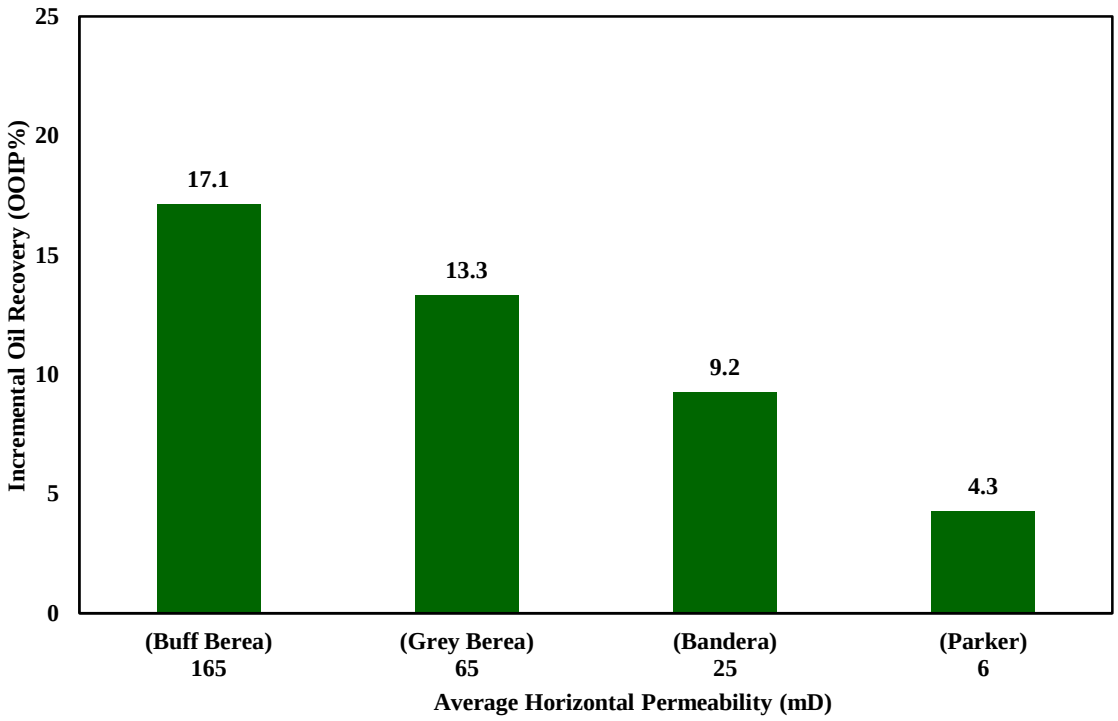


**Figure 21—Incremental oil recovery (OOIP%) versus average horizontal permeability during secondary recovery mode.**

### 4.6. Effect of the Pore-Throat Radius Distribution on the LSW

In the present work, high-pressure mercury injection measurements were performed to characterize the pore geometry and provide capillary pressure curves. Dry, clean core plugs with dimensions of 1 in. diameter and 1 in. length were used. An automated, high pressure mercury injection device operates at injection pressures of 0 to 55,000 psia. **Figure 22** presents the capillary pressure curves as a function of water saturation for water-oil fluid system for the Buff Berea, Grey Berea, Bandera, and Parker sandstones. The capillary pressure is inversely proportional to pore radius. It can be seen

that the parker sample has the highest capillary pressure values and Buff Berea has the lowest capillary pressure values.

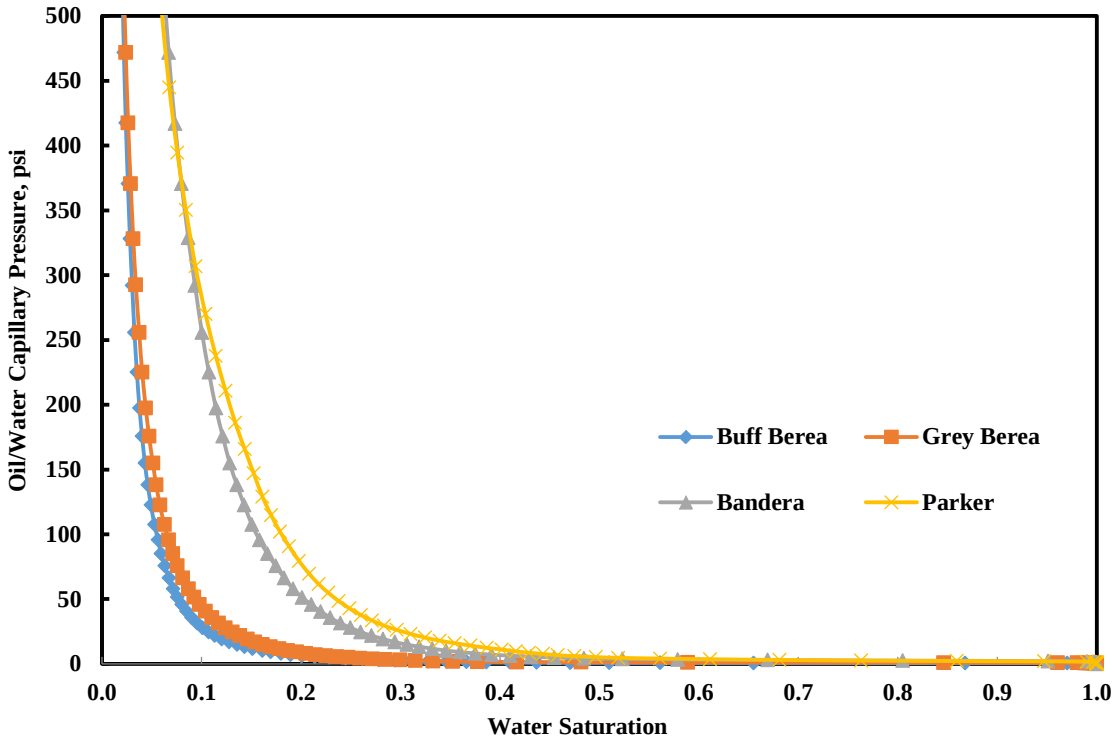


**Figure 22—Capillary pressure curves for the Buff Berea, Grey Berea, Bandera, and Parker sandstones.**

The relationship of injection pressure to mercury saturation was used to calculate the pore-throat size distribution. For Buff Berea, the measured pore-throat radius was 11 microns at a mercury saturation of 35%, while the median pore-throat radius was 8.8 microns. **Figure 23**, shows that the largest pore-throats are located on the mega (25 microns). The predominant pore-throat ranges from 2.5 to 25 microns. For Grey Berea, the measured pore-throat radius was 7 microns at a mercury saturation of 35%, while the

median pore-throat radius was 6.3 microns. The predominant pore-throat ranges from 2.5 to 10 microns.

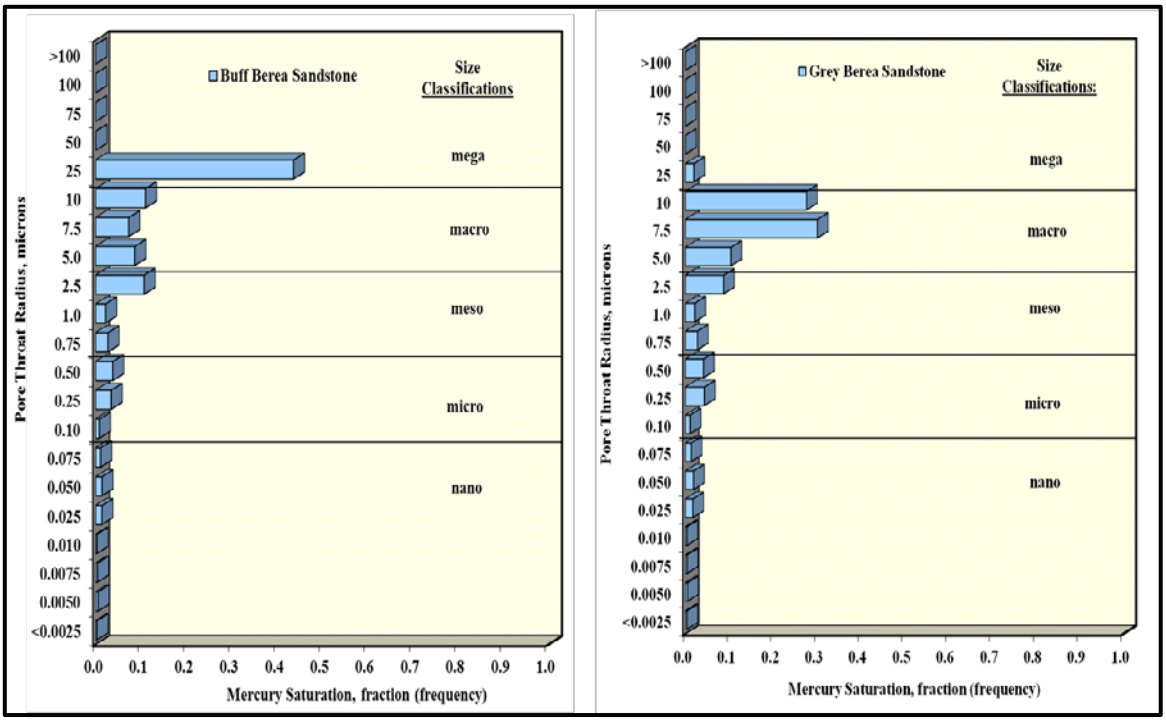


**Figure 23—Pore throat size histogram for Buff Berea and Grey Berea sandstone samples using a high-pressure mercury injection test.**

On the other hand, for Bandera sandstone, the measured pore-throat radius was 2.6 microns at a mercury saturation of 35%, and the median pore-throat radius was 1.8 microns. The pore-throat size histogram shows that the predominant pore-throat range from macro (5 microns) to micro (0.25 micron) rock types (**Figure 24**). The measured pore-throat radius was 2 microns, while the median pore-throat radius was 1.7 microns for the Parker sandstone sample.

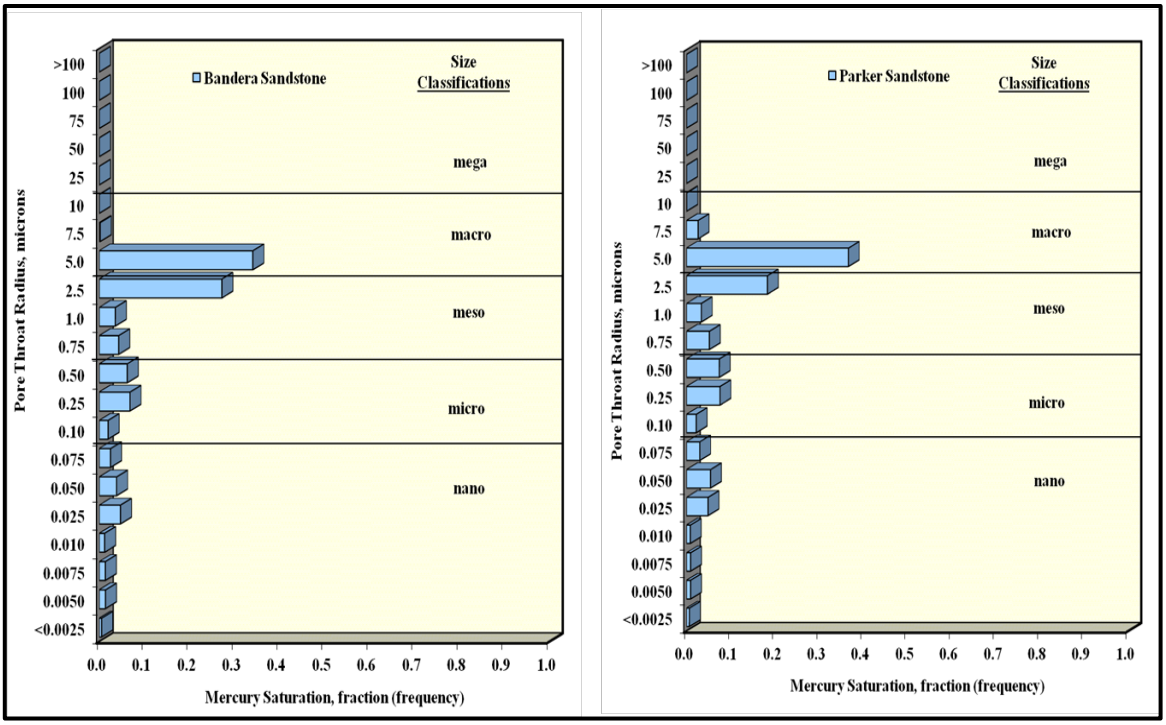


**Figure 24—Pore throat size histogram for Bandera and Parker sandstone samples using a high-pressure mercury injection test.**

**Figures 25** and **26** show the pore-throat radius distribution for Buff Berea, Grey Berea, Bandera, and Parker sandstone samples using a high-pressure mercury injection test. A single peak was noticed for Buff Berea, Grey Berea, Bandera, and Parker rock types. It indicates that these rock types are homogeneous, and all of the pores have a similar geometric shape.

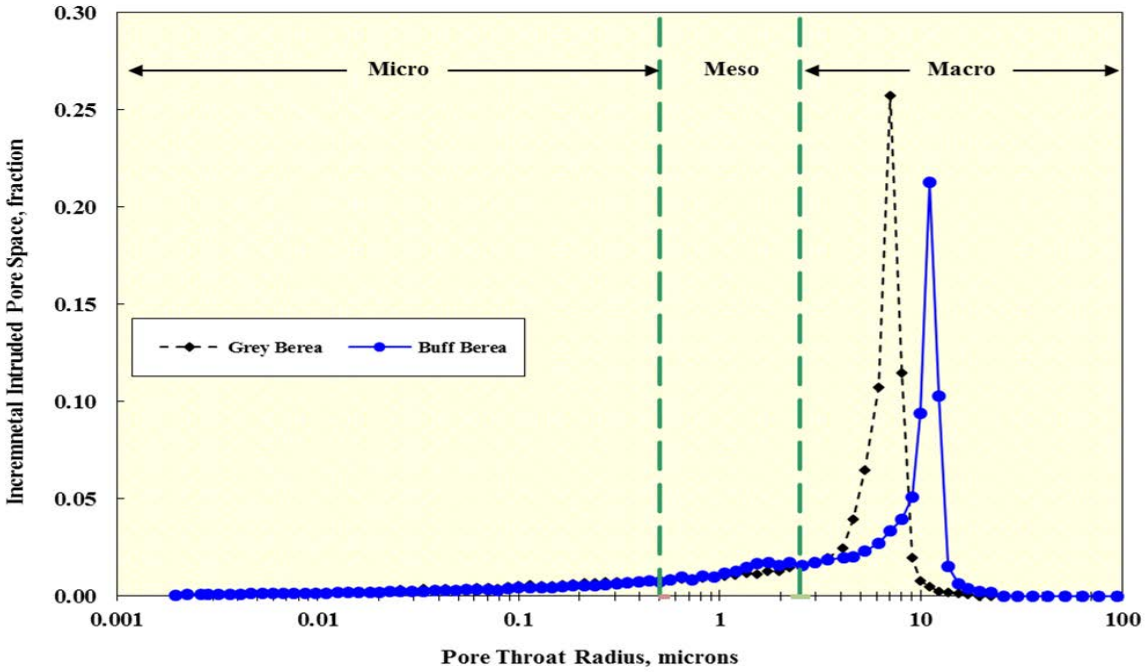


**Figure 25—Pore-throat radius distribution for Buff Berea and Grey Berea sandstone samples using a high-pressure mercury injection test.**

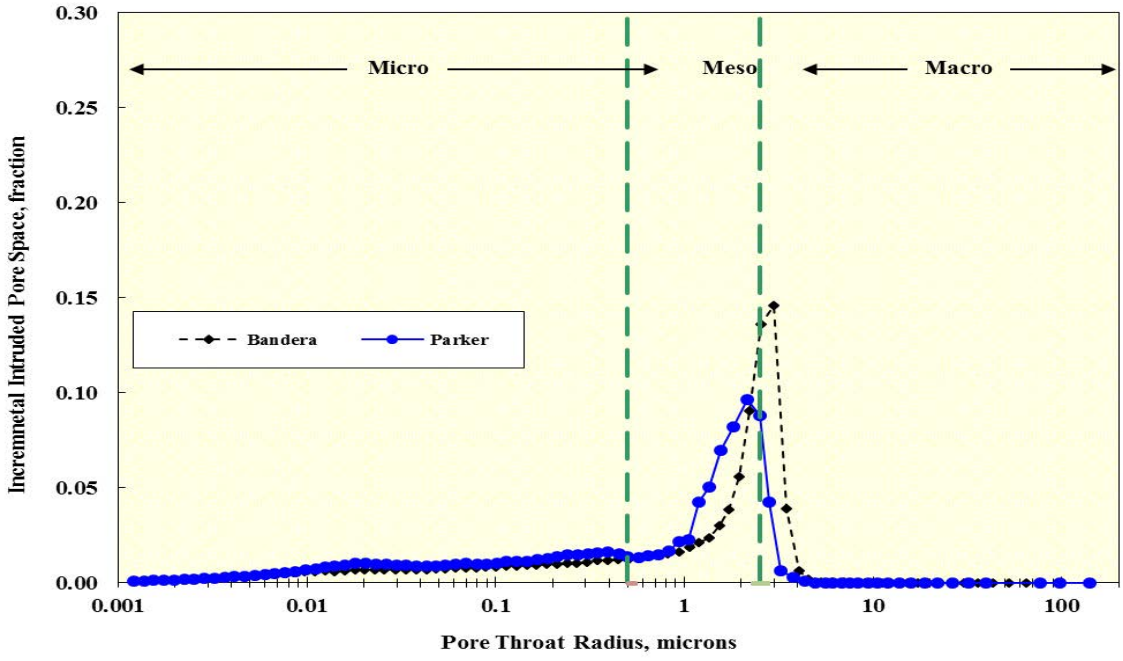


**Figure 26—Pore-throat radius distribution for Bandera and Parker sandstone samples using a high-pressure mercury injection test.**

In addition, Nuclear Magnetic Resonance (NMR) measurements were conducted on the four sandstones types saturated with FW. The NMR measurements were conducted using a 2 MHz NMR benchtop spectrometer (GeoSpec2 Core Analyzer). Core plugs with dimensions of 1.5 in diameter and 1.5 in length were used. From this test, the rate of decay of the NMR signal was determined. It is described by a distribution of decay times, $T_2s$, which are called transverse relaxation times. Coates et al. (1999) stated that in water-saturated rocks, the $T_2$ distributions are qualitatively directly proportional to pore-size distributions. The largest pores have the longest $T_2$, while the smallest pores have the shortest $T_2$ values.

**Figure 27** shows the $T_2$ distribution for the four sandstone types. The area under the $T_2$ distribution is proportional to the total porosity of the samples. The total NMR porosities for Buff Berea, Grey Berea, Bandera, and Parker are 19.6, 20.5, 17.8, and 14%, respectively. These values are quite similar to values obtained from a routine core analysis. Buff Berea has the highest $T_2$ peak values (222 ms), while the $T_2$ response of Grey Berea and Bandera rock types shift to lower values of 158.5 and 89.1 ms, respectively. This means that Buff Berea has the largest pore radius, followed by Grey Berea and then Bandera. Parker has the lowest pore size because this leads to a shifting of the major $T_2$ peak to a shorter time.

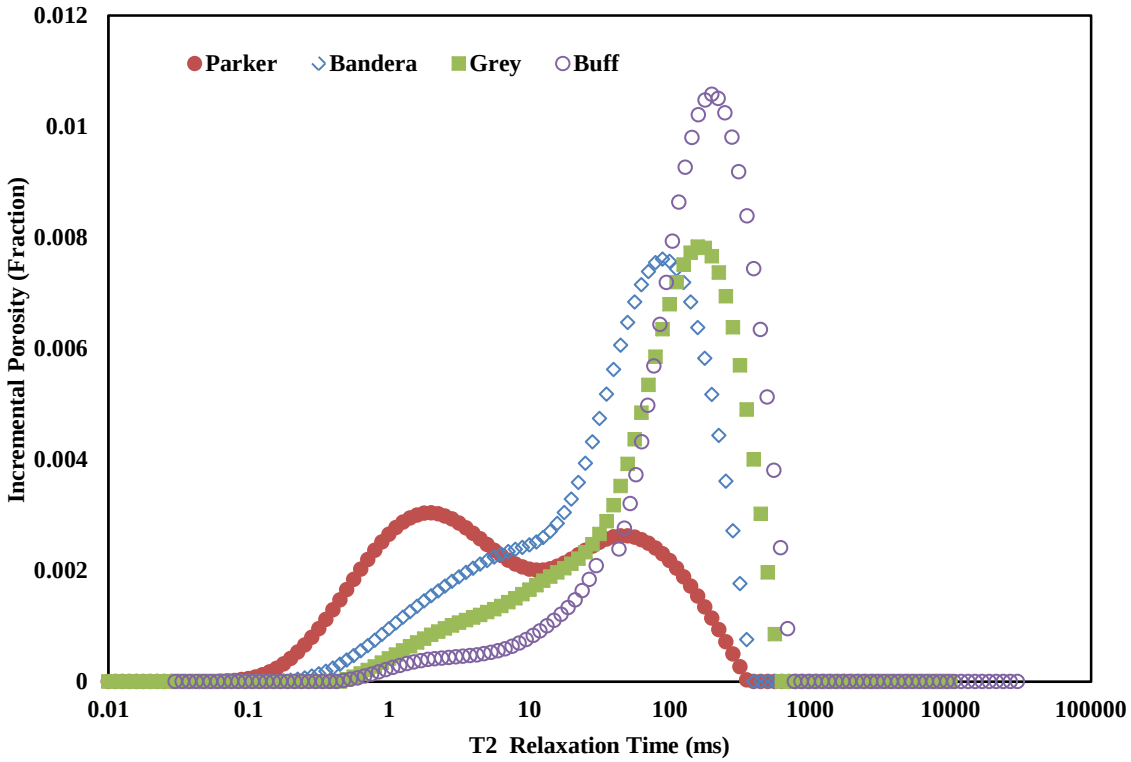


**Figure 27—NMR $T_2$ distributions for the Buff Berea, Grey Berea, Bandera, and Parker sandstones.**

Then, the average pore-throat radius was calculated for each core to define the rock type (flow units) using Winland's empirical equation (**Eq.2**) (Kolodzie 1980). Eq. 2 was developed with data from more than 2,500 sandstone and carbonate samples. Where R35 is the calculated pore throat radius (microns) at 35% mercury saturation from a mercury-injection capillary pressure test, permeability is in md, and porosity is a percentage (Guo et al. 2005). The Buff Berea, Grey Berea, and Bandera are located in the macro-porous flow unit, while Parker was located in the meso-porous flow unit with smaller pore throat radius (Martin et al. 1997). **Figure 28** shows a cross plot of the permeability versus the porosity for the four sandstone types.

$$log(R35) = 0.732 + 0.588\ log(k) - 0.864\ log(\varphi)$$ ..... (2)

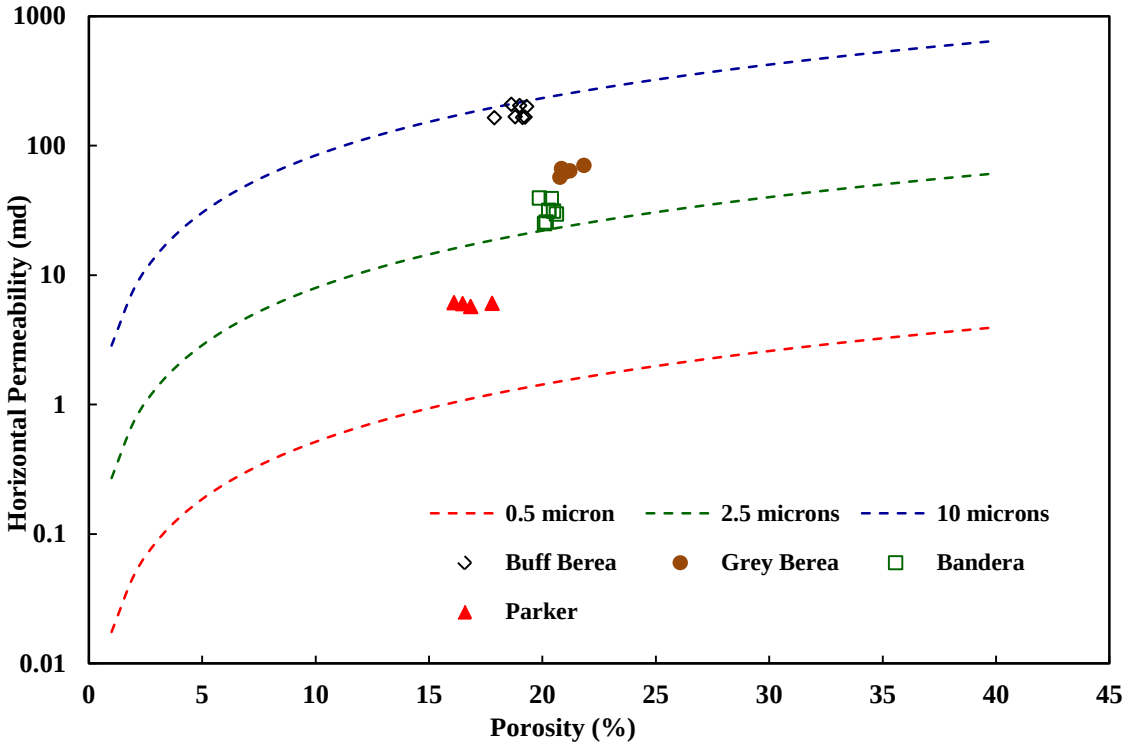


**Figure 28—Cross plot of permeability versus porosity for the used sandstone cores. The dotted points represent the average pore-throat radius for each sandstone core. The dashed lines represent the ` pore-throat radius calculated using Eq.2.**

In this study, a comparison of oil recovery obtained by the injection of NaCl (5,000 ppm) as LSW compared to the injection of FW as HSW during secondary recovery mode is given in **Figure 29**. **Figure 30** shows the incremental oil recovery using LSW compared to HSW versus the average pore-throat radius R35 (microns) during the secondary recovery mode. Quantification of the pore space has improved the understanding of the influence of LSW on oil improvement. The rate of oil recovery by

coreflood experiments were in the decreasing order of Buff Berea > Grey Berea > Bandera > Parker. The oil recovery appeared to increase for sandstone cores with a higher pore throat radius. For HSW, increases in oil recovery by 9% was observed when the average pore-throat radius increased from 1.4 (Parker) to 2.7 (Bandera) microns. On the other hand, the oil recovery increased by 20% when the average pore-throat radius increased from 1.4 (Parker) to 8.5 (Buff Berea) microns. For LSW, increases in oil recovery by 10.2% was observed when the average pore-throat radius increased from 1.4 (Parker) to 2.7 (Bandera) microns, while the oil recovery increased by 32.9% when the average pore-throat radius increased from 1.4 (Parker) to 8.5 (Buff Berea) microns.

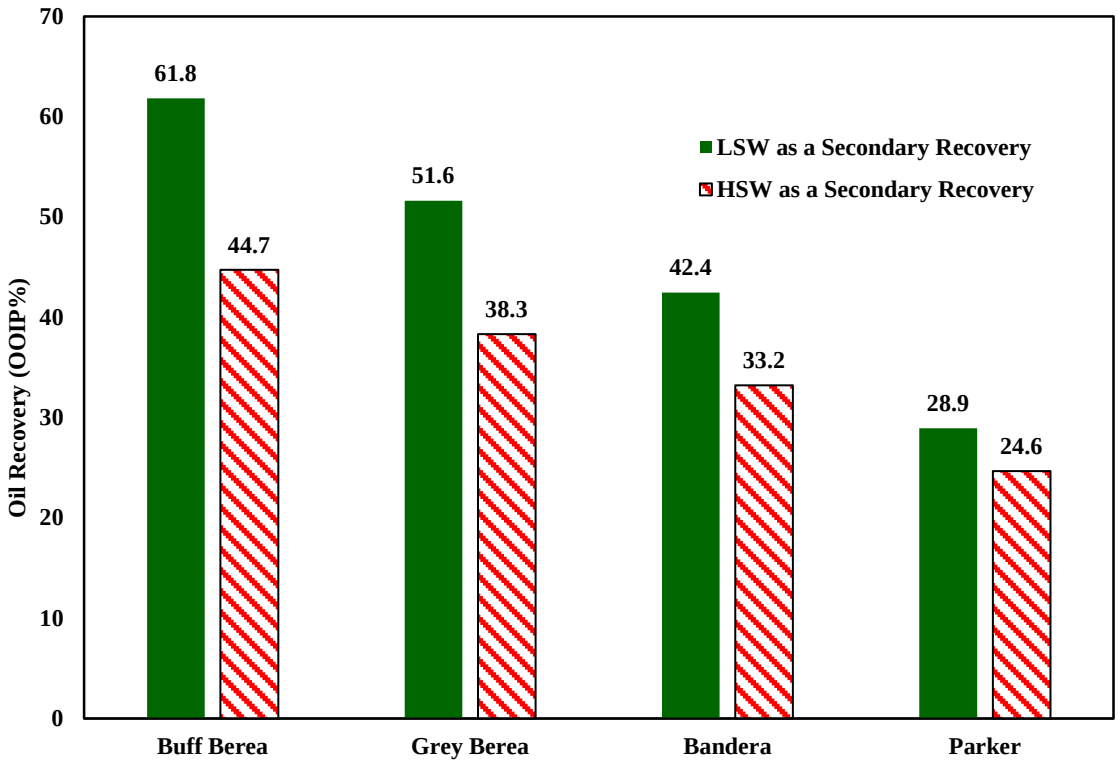


**Figure 29—Comparison of oil recovery (OOIP%) using LSW and HSW during secondary recovery mode for Buff Berea, Grey Berea, Bandera, and Parker sandstone cores.**

From the results obtained, it was obvious that the sandstone rock quality plays a key role in the effectiveness of LSW. The results reflect the variation in oil recoveries obtained by LSW for the different sandstone cores. The incremental oil recovery increased from 4.3 to 17% when the average pore-throat radius (R35) of the core increased from 1.3 to 8.5 microns. A quantitative comparison between the oil recovery shows that the effect of average pore–throat radius is higher in case of LSW compared to HSW on the secondary recovery mode.

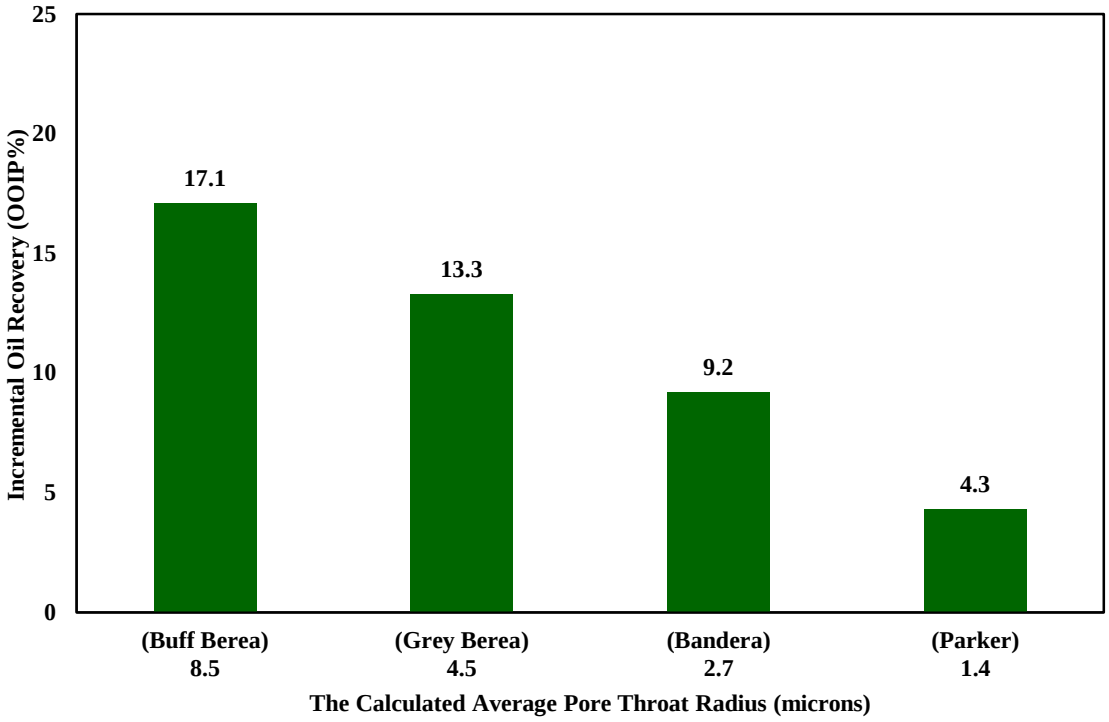


**Figure 30—Incremental oil recovery (OOIP%) versus average pore-throat radius during the secondary recovery mode.**

# CHAPTER V

# IMPACT OF SANDSTONE MINERAL COMPOSITION ON LOW-SALINITY WATERFLOODING PERFORMANCE

Sandstone reservoirs contain numerous minerals, such as quartz, clays, feldspars, mica, and carbonates. Sandstone formations may contain various amounts of quartz, clays, feldspars, zeolites, carbonates (calcite and dolomite), and iron-based minerals (Nasr-El-Din et al. 2007). Clays act as cation exchangers, and the relative affinity of cations towards the clay surface is: $Li^+<Na^+<K^+<Mg^{2+}<Ca^{2+}<H^+$ (Civan 2007). Aksulu et al. (2012) stated that because the clay minerals are permanent negative charges, they act as cation exchangers to be charge-balanced. Researchers have noted that the impacts of clay content, rock permeability, and pore-throat radius are still questionable on the performance of low-salinity waterflooding.

Researchers have noted that the impacts of clay content and sandstone mineral composition are still uncertainties in on the performance of low-salinity waterflooding. In this chapter, the results of coreflood and zeta potential experiments were presented. The main objectives of this work were to investigate the role of clay content on the performance of low-salinity waterflooding and evaluate the effects of mineral type, brine salinity, cation type, and pH on the zeta potential measurements.

### 5.1. Crude Oil/Brine Interaction

The magnitude of zeta potential is related to the thickness of the double layer and surface charge at the mineral/brine or crude oil/brine interfaces. In this study, the crude oil samples were dispersed in the different connate water compositions to evaluate the effect of interaction between crude oil and brine. Several brines of CW (H-1), CW (H-2), CW (H-3), and 5000 ppm NaCl were used. The zeta potential of oil droplets in conventional connate water (H-1) of 174,156 is 2.92 mV. The zeta potential values of crude oil in deionized water is very small and close to zero. This means that at this condition, the crude-oil droplets will be unstable, and the crude oil will tend to attach to the rock. The conventional connate water was considered to be the base case for comparison with other solutions. **Figure 31** shows zeta potential of crude oil as a function of salinity and cation type at a pH of 7. The connate water with monovalent cation (H-2) of 138,281ppm reduced the zeta potential of crude oil to -3.8. For connate water (H-3) of 35,659 without monovalent ions, zeta potential of crude oil was -5.1 mV.

Polar crude oil components can either adsorb directly onto charged surfaces or multivalent cations can bind polar crude oil components to the mineral surfaces by cationic bridging (Fjelde et al. 2014). The retention of polar oil components onto the reservoir rock mineral surface has been found to depend on both the composition of brine and/or crude oil. Fjelde et al. (2013a) reported that the retention of polar crude oil components onto clay minerals and reservoir rock increases with increasing total concentration of divalent cations onto clay surfaces. Fjelde et al. (2013b) reported that

the water wetness was found to increase with decreasing retention of polar oil components.

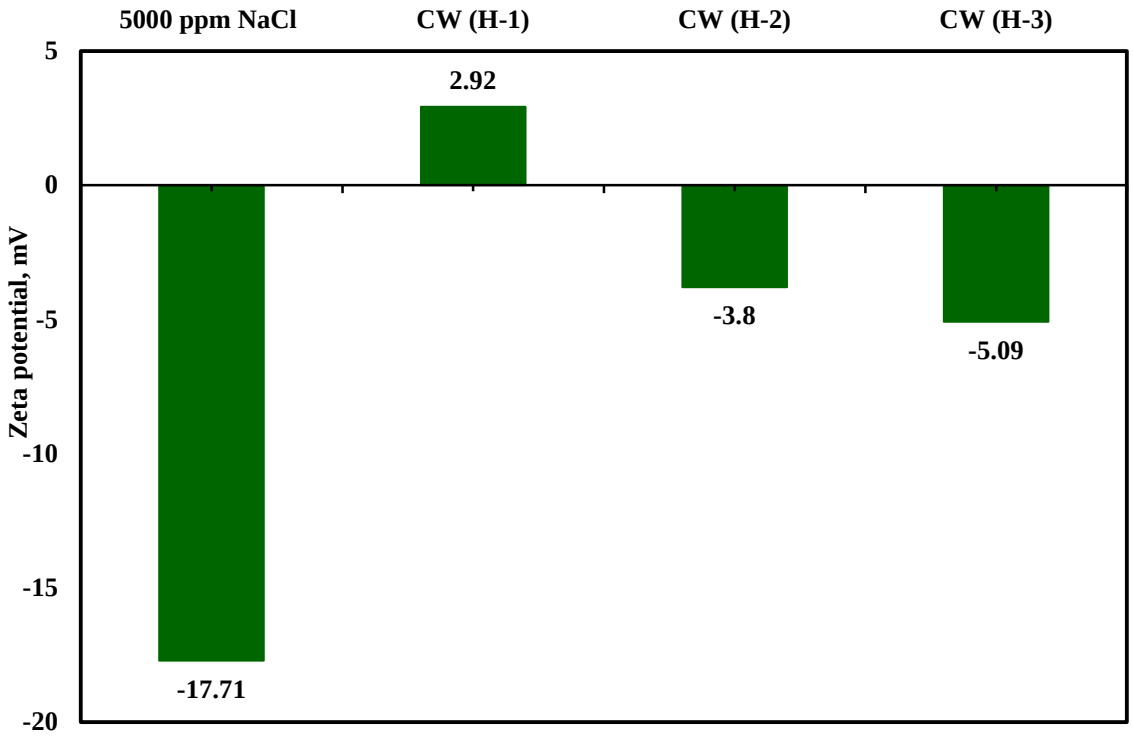


**Figure 31—Comparison of zeta potential results of crude oil droplets at 77°F and 14.7 psi.**

These results demonstrate the influence of brine salinity and cation composition on the electric surface charge at sandstone/brine interfaces. Zeta potential values decrease with the decrease in the salinity of brine. Zeta potential values indicated a less negative charge on the crude-oil droplets in 0.5 wt% NaCl than the other brines. The crude-oil droplet in 0.5 wt% NaCl had a negative charge of -17.71 mV at a pH of 7. Alotaibi and Nasr-El-Din (2011) stated that the surface potential of crude-oil droplets was affected by 10% diluted seawater (−24.94 mV), seawater without $Ca^{2+}$ and $Mg^{2+}$ ions (−17.7 mV),

as well as deionized water (−26.37 mV) because of hydroxide-ion adsorption at the O/W interface.

### 5.2. Effect of Salinity, Cation Type, and pH on Zeta Potential Measurements

In this section, the results of zeta potential measurements are presented and discussed. The main objectives are to determine the suitable injection low-salinity brine for sandstone coreflood experiments and examine the effects of brine salinity and pH on the zeta potential measurements. SW was used as the high-salinity brine. Brines diluted to 20% salinity of seawater (10,936 mg/l) and 5,000 ppm of NaCl, $CaCl_2$, and $MgCl_2$ solutions were used as low-salinity brines. The original pH of rock/brine samples was measured. Then, zeta potential for Buff Berea, Grey Berea, Parker, and Bandera sandstone was conducted at the original pH without adding the pH buffer.

**Table 24** shows zeta potential of sandstone rocks as a function of salinity and cation type at the original pH. The surface charge of sandstone powder in a SW solution has a tendency to become positive. This means that at this condition, the rock surface will be more oil wet. The zeta potential values of rock/SW brine were all very small and close to zero. The zeta potential become negative as the salinity of the brine decreased. Brine diluted to 20% salinity of seawater showed a stronger negatively charged of sandstone more than the seawater brine. The 0.5 wt% NaCl brine solution showed the lowest zeta potential of -30.8 to -33.8 mV.

**Table 24—Zeta Potential of Sandstone Rocks in Seawater, 20% Diluted Seawater, 0.5 wt% NaCl, 0.5 wt% $MgCl_2$, and 0.5 wt% $CaCl_2$ Aqueous Solutions AT T = 25°F and Atmospheric Pressure.**

| Rock Type | Aqueous Phase | pH | Zeta potential, mV |
|---|---|---|---|
| Buff Berea | Seawater | 7.8 | 4.1 |
| | 20% diluted seawater | 6.7 | -14.1 |
| | 0.5 wt% NaCl | 9.4 | -30.8 |
| | 0.5 wt% $MgCl_2$ | 8.7 | -2.1 |
| | 0.5 wt% $CaCl_2$ | 7.8 | -6.0 |
| Grey Berea | Seawater | 7.9 | 2.6 |
| | 20% diluted seawater | 7.7 | -17.7 |
| | 0.5 wt% NaCl | 8.5 | -33.7 |
| | 0.5 wt% $MgCl_2$ | 7.4 | -5.8 |
| | 0.5 wt% $CaCl_2$ | 6.6 | -3.8 |
| Parker | Seawater | 7.9 | -1.9 |
| | 20% diluted seawater | 7.2 | -18.2 |
| | 0.5 wt% NaCl | 7.4 | -33.8 |
| | 0.5 wt% $MgCl_2$ | 7.4 | -7.2 |
| | 0.5 wt% $CaCl_2$ | 7.3 | -8.1 |
| Bandera | Seawater | 8 | 1.1 |
| | 20% diluted seawater | 7.8 | -11.9 |
| | 0.5 wt% NaCl | 7.5 | -30.8 |
| | 0.5 wt% $MgCl_2$ | 6.8 | -4.7 |
| | 0.5 wt% $CaCl_2$ | 6.7 | -3.1 |

The surface charge was slightly negative in brine containing calcium and magnesium ions. The zeta potential values for 0.5 wt% $CaCl_2$ and $MgCl_2$ ranges from -2.1 to -8.1

mV. The divalent cations changed the surface charges to be weak negative compared to the zeta potential values using the monovalent cations. Zhao et al. (2006) investigated the effects of divalent cations on interactions between silica and bitumen by surface force and zeta potential distribution measurements. These researchers found that calcium and magnesium cations increase adhesion force and decrease long-range repulsive forces between silica and bitumen. The zeta potential distribution measurements indicated heterocoagulation between silica and bitumen in the presence of calcium.

As the next step in the present study, the effects of salinity and cation type were evaluated at the same pH of 7. **Figure 32** shows the zeta potential of the sandstone rocks as a function of brine salinity at 25°C and pH 7. Zeta potential values decrease with the decrease in salinity. These results demonstrate the influence of brine salinity and cation composition on the electric surface charge at sandstone/brine interfaces. Lee et al. (2010) identified the presence of thin water layer around sand and clay particles. They observed the variation of water layer thickness of sand system with brine salinity for different cation and anion valence. They noticed that lowering the water salinity developed a thicker water film when compared to the high-salinity water, which allows the opportunity for more oil to be displaced. The increase in thickness of the water layer was smaller for divalent ions, compared to monovalent cations. The surface charge for sandstone rock became more negative using 0.5 wt% NaCl. The zeta potential values at the measured conditions ranges from -21.4 to -30.8 mV. On the other hand, the zeta potential values for 0.5 wt% $CaCl_2$ and $MgCl_2$ ranges from -1.5 to -9 mV. This occurs because the charge number of $Mg^{2+}$ and $Ca^{2+}$ is twice as high as $Na^{+}$. Based on zeta

potential results, the NaCl brine (5,000 ppm) was used as the low-salinity brine in the dynamic core displacement experiments.

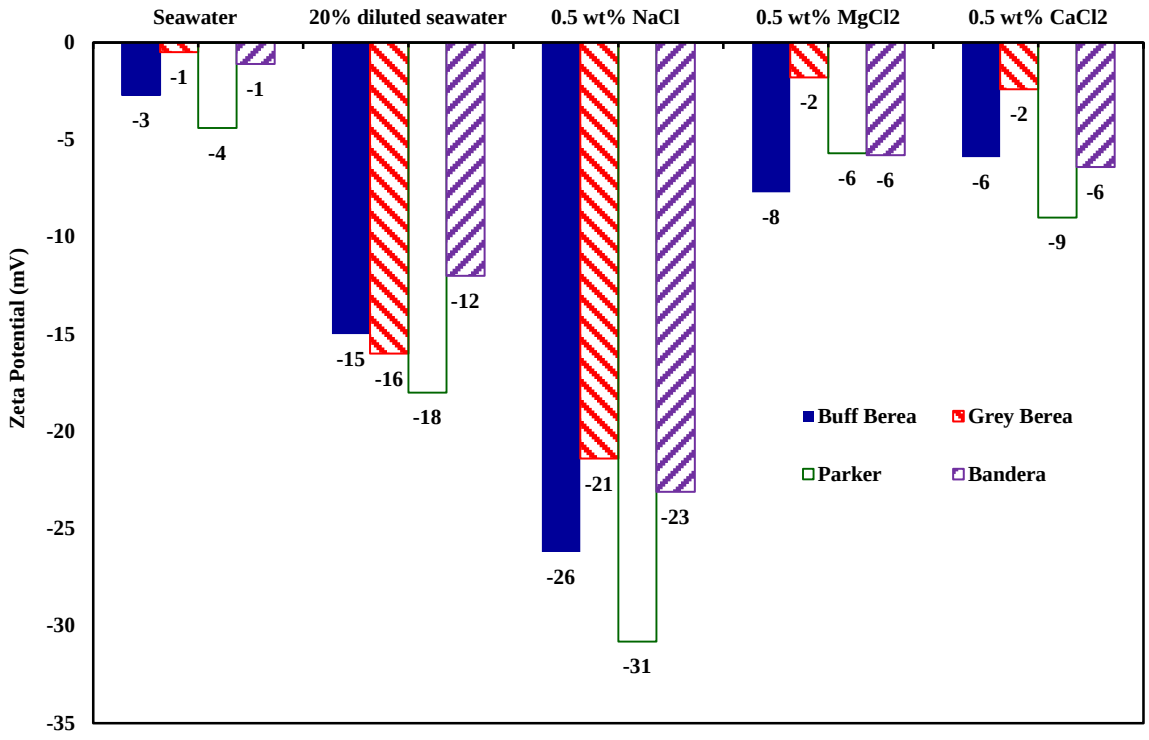


**Figure 32—Effect of brine salinity and composition on zeta potential for Buff Berea, Grey Berea, Bandera, and Parker sandstone rocks at 77°F and pH 7.**

Furthermore, the surface charge of the Buff Berea and Bandera sandstone particles were evaluated over a wide pH range, from 5 to 11. **Figure 33** shows a comparison between the measured values of zeta potential versus pH at 77°F for Buff Berea and Bandera. It can be observed that a small change in solution pH can impose a significant change in the surface charge of the rock. The comparison showed that the magnitude of the negative zeta potential increased as the solution pH increased. The zeta potential of

Bandera was more negative than that of Buff Berea at a pH in the range of 5 to 10. When the electric charges became more negative at rock/brine interfaces, the repulsion forces between rock and oil increased and made the rock more water-wet as a result of the expansion of the electric double-layer and stabilization of the water film surrounding the rock. These observations and trends are in agreement with the literature of sandstone rock (Nasralla and Nasr-El-Din 2014). It is, therefore, verified that this measurement system gives reliable zeta potential values.

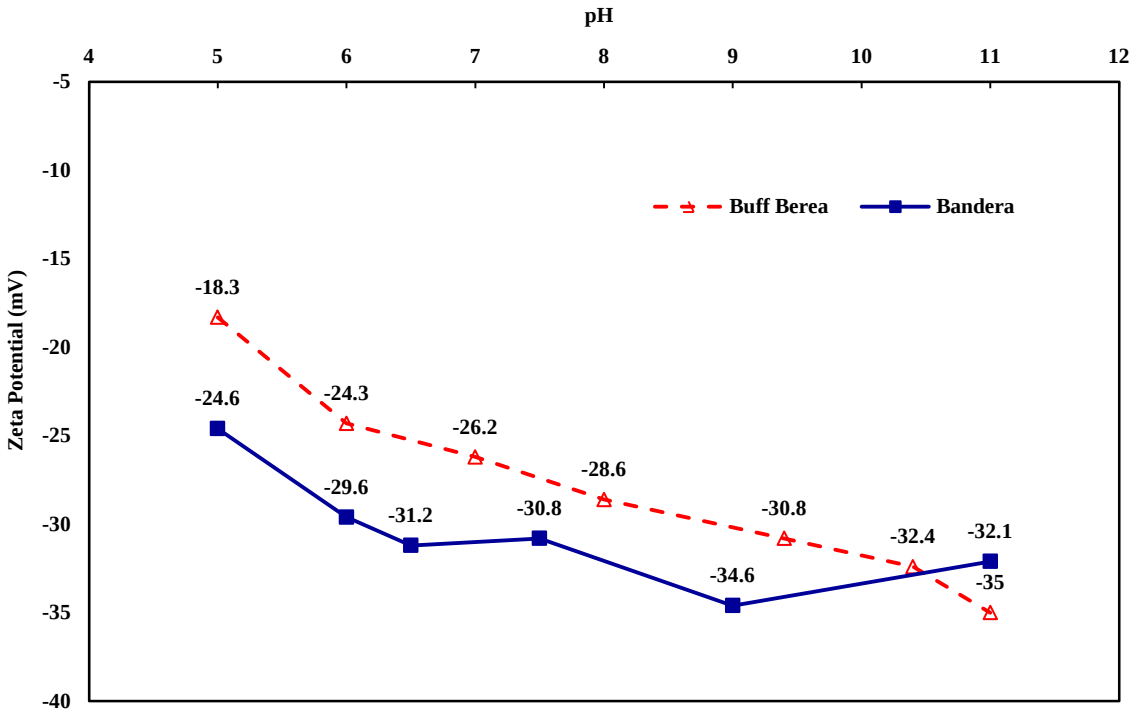


**Figure 33—Impact of pH on zeta potential of Buff Berea and Bandera sandstone rocks in 0.5 wt% NaCl at 77°F.**

### 5.3. Effect of Total Clay Content on the LSW

The amount of sandstone clays have been cited as key in the performance of LSW. The clay content was noticed by Seccombe et al. (2008) to correlate with additional oil recovery during LSW. Seccombe et al. (2010) presented a simple linear correlation between additional oil recovery (%PV) due to LSW and the proportion of clay content in the rock for Endicott field. This correlation indicates that the additional recovery will increase when the clay content increases. Pu et al. (2010) reported up to 9.5% additional recovery by injecting low-salinity coalbed methane water in sandstone cores with very low clay content. RezaeiDoust et al. (2010) stated that the low salinity effect decreased from 6 to 2% when the clay content of the core material decreased from 16 to 8 wt%. Austad et al. (2010) stated that the low-salinity effect would decrease in the order of montmorillonite > illite/mica > kaolinite based on the cation exchange capacity relations.

**Figure 34** shows the incremental oil recovery compared to the total clay content (wt %) based on the bulk measurements from XRD during the secondary recovery mode. The rate of oil recovery by coreflood experiment decreased in the order of Buff Berea > Grey Berea > Bandera > Parker. Consequently, the incremental oil recovery could vary over a wide range from 4.3 to 17.1% of OOIP. The results revealed no direct relationship between the incremental oil recoveries and total clay content of the cores. This total clay content does not relate to actual surface coverage of the clays. This conclusion agrees with the reported results by Wickramathilaka et al. (2011) that there is no connection between clay content and oil recovery. Emadi and Sohrabi (2013) explained that the formation and coalescence of water micro-dispersions is a result of the salinity change in

the aqueous phase based on the micromodel results and fluid characterization tests. Suijkerbuijk et al. (2013) stated that correlating the low-salinity waterflooding effect to bulk clay content (using XRD) does not result in a robust approach. This occurs because the bulk contents of clay as determined by XRD do not correlate with these surface coverages. Law et al. (2015) examined the effect of clay content and type on the incremental oil recovery from the United Kingdom continental shelf oil reservoir. The authors modeled the effect of clay content on the reservoir response by altering the cation exchange capacity relative to the clay mineral fraction present in the reservoir. The clay surface minerals are the dominant reactive surface areas seen by oil because of their smaller grain size, sheet morphology, and much higher surface areas. Kaolinites have surface areas of 14-23 $m^2/g$; illite, 76-91 $m^2/g$; and montmorillonite, 700–749 $m^2/g$, compared with quartz and feldspars) with 0.1 $m^2/g$ (Diamond and Kinter 1956). Thus, effect of each clay content will depend on the amount and the surface area of each type of clay.

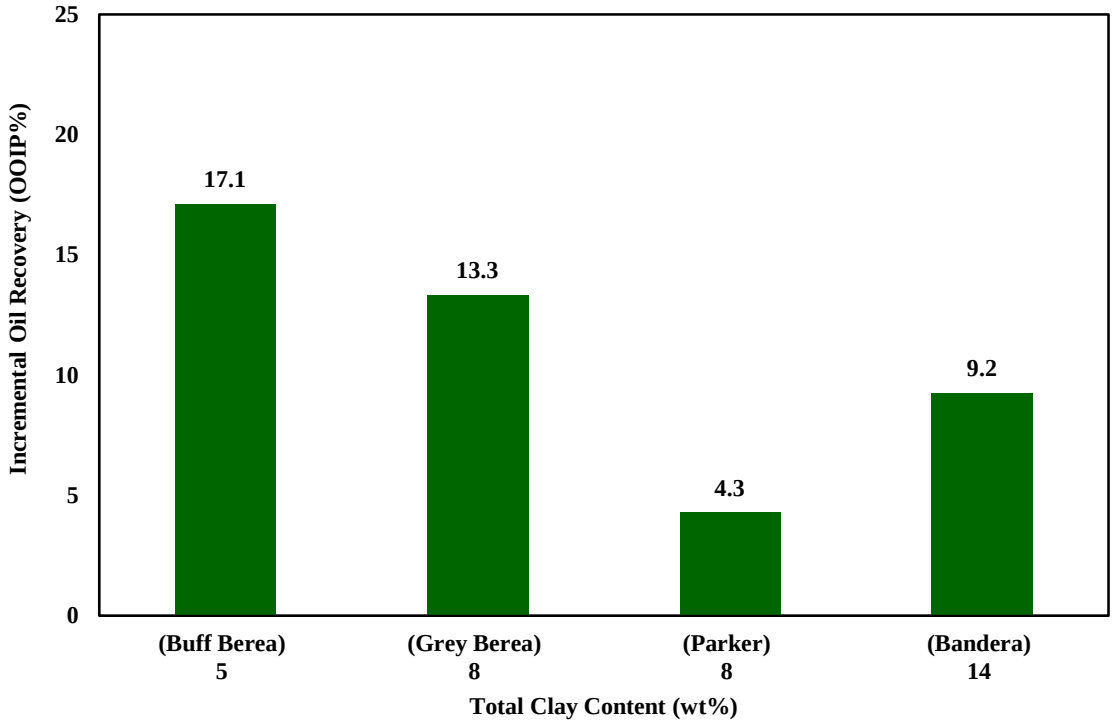


**Figure 34—Incremental oil recovery (OOIP%) versus total clay content during the secondary recovery mode.**

### 5.4. Effect of Specific Minerals on LSW

The following discussion takes up each mineral type to examine its impact on LSW. Nasralla and Nasr-El-Din (2014) demonstrated that the electrical-double layer expansion, which is a function of brine salinity and pH, could be the primary mechanism of IOR by LSW during the secondary oil recovery mode. A question remains on the effect of each mineral on the low-salinity waterflooding performance. In this work, however the effect of each sandstone mineral on the electrical double-layer expansion was investigated. The zeta potential was measured to evaluate the effect of electrical surface charge and double-layer expansion for each sandstone minerals at a pH of 7 and 77°F for SW and 5,000 ppm NaCl. The pH of 7 was selected because it was noticed

during coreflood experiments that the pH values were in the range of 6.3 to 8. Quartz, carbonates (calcite and dolomite), clays (kaolinite, chlorite, and smectite), micas (muscovite and illite), and feldspars (microcline) were tested in this work. **Table 25** presents the zeta potential of common sandstone minerals.

### 5.4.1. Quartz

The measured zeta potentials in SW and 5,000 ppm NaCl brine was -2.5 and -20.5 mV, respectively. The quartz ($SiO_2$) has a low cation exchange capacity (CEC) of 0.6 cmol $kg^{-1}$ in the silt fraction (2 to 63 μm) and 5.3 cmol $kg^{-1}$ in the clay fraction (lower than 2 μm). Kaya and Yukselen (2005) reported that the zeta potential for quartz powder ranged from -30.2 mV at a pH of 3 to -65.4 mV at a pH of 11. Júnior and Baldo (2014) reported that for pH values above the isoelectric point, the zeta potential values of crystalline forms of silica (α-quartz and α-cristobalite) were negative. However, it was found that the crystalline samples of silica had a positive zeta potential for pH values below the isoelectric point. The isoelectric point pH was around 2.5. As quartz content increases, there is a decrease in CEC and surface area (Wilding et al. 1977).

**Table 25—Zeta Potential of Sandstone Minerals in Seawater and 0.5 wt% NaCl Brines AT pH = 7, T = 77°F, and Atmospheric Pressure.**

| Mineral Type | Zeta potential, mV | |
|---|---|---|
| | Seawater | 0.5 wt% NaCl |
| Quartz | -2.5 | -20.5 |
| Montmorillonite | -8.7 | -29.4 |
| Kaolinite | -11 | -26.5 |
| Chlorite | 6.5 | -21.5 |
| Albite | -5.5 | -31.5 |
| Microcline | 9.8 | -28.5 |
| Illite | -4.3 | -18.5 |
| Muscovite | 1.8 | -33.8 |
| Dolomite | 6.5 | -4.5 |
| Calcite | 6.1 | 1 |
| Ilmenite | -1.4 | -18.7 |

### 5.4.2. Kaolinite

Based on previous work, the presence of kaolinite was believed to be important for the success of LSW. The recovery benefit appeared to increase with clay content, especially with kaolinite content (Seccombe et al. 2008). **Figure 35** shows the incremental oil recovery using LSW compared to HSW in conjunction with the kaolinite content (wt%) during the secondary recovery mode. Hence, no direct relationship between the incremental oil recoveries and the kaolinite content of the cores. Kaolinite is

a clay mineral with the following chemical formula: $Al_2Si_2O_5$ (OH) $_4$. The surface area for kaolinite depends upon the particle size. Values as low as 5 and as high as 39 $m^2.g^{-1}$ have been reported (Dixon 1989). The zeta potential measurements for kaolinite was conducted at the original pH value using SW and 0.5 wt% NaCl. The results in 5,000 ppm NaCl brine showed a negative surface charge (-24.6 mV) at a pH of 4.3, while the zeta potential become -26.5 mV at a pH of 7. The results of zeta potential of kaolinite at a pH of 4.33 and 7 are close to each other. The original pH for kaolinite particles in SW was 7.2. Kaolinite particles in SW displayed a negative zeta potential of -11 mV.

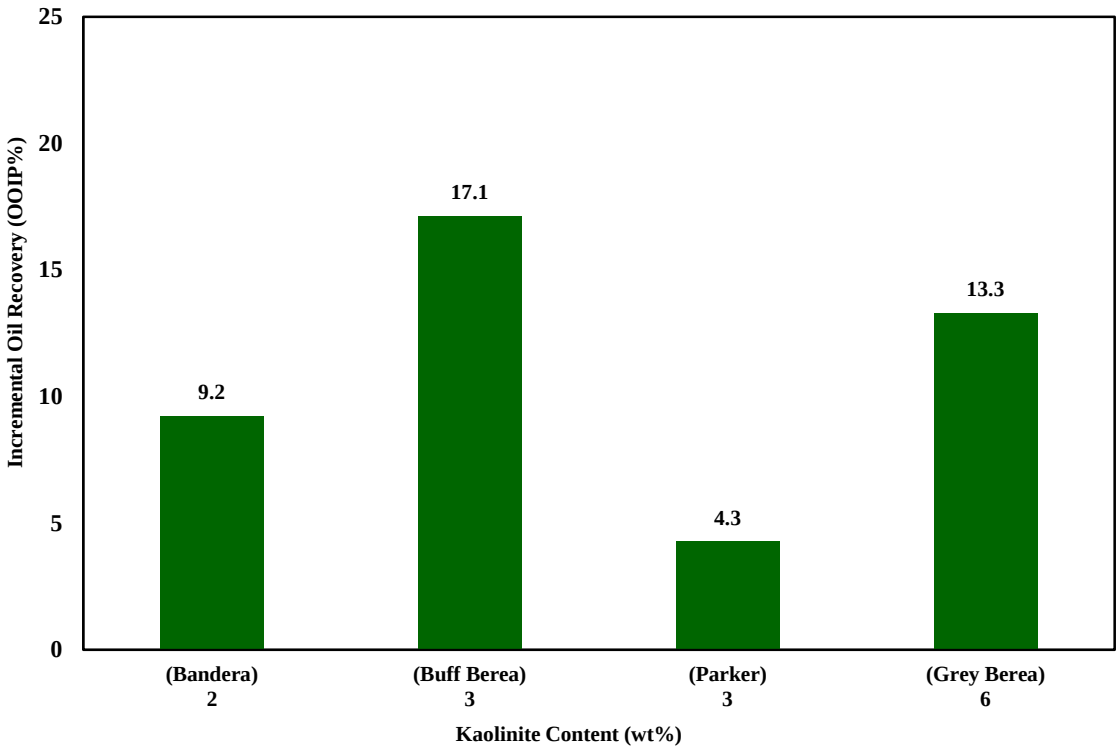


**Figure 35—Incremental oil recovery (OOIP%) versus kaolinite content during secondary recovery mode.**

### 5.4.3. Smectite

Buff Berea sandstone contains 1 wt% of smectite. The smectite group consists of expansive minerals with a 2:1 structure. Montmorillonite is the most common smectite mineral. Water and exchangeable cations occupy the region between layers. The range of measured CEC is 47 to 162 $cmol.kg^{-1}$ (Borchardt 1989). Montmorillonite gives a more negative value for zeta potential than kaolinite particles of -29.4 mV in 5,000 ppm NaCl and -8.7 mV in SW.

### 5.4.4. Feldspar

It was found in the used sandstone cores with different concentration in the range of 3 to 12 wt%. The zeta potentials of microcline ($KAlSi_3O_8$) and albite ($(Na,K)AlSi_3O_8$) have been tested at a pH of 7. The values of zeta potential of microcline and albite with 0.5 wt% NaCl are -28.5 and -31.5 mV, respectively. These values reveal that the aqueous suspensions are quite stable. **Figure 36** shows the incremental oil recovery compared to the feldspar content (wt%) during the secondary recovery mode. It indicates that there is no direct relationship between the incremental oil recoveries and the feldspar content of the cores. Zeta potential data demonstrates that the presence of feldspars could be useful to increase the incremental oil recovery during LSW.

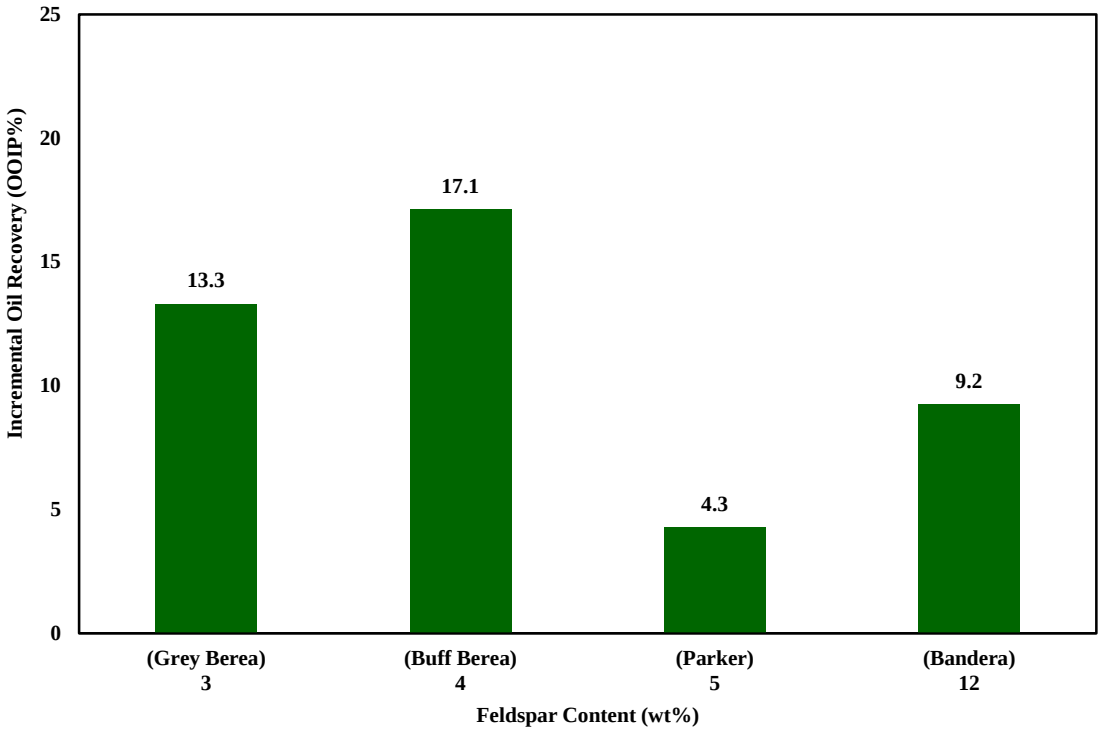


**Figure 36—Incremental oil recovery (OOIP%) versus feldspar content during secondary recovery mode.**

### 5.4.5. Chlorite

A small amount of chlorite (1%) was noticed in Bandera sandstone rock. Zeta potential for chlorite $\{(Mg, Fe)_3(Si,Al)_4O_{10}(OH)_2(Mg,Fe)_3(OH)_6\}$ was conducted at a pH of 7. The specific surface area reported between 26 to 45 $m^2\ g^{-1}$, while CEC values of 1, 1.5, 1.8, and 2.5 $cmol.kg^{-1}$ have been reported (Kohut and Warren 2002). The zeta potential of chlorite in SW was 6.5 mV, while the surface charge became more negative (-21.5 mV) using 0.5 wt% NaCl. For the 0.5 wt% NaCl brine, the zeta potential values indicated a less negative charge on the chlorite particles than that of the other clay minerals. It seems that chlorite has a smaller contribution to electrical-double layer

expansion than kaolinite and feldspars. This might be because chlorite is a nonexpanding clay with a low specific surface area and CEC. Also, chlorite contains some iron.

### 5.4.6. Ilmenite

It was used to investigate the effect of iron on the zeta potential values. The surface charge and zeta potential of ilmenite particle was evaluated using SW and 0.5 wt% NaCl. Ilmenite has composition of 49% $TiO_2$ and 51% FeO. The zeta potential for ilmenite particles were -1.4 and -18.7 mV for seawater and 0.5 wt% NaCl, respectively. These results confirm that the presence of iron decreases the effect of low-salinity brine on the double layer expansion.

### 5.4.7. Mica

Bandera, Parker, and Grey Berea sandstones contain 10, 4, and 2 wt% of illite, respectively. Mica in the clay fraction is usually identified as illite $\{K_{0.75}\ (Al_{1.75}\ [MgFe]_{0.25})\ (Al_{0.5}Si_{3.5})\ O_{10}\ (OH)_2\}$. The other type of mica that was found in Buff Berea rock is muscovite (1 wt%). Muscovite $\{KAl_2(AlSi_3)\ O_{10}\ (OH)_2\}$ is the most abundant dioctahedral primary mica. The average zeta potential for the used micas minerals was found to be negative, except for the case of muscovite in SW, where the zeta potential was positive (1.8 mV). For the 0.5 wt% NaCl brine, the resulting zeta potentials for the illite and muscovite were -18.5 and -33.8 mV, respectively. The zeta potential values indicated a stronger negative charge on mica minerals (muscovite) compared to quartz,

clays, and feldspars. The low-salinity effect may increase in the presence of feldspars, kaolinite, and mica based on the zeta potential relationship. The diffused layer near a rock particle surface will expand in thickness. These values agree with the reported results by Alotaibi et al. (2011) for kaolinite, illite, chlorite, and, montmorillonite. **Figure 37** shows the incremental oil recovery compared to the illite content (wt%) during the secondary recovery mode. The comparison revealed that the incremental oil recovery decreased from 13.3 to 4.3 OOIP% when the illite content increased from 2 to 4%. Then the incremental oil increased to 9.2 OOIP% when the elite content increased to 10%.

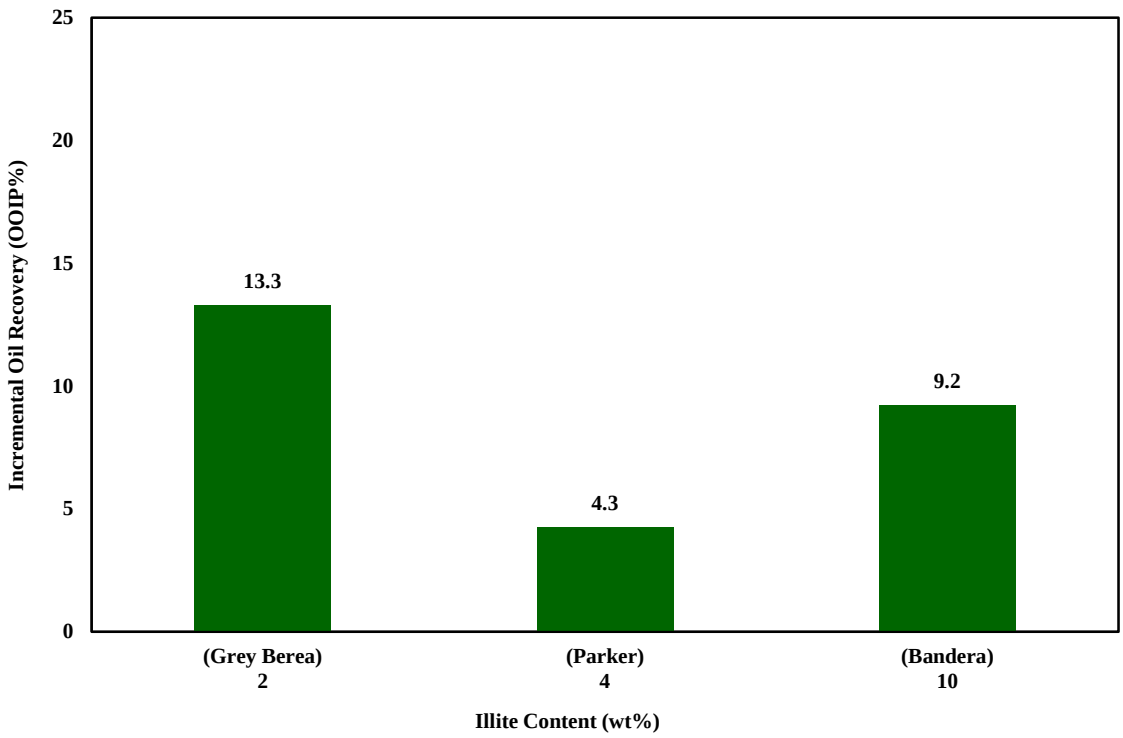


**Figure 37—Incremental oil recovery (OOIP%) versus illite content during secondary recovery mode.**

### 5.4.8. Carbonates

For the carbonate minerals, Grey Berea and Bandera sandstone cores contain about 2 wt% calcite ($CaCO_3$) and 15 wt% dolomite ($CaMg(CO_3)_2$), respectively. **Figure 38** shows the incremental oil recovery compared to the carbonate content (wt%) during the secondary recovery mode. The LSW performance in the Bandera was noted that, which had a higher carbonate mineral that was poorer than the performance of Grey Berea cores. The resulting zeta potentials for the dolomite and calcite minerals showed a different trend from the other sandstone minerals for low-salinity brine. For the 0.5 wt% NaCl brine, the zeta potential values indicated a weaker negative charge on carbonate minerals compared to that of other sandstone minerals. The 0.5 wt% NaCl created positive charge of one mV for the calcite mineral and -4.5 mV for the dolomite particles at a pH of 7. The effect of double layer expansion would decrease in the presence of dolomite and calcite minerals which affect on the performance of low-salinity waterflooding.

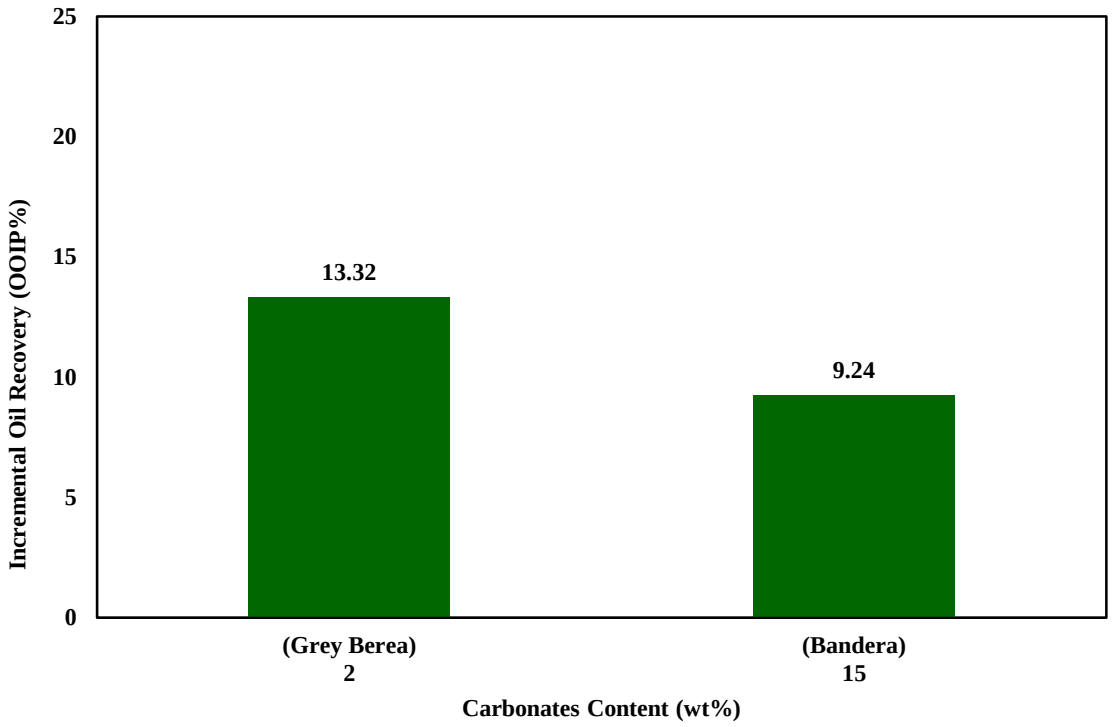


**Figure 38—Incremental oil recovery (OOIP%) versus carbonates content during secondary recovery mode.**

# CHAPTER VI

# EFFECT OF CONNATE WATER COMPOSITION ON LOW-SALINITY WATERFLOODING IN SANDSTONE RESERVOIRS

Most previous the low-salinity waterflooding studies focused on the injection brine salinity and composition. The question remains: how does the salinity and composition of the reservoir connate water affect the low-salinity waterflooding performance? Therefore, in this work, different connate water compositions were used to investigate the role of reservoir connate water on the performance of low-salinity waterflooding for sandstone reservoirs.

Reservoir connate water salinity and composition vary from one reservoir to another. $Na^+$, $Ca^{2+}$, and $Mg^{2+}$ are the main cations. The salinity of the brine is represented by the Total Dissolved Solids (TDS). TDS is the total mass content of dissolved ions and molecules or suspended micro granules in a liquid medium (Sheng 2011). The ions were divided into two groups: monovalent (represented by the sodium ion, $Na^+$) and divalent (represented by calcium $Ca^{2+}$ and magnesium $Mg^{2+}$ ions).

The main objectives of this work are to: (1) examine the effect of the salinity of the reservoir connate water, (2) investigate the role of the composition ($Na^+$, $Ca^{2+}$, and $Mg^{2+}$) of the reservoir connate water, and (3) study the effect of temperature on the performance of low-salinity waterflooding. This paper combines the results of spontaneous imbibition and coreflood tests to understand the role of connate water

composition on the performance of LSW recovery for sandstone rocks. The results of eleven spontaneous imbibition experiments and six coreflood experiments were presented. This study includes two types of sandstone cores (Bandera and Buff Berea) with different permeability's, rock qualities, and mineral compositions. Connate water compositions with wide ranges of salinity were used. The $Na^{+}$, $Ca^{2+}$, and $Mg^{2+}$ ions were excluded from the connate water to determine their individual impact on the oil recovery. X-ray computed tomography (CT) imaging was used to investigate the effect of the initial water saturation distribution across the core on oil recovery.

This work describes the experimental studies of the spontaneous imbibition of oil by low-salinity and high-salinity brines using 20 in. length outcrop samples. The volume of produced oil was monitored and recorded against time on a daily basis. Imbibition brine samples were analyzed at the end of each experiment. In addition, coreflood experiments were performed to validate the spontaneous imbibition results and examine the effect of the connate water salinity variation. The coreflood experiments were conducted using 6 in. length outcrop Buff Berea sandstone cores at 160°F and 500 psi. The oil recovery, pressure drop across the core, pore volume injected, and core effluent samples were analyzed for each coreflood experiment.

The results demonstrate that the spontaneous imbibition oil produced oil ranging from 38 to 69% OOIP for high permeability Buff Berea cores (164-207.7 md), while the produced oil of the low permeability Bandera cores (31.1-39.2 md) ranged from 20 to 51.5% OOIP at 77°F and 14.7 psia. The produced oil recovery decreased when the average pore-throat radius (rock quality) decreased. As the temperature increased from

77 to 150°F, additional produced oil up to 15% of OOIP was observed by spontaneous imbibition for Buff Berea cores. The reservoir connate water composition had a dominant influence on the oil recovery rate. The changes in the ion composition of reservoir connate water ($Ca^{2+}$, $Mg^{2+}$, and $Na^{+}$) showed a measurable change in the oil production trend. Reservoir cores saturated with connate water containing divalent cations of ($Ca^{+2}$ and $Mg^{+2}$) showed higher oil recovery than for cores saturated with monovalent cations ($Na^{+}$). In all cases, a measurable ion exchange was observed, while there was no significant change in the pH of the imbibition brine during the experiment. The ion exchange effect was more pronounced than the pH effect in the low-salinity waterflooding performance for Buff Berea and Bandera sandstone. The total oil recovery increased from 51.9 to 58.9% OOIP when the divalent cation ($Ca^{+2}$ and $Mg^{+2}$) concentration of the reservoir connate water increased from 709 to 12,210 ppm for injected brine salinity of 500 and 5,000 ppm, respectively. On the other hand, increasing the monovalent cation ($Na^{+}$) concentration from 610 to 54,400 ppm resulted in a slight increase in oil recovery (2.3% OOIP).

### 6.1. Spontaneous Imbibition Studies: Effect of Connate Water Composition

Three SI experiments were initially conducted using Buff Berea sandstone Cores O-1, O-2, and O-3. For a Buff Berea sandstone sample, quartz was the dominant mineral. Also, kaolinite, muscovite, feldspars (microcline), and mica were found. Core O-1 was saturated with connate water containing only monovalent cations ($Na^{+}$). The salinity of the connate water for this core before the start of the test was approximately 54,400 ppm.

Core O-2 was saturated with high-salinity connate water (174,156 ppm). Core O-3 was saturated with reservoir connate water containing only divalent cations ($Ca^{2+}$ and $Mg^{2+}$). The concentration of $Ca^{2+}$ and $Mg^{2+}$ was 10,600 and 1,610 ppm, respectively. NaCl brine (5,000 ppm) was used as the imbibition brine. The pH of this imbibition fluid at the beginning of the experiments was 6.86. These three experiments were conducted under the same temperature of 77°F and pressure of 14.7 psi. The volume of the produced oil was monitored and recorded against time on a daily basis. **Figure 39** provides comparison of the effect of reservoir connate water composition on oil production performance. The rates of oil production by SI were in the order of O-3 > O-2 > O-1. The oil production by spontaneous water imbibition for these three cores ranged from 39 to 68.9% of OOIP with an average of 51.7% OOIP. Core O-1, which was saturated with FW that contained only monovalent cations ($Na^{+}$), had the lowest imbibition production of 38.9% of OOIP after 50 days.

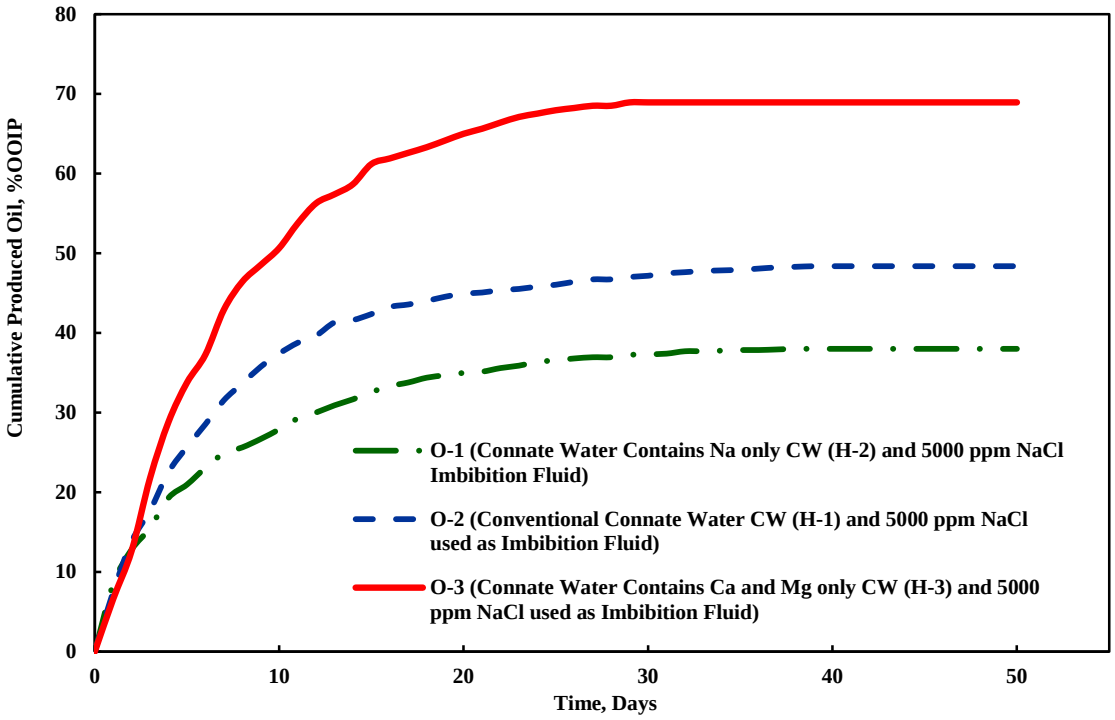


**Figure 39—Comparison of cumulative produced oil (%OOIP) by spontaneous imbibition as a function of time (days) for three different Buff Berea sandstone Cores (O-1, O-2, and O-3) at 77°F and 14.7 psi.**

As illustrated in figure 39, connate water containing only divalent cations increased the imbibition rate and the oil production by SI. The oil production from Core O-3 reached approximately 69% of OOIP, while only 48% of the oil was recovered from Core O-2 when the tests were abandoned after 50 days. Multivalent metal cations in the brine, such as $Ca^{2+}$ and $Mg^{2+}$, are believed to act like bridges between the negatively charged oil and clay minerals (Anderson 1986). It is also shown in the data presented by Lager et al. (2006) that when multivalent cations were present in the connate brine, flooding with LSW led to higher oil production. Thus, changing the composition of the connate water had a significant effect on the LSW performance. The imbibition rate is

influenced by the reservoir connate water composition of the core. The peak production rate for Core O-3 appeared earlier, after 28 days of imbibition, compared to Cores O-2 and O-1, which reached maximum production after 37 and 38 days, respectively. This recovery range agrees with similar values determined previously (Yildiz and Morrow 1996). They stated that waterflood recoveries of Moutray crude oil, which could be ascribed to differences in initial and injected brine composition and neutral brine saturation, ranged from 59-72% of original oil-in-place. Lee et al. (2010) concluded that the exchange of divalent ions for monovalent ions at low concentration can significantly enhance the thickness of the water layer of the mineral surface. They reported that the sodium chloride water layer increased from 10.8 to 11.8 Å for a reduction in salinity from 0.1 Molar to 0.001 Molar (6000 ppm to 60 ppm). For $MgCl_2$, the water layer thickness increased from 8.14 to 14.8 Å. Nasralla et al. (2011) demonstrated the occurrence of cation exchange between LSW, connate water, and the rock surface. They showed that LSW leaches cations from the rock surface, which results in a change of the surface charges of the rock. Skrettingland et al. (2011) suggested that the initial wetting condition is crucial to the performance of a low-salinity drive. They demonstrated that when multivalent cations were present in the connate brine, flooding with LSW led to higher oil recovery. Polar crude oil components can either adsorb directly onto charged surfaces or multivalent cations can bind polar crude oil components to the mineral surfaces by cationic bridging (Fjelde et al. 2014). The retention of polar components onto rock surfaces has been found to depend on both the composition of brine and crude oil.

In addition, two SI experiments were performed at a temperature of 150°F using Buff Berea sandstone Cores O-4 and O-5. The objective of these two experiments was to study the influence of temperature on the oil production performance using SI tests. Cores O-4 and O-5 were saturated with high-salinity connate water (174,156 ppm) similar to Core O-2. One of the cores was immersed in low-salinity imbibition brine (5,000 ppm NaCl), while the other core was immersed in brine with the same composition of the connate water (H-1) to simulate high-salinity waterflooding. Then, the two cells were placed in an oven set at 150°F. The pH values of the imbibition fluid for Cores O-4 and O-5 at the beginning of the experiments were 6.86 and 6.34, respectively.

**Figure 40** presents the results for high-temperature experiments. The produced oil, by using (5,000 ppm NaCl) as imbibition fluid, could reach 63.8% of OOIP in 40 days. It is even higher than the produced oil of 52.2% of OOIP using high-salinity imbibition fluid. Lee et al. (2010) suggested that during high-salinity water flooding, the polar and charged components of the oil are retained on the surface of the clay resulting in higher post-waterflood residual oil saturation. Reducing the water salinity developed a thicker water film compared to that of high-salinity water, which demonstrated the expansion of the double layer by LSW, which provided a greater opportunity for the oil to be swept. The comparison between Cores O-2 and O-4 confirms that the imbibition rate is influenced by the temperature condition. An additional oil production up to 15.8% of OOIP was clearly observed when the temperature increased from 77 to 150°F. The breakthrough time for Cores O-4 and O-5 decreased with an increased temperature. The

initial fast production during the first days was due to thermal fluid expansion. An increase in temperature reduced the oil to water viscosity ratio, so as to yield a less resistant force to water imbibition, and also enhanced the water wetness of solid surfaces. Hoffman and Kovscek (2004) stated that the wettability of the reservoir rock was a key factor in thermal displacement efficiency. Tang and Morrow (1997) demonstrated that an increase in temperature always results in increased water-wetness and increased oil recovery.

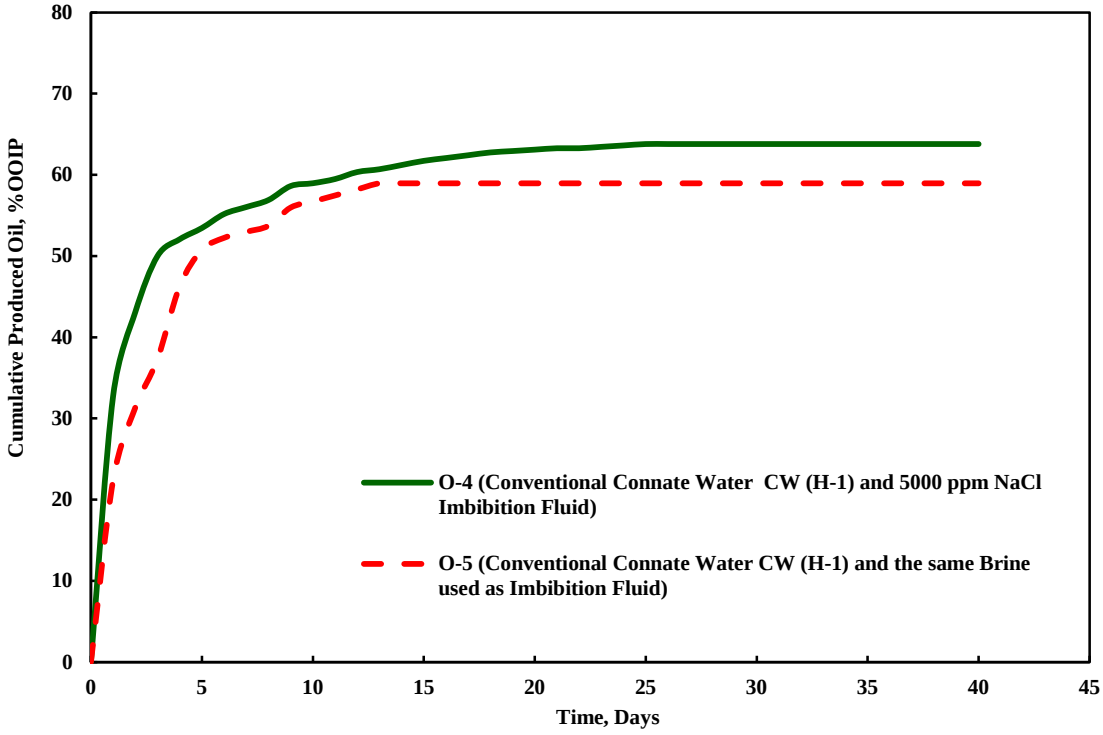


**Figure 40—Comparison of cumulative produced oil (%OOIP) by spontaneous imbibition as a function of time (days) for two Buff Berea sandstone Cores (O-4 and O-5) at 150 °F and 14.7 psi.**

Results of this study indicate that an increase in exposure time in the low-salinity brine makes a crude oil/brine/rock system more water-wet. Furthermore, the extent of

wettability modification toward more water-wet depends on the types of cations present in the formation water. Keeping the core samples in the imbibition brine allows for more interaction between the connate water, minerals, crude oil, and imbibition fluid. Shehata and Nasr-El-Din (2014) tested the low-salinity waterflooding performance in Buff Berea sandstone using a coreflood test. Continuous injection of 5000 ppm NaCl resulted in a final oil recovery of 60.9% OOIP. In the present work, the oil production from Core O-4 using spontaneous imbibition was reached approximately 63.8% of OOIP.

For these five SI experiments, the pH of the imbibition fluids was measured before and after the experiments. The pH after the SI varied between 6.3 and 7.1. In some cases, the pH was unchanged. A slight increase in pH was observed for Cores O-4 and O-2. The mineral composition analysis of Buff Berea sandstone showed that there were no carbonate or gypsum minerals in this rock. This confirms that there was no pH increase due to the carbonate dissolution. The oil production trend was not related to the increase in pH for the Buff Berea sandstone core.

Then, samples were collected from the imbibition fluid at the end of the tests. The samples were analyzed using ICP-OES to determine the concentrations of sodium, calcium, and magnesium cations. The comparison between the imbibition brine samples provided insight into whether any interactions or cation exchange could take place. **Figure 41** shows the concentration of $Ca^{2+}$, $Mg^{2+}$, and $Na^{+}$ ions in the imbibition fluid for experiments O-1 to O-4. The chemical analysis results show that the $Na^{+}$ ion concentrations were higher than that in the original imbibition brine for all the experiments. Also, $Ca^{2+}$ and $Mg^{2+}$, ions were detected in the imbibition fluid at the end

of the tests. Similar observations were noticed in experiment O-1 despite the absence of $Ca^{2+}$ and $Mg^{2+}$ cations in the initial connate water. The Mg cations were lower than the Ca and Na cations. The ratio of Ca to Mg cation composition in the imbibition fluid sample at the end of tests was in the range of 10 to 18. XRF analysis showed that Buff Berea contained 0.6, 0.7, and 0.7 as a weight percent of $Na^{+}$, $Ca^{2+}$, and $Mg^{2+}$ cations, respectively.

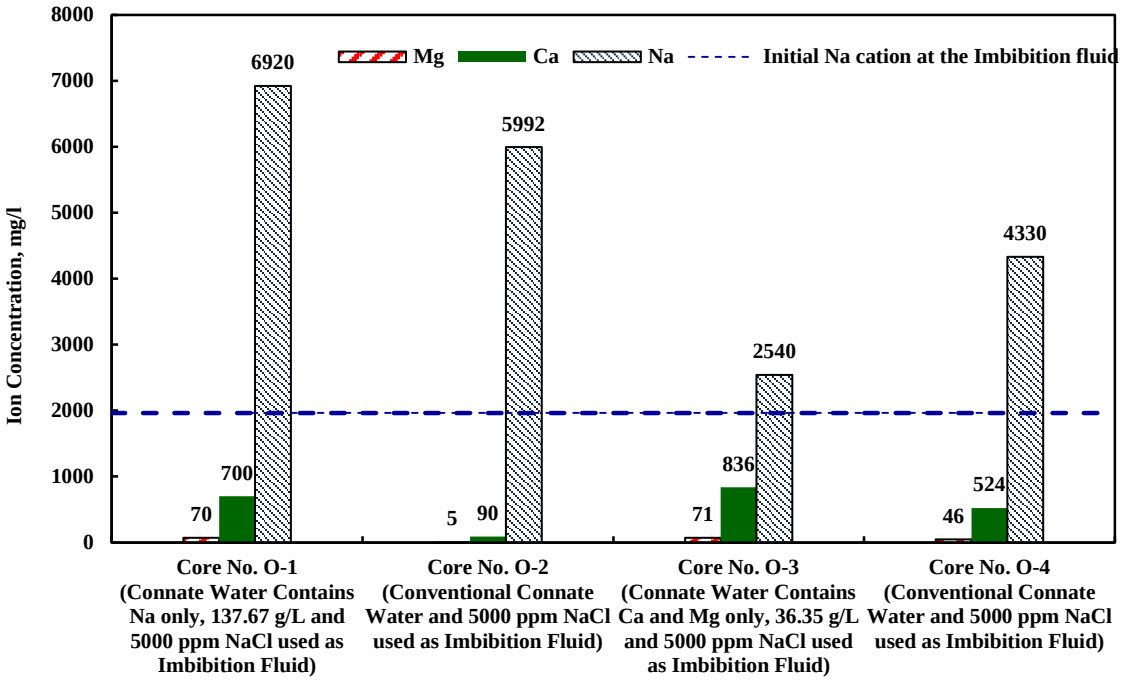


**Figure 41—Concentrations of $Ca^{2+}$, $Mg^{2+}$, and $Na^{+}$ ions in the imbibition fluid for Buff Berea sandstone cores at the end of the experiment.**

Initial oil saturation plays a significant role in waterflood performance. Jadhunandan and Morrow (1995) described that wettability depends on the initial water saturation,

aging temperature, crude oil, and brine composition. Two SI experiments were performed using Buff Berea sandstone Cores R-20 and R-40. The objective of these two experiments was to study the effect of initial water saturation distribution across the core on the oil production using X-ray Computed tomography (CT) imaging. The Toshiba TSX-101A/RG CT-Scan system with a resolution of 0.3 mm was used to collect cross-sectional images along the core. The data obtained from the CT scanner was transferred to a PC for image processing (**Figure 42**). The cross-sectional images can then be used for porosity and saturation determination, or reconstructed for flow visualization. The following equations were used to determine the saturation (Bataweel et al. 2011; Alshehri and Kovscek 2015):

$$S_w + S_o = 1 \quad \text{..... (3)}$$

$$S_w = \frac{CT_x - CT_{or}}{CT_{wr} - CT_{or}} \quad \text{.....(4)}$$

$$CT_{or} = CT_{dry} + (CT_{wr} - CT_{dry}) * \frac{CT_o - CT_A}{CT_w - CT_A} \quad \text{..... (5)}$$

where: $S_w$ is water saturation (%), $S_o$ is oil saturation (%), $CT_x$ is CT-number for image in question, $CT_{or}$ is CT-number of 100% oil saturated core, $CT_{wr}$ is CT-number of 100% brine saturated core, $CT_A$ is CT-number of air, $CT_o$ is CT-number of crude oil, and $CT_w$ is CT-number of brine.

**Figure 42— Image of the X-ray computed tomography (CT).**

A CT scan was performed for the two cores after drying the cores. Then, Core R-20 was saturated with connate water containing only monovalent cations ($Na^+$). The salinity of the connate water for this core before the start of test was approximately 50,000 ppm. On the other hand, Core R-40 was saturated with connate water containing only divalent cations ($Ca^{2+}$ and $Mg^{2+}$). The concentration of $Ca^{2+}$ and $Mg^{2+}$ was 25,000 and 25,000 ppm, respectively. Then the two saturated cores were scanned. The brine-saturated cores were flooded with crude oil until no more water was produced from the cores to establish the initial water saturation. The CT scan was performed for the two cores at initial water saturation. The two cores were immersed in low-salinity imbibition brine (5,000 ppm NaCl). The pH of this imbibition fluid at the beginning of the experiments was 6.94. Then, the two cells were placed in an oven set at 150°F. The volume of the

produced oil was monitored and recorded against time on a daily basis.

**Figure 43** shows a comparison of cumulative produced oil (%OOIP) by spontaneous imbibition for two Buff Berea sandstone Cores (R-20 and R-40) at 150°F and 14.7 psi. An increase in temperature enhanced the production in the first period and made the breakthrough time earlier. It was observed that the core saturated with monovalent cations had higher oil production in the early stages compared to the core saturated with divalent cations. The peak production rate for Core R-20 appeared earlier after 19 days of imbibition compared to Core R-40, which reached maximum production after 25 days. The oil production from Core R-40 reached approximately 59.6% of OOIP when the tests were abandoned after 32 days. Only 55.1% of the oil was recovered from Core R-20, when the tests were abandoned after 35 days. Then, a final CT scan was performed for the two cores at end of the SI test. The calculated saturation at each point was based on the images scanned at exactly the same location.

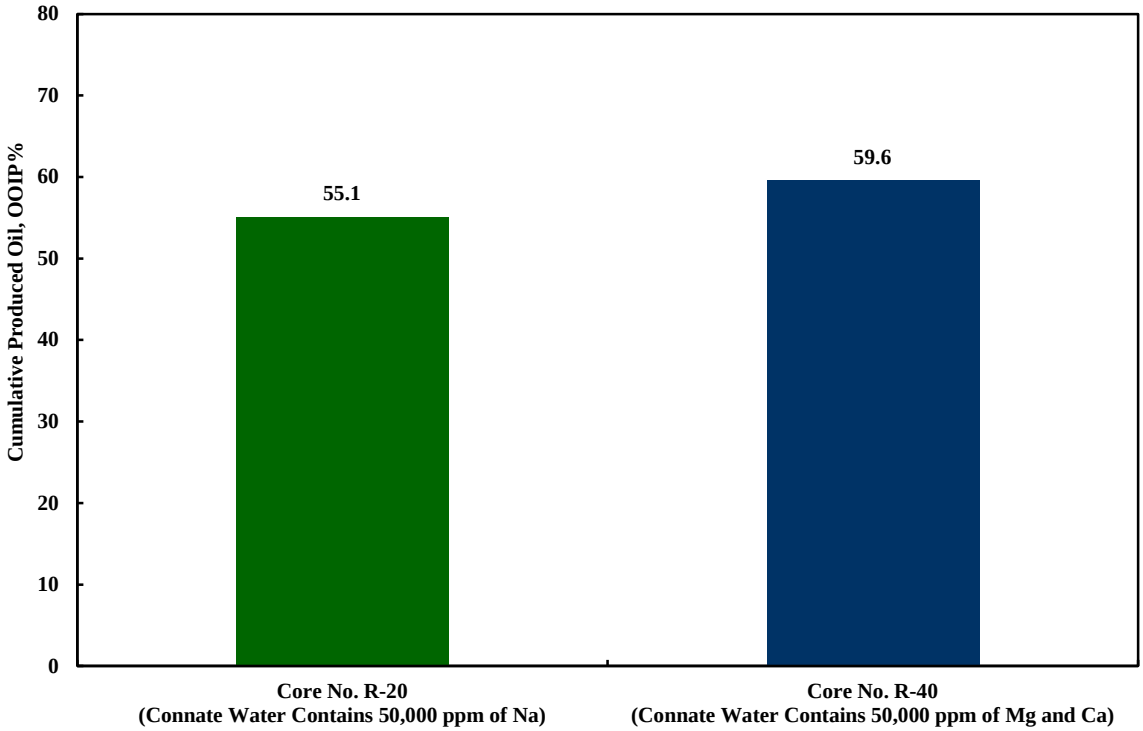


**Figure 43—Comparison of cumulative produced oil (%OOIP) by spontaneous imbibition for two Buff Berea sandstone cores (R-20 and R-40) at 150°F and 14.7 psi.**

**Figures 44** and **45** shows a comparison between the water saturation distribution across Core R-20 and Core R-40. The initial water saturation of the two cores were homogenous and similar across the core. The initial water saturation at the end of the cores was slightly higher than those at the middle of the cores. Overall, the average initial water saturation values throughout Core R-20 and Core R-40 was 38.52 and 37.8, respectively. The distribution of final water saturation within Core R-40 was quite different the initial water saturation distribution. The final water saturation distribution across core R-20 was more heterogeneous than Core R-40. No relationship was noticed between the produced oil and the initial water saturation distribution at Core R-40 and

Core R-40.

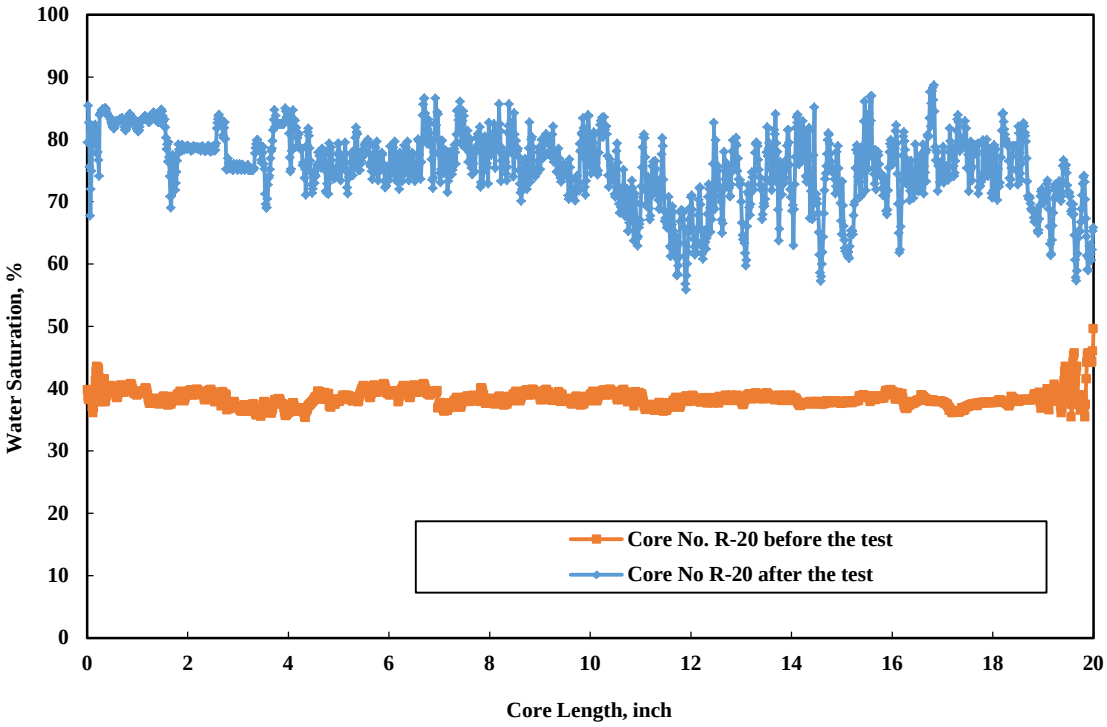


**Figure 44—Water saturation distribution along Buff Berea sandstone cores (R-20 and R-40) at the beginning and at the end of the SI experiment.**

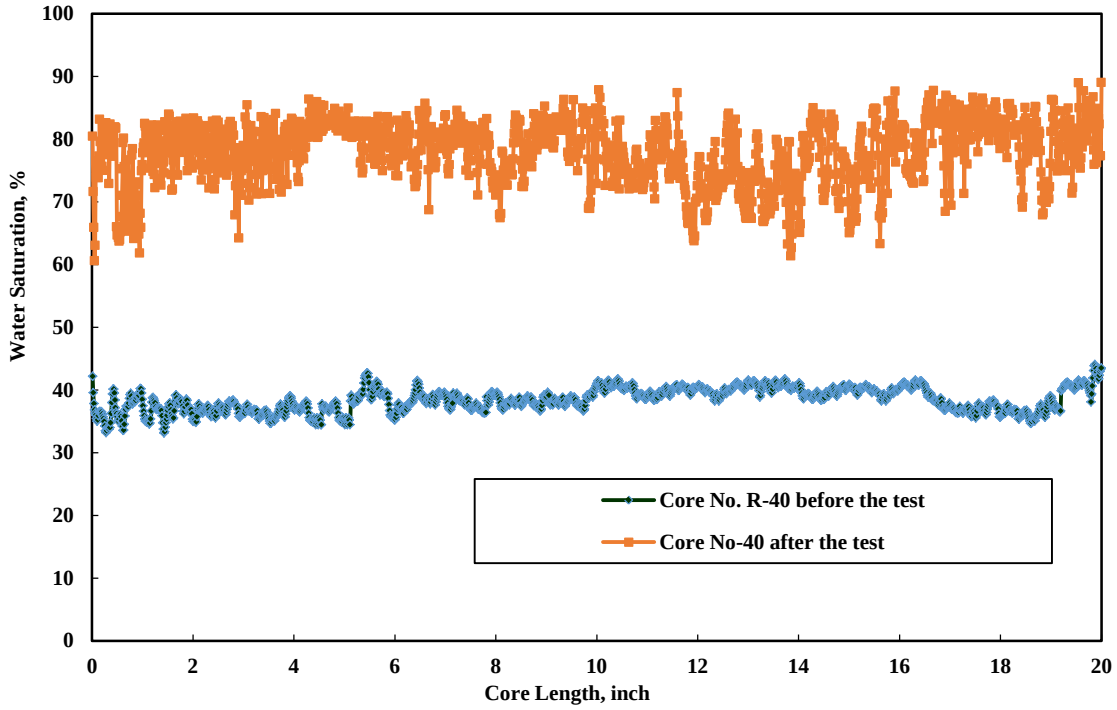


**Figure 45—Water saturation distribution along Buff Berea sandstone cores (R-20 and R-40) at the beginning and at the end of the SI experiment.**

The size and shape of crude oil droplets on the rock surface was observed during the imbibition tests. **Figure 46** shows the oil droplet on the top and at the outer surface of the cylindrical for core R-20 and R-40 immersed in the imbibition brine as a function of time. A mix of large and small spherical oil droplets was noticed on the top surface of Core R-40. Oil droplets had contact angle smaller than 90 degrees. The oil droplets sizes on core R-40 were qualitatively larger than oil droplets on Core R-20. For Core R-20, several spherical small oil droplets were produced on all surfaces of the core. The scatter droplets had a similar contact angle lower than 90 degrees. The size of the oil droplets was noticed to be homogeneous on each core. The size of oil droplets become smaller during the entire period of imbibition.

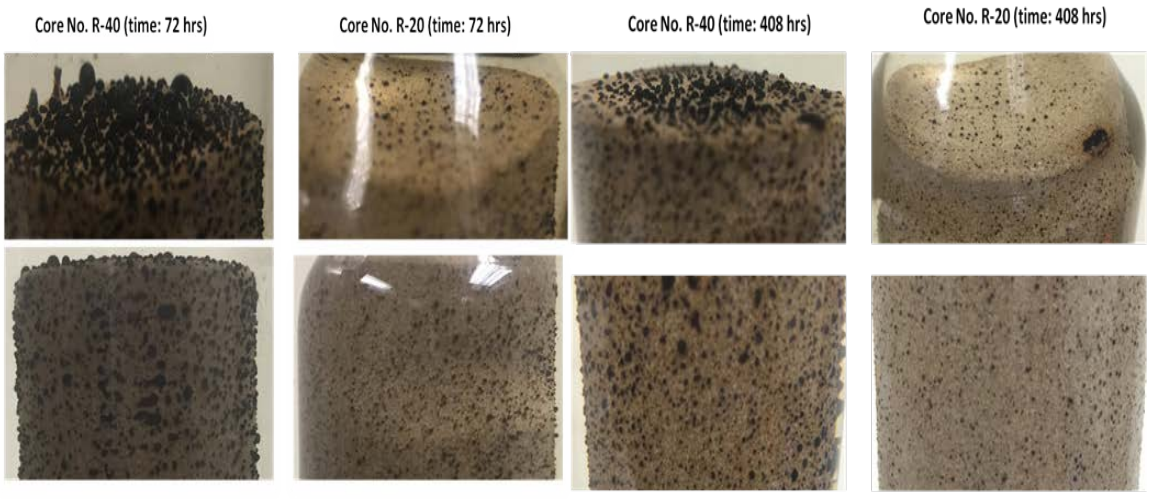


**Figure 46—Droplets of crude oil on the top and at the outer surface of the cylindrical of Buff Berea sandstone cores (R-20 and R-40) immersed in the NaCl (5000 ppm) at 150°F and 14.7 psi.**

The influences of connate water brine composition and average pore-throat radius on oil recoveries from Bandera sandstone have been investigated using SI tests. Four SI tests were carried out using Bandera sandstone cores at 77°F and 14.7 psi. From the XRD analyses, Bandera samples contained a higher amount of clay minerals than Buff Berea and Grey Berea. Bandera contains a considerable amount of illite (10%) and kaolinite (3%) and small proportions of chlorite clays (1%). Also, it contained a large amount of albite minerals (12%). The Bandera cores were rich in carbonate cement minerals (15%), while quartz made up the remainder.

Core R-3 was saturated with connate water containing only monovalent cations ($Na^+$) with a salinity of 54,400 ppm. The second and third Cores, R-1 and R-4, were saturated with high salinity connate water (174,156 ppm). Core R-2 was saturated with connate water containing only divalent cations ($Ca^{2+}$ and $Mg^{2+}$). The concentrations of $Ca^{2+}$ and

$Mg^{2+}$ in the connate water were 10,600 and 1,610 ppm, respectively. In the low-salinity water imbibition, NaCl brine (5,000 ppm) was used as the imbibition brine for Cores R-2, R-3, and R-4. On the other hand, connate water (174,156 ppm) was used as the imbibition brine for Core R-1 to simulate high-salinity waterflooding. The oil production value was compared with the value obtained from Core R-4. Water imbibition was monitored versus time on a daily basis during a period of 93 days by measuring the oil volume. The imbibition rate also varied from core to core. The rate of oil production by SI was in the order of R-2 > R-4 > R-1 > R-3 as shown in **Figure 47**. The Bandera sandstone gave oil recoveries by SI at 77°F ranging from 20-51.5% OOIP, according to the choice of initial and injected brine compositions.

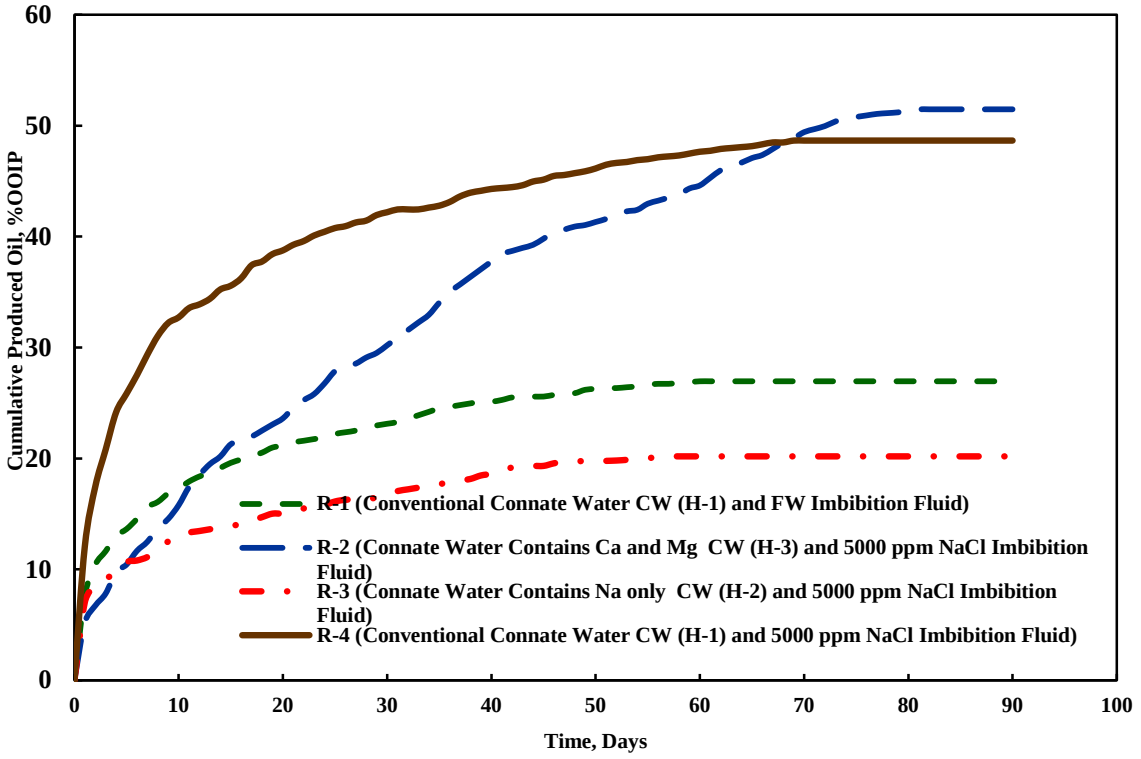


**Figure 47—Comparison of cumulative produced oil (%OOIP) by spontaneous imbibition as a function of time (days) for four Bandera sandstone cores (R-1, R-2, R-3, and R-4) at 77°F and 14.7 psi.**

Produced oil with Core R-1 reached approximately 27% of OOIP. The change to 5,000 ppm NaCl as imbibition brine for Core R-4, instead of high-salinity brine CW (H-1) for Core R-1, increased the produced oil by 21.7% of OOIP. Thus, there was a distinct improvement in oil production with the change to low-salinity brine as the imbibition fluid. The low-permeability sandstone cores showed a positive result using LSW compared to high-salinity waterflooding. From the previous results, a significant difference in the magnitude of the oil production between the Buff Berea and Bandera cores was noticed. For high permeability Buff Berea cores (164 - 207.7 md), the spontaneous imbibition oil produced ranged from 38 to 69% OOIP, while the oil produced from the low permeability Bandera cores (31.1 - 39.2 md) ranged from 20 to 51.5% OOIP at 77°F and 14.7 psia. Low-salinity waterflooding showed good potential to improve oil production in the spontaneous imbibition experiments at different permeability levels.

The average produced oil for Core R-1 was 27% of OOIP compared to 20.2% for Core R-3. Core R-3, saturated with connate water containing only monovalent cations ($Na^+$), had the lowest production of 20.2% of OOIP after 93 days. This result affirmed the importance of the existence of divalent cations in the connate water. For 66 days, the produced oil of Core R-4 was consistently higher compared to that of Core R-2. Conditions for Core R-2 and R-4 were similar except for the initial connate water composition. This is because Core R-4 was saturated with high-salinity connate water CW (H-1), while Core R-2 was saturated with connate water containing only divalent cations ($Ca^{2+}$ and $Mg^{2+}$). After 66 days, the oil produced from the R-4 experiment was

stopped. On the other hand, the cumulative oil produced for the R-2 experiment increased with further brine imbibition. At the end of the experiment, oil recoveries of 48.7 and 51.5% of OOIP were achieved for experiments R-4 and R-2, respectively.

The pH of the imbibition fluids was measured before and after the experiments for the Bandera SI experiments. The pH after the SI varied between 6.4 and 7.1. A slight increase in the pH was observed. Also, Bandera SI experiments showed that the produced oil was not related with the increase in pH. These results matched with the previous Buff Berea experiments.. Also for experiments R-2 to R-4, samples were collected and analyzed from the imbibition fluid at the end of the tests. **Figure 48** shows the concentration of $Ca^{2+}$, $Mg^{2+}$, and $Na^{+}$ ions in the imbibition fluid. Analyzing the sample for R-2 showed a much higher concentration of $Na^{+}$ than was originally in the imbibition brine. A similar observation was also noticed in experiment O-3, despite the absence of $Na^{+}$ cations in the initial connate water. However, Core R-3 was initially saturated with connate water containing only monovalent cations ($Na^{+}$). Also, $Ca^{2+}$ and $Mg^{2+}$, ions were detected in the imbibition fluid at the end of the tests. XRF analysis showed that Bandera sandstone contains 1.3, 1.4, and 1.7 as a weight percent of $Na^{+}$, $Ca^{2+}$, and $Mg^{2+}$ cations, respectively.

The change in ion concentration noticed in the imbibition brine for Bandera sandstone cores was similar to what was noticed for the Buff Berea sandstone. Sheng (2014) reported that when the salinity of injection water is different from that of initial water, a new equilibrium must be reached. The equilibrium must be governed by the law of mass action. Cation adsorption or desorption is not only determined by the injected brine

composition, but also by the adsorbed concentrations. Meyers and Salter (1984) observed that the steady-state effluent concentrations of calcium and magnesium were observed to be slightly greater than the injected concentrations. These excesses in concentration increased as the injection concentrations decreased. When NaCl brine was injected into the cores, "residual" calcium and magnesium concentrations were still observed in the effluent.

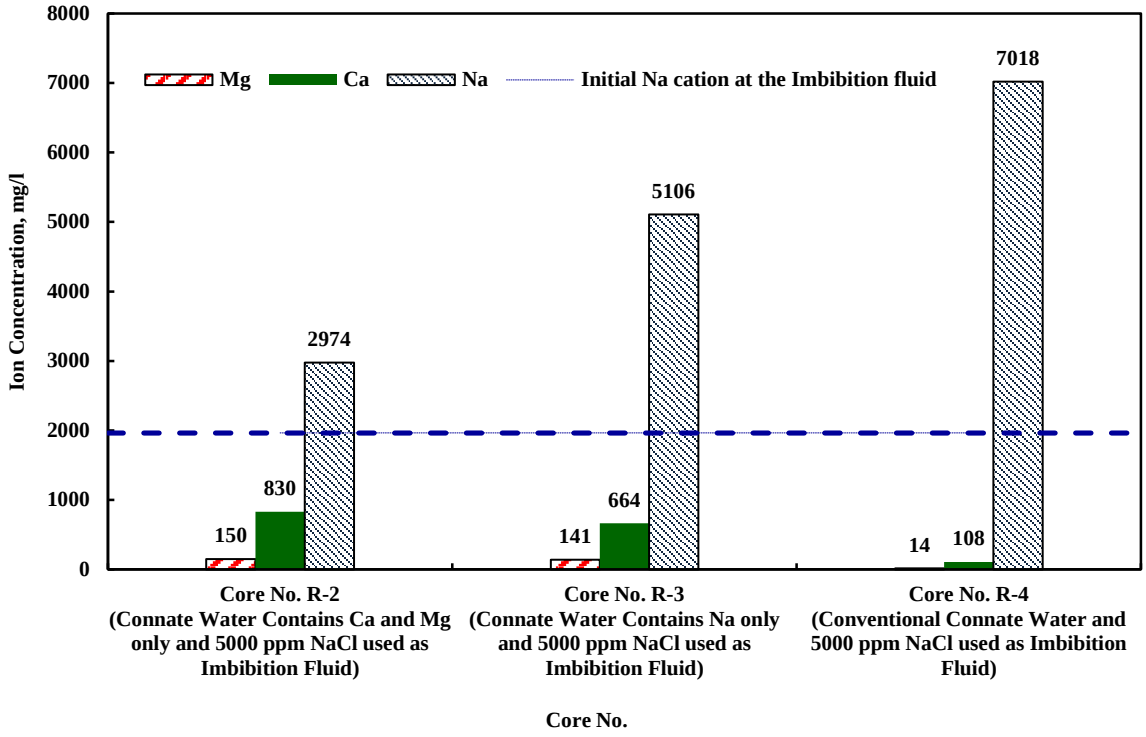


**Figure 48—Concentrations of $Ca^{2+}$, $Mg^{2+}$, and $Na^{+}$ ions in the imbibition fluid for Bandera sandstone cores at the end of the experiment.**

From the above results, reservoir connate water composition has a dominant influence on the produced oil rate. The $Ca^{2+}$, $Mg^{2+}$, and $Na^{+}$ ions play a key role in oil mobilization in different sandstone rocks. Reservoir cores saturated with connate water containing

divalent cations, $Ca^{+2}$ and $Mg^{+2}$, showed higher oil production than cores saturated with monovalent cations $Na^{+}$. Also, the oil production appeared to increase for sandstone cores with larger pore-throat radii. Therefore, a large pore-throat radius helped to recover more oil by the invaded water. These results indicated that the rock quality had a significant effect on the performance of LSW.. Jadhunandan and Morrow (1995) performed more than 50 slow-rate laboratory waterflood to investigate the relationship between wettability and oil recovery by waterflooding using Berea sandstone. The cores were 3.79 cm in diameter and 8 cm long. They observed that wettability depended on the initial water saturation, aging temperature, crude oil, and brine composition.

### 6.2. Coreflood Studies: Effect of Connate Water Composition

Six waterflood experiments were conducted on 6 in. length and 1.5 in. diameter cores of Buff Berea sandstone. The objectives were to validate the spontaneous imbibition results and to examine the effect of the connate water salinity and composition on the performance of the LSW recovery during secondary recovery mode. In this work, high-salinity reservoir connate water was defined as brine having a salinity of 174,156 ppm, while low-salinity connate water included brines of 4,633 ppm salinity. NaCl brines with two concentrations of 500 and 5,000 ppm were used as the injection brine. All experiments were conducted at the same temperature of 160°F, back flow pressure of 500 psi, and an overburden pressure of 1800 psi. **Table 26** summarizes the results of coreflood experiments.

Three coreflood experiments (S-2, S-4, and S-20) were conducted on cores saturated with high-salinity reservoir connate water. Core S-2 was saturated with connate water containing only divalent cations ($Ca^{2+}$ and $Mg^{2+}$). The concentration of $Ca^{2+}$ and $Mg^{2+}$ water was 10,600 and 1,610 ppm, respectively. A constant injection flow rate of 0.5 $cm^3$/min was used. Then the injection rate was increased to 1, 2, and 4 $cm^3$/min to ensure that no oil was produced from the core in each stage and that the remaining oil was the residual oil. The continuous injection of NaCl (5,000 ppm) brine from the initial water saturation resulted in a total recovery of 58.9% of OOIP. Gains in oil recovery occurred mainly in the first three pore volumes and were accompanied by pressure drop increases. According to the production data monitoring, around 36% of OOIP was recovered from core S-2 during the first 0.3 pore volume injected. Then, another 27% of OOIP was recovered between 0.3 to 3.7 pore volume injected. A small increase, 1.46% OOIP, in oil recovery was noted after flooding the core at 1 $cm^3$/min.

For Core S-4, high-salinity reservoir connate water with a salinity of 174,156 ppm was used to saturate the core. This core was flooded by NaCl (5,000 ppm) brine on an initial water injection rate of 0.5 $cm^3$/min. The oil recovery stabilized at 40.7% OOIP during 6.75 PV. Most of the recovered oil was produced during the 4.5 PV injection. After oil production ceased, the rate was increased to 1, 2, and 4 $cm^3$/min. The continuous injection of NaCl (5,000 ppm) brine from the initial water saturation resulted in a total recovery of 44.2% of OOIP. In this test 24.7% of OOIP was noticed during the first 0.2 pore volume injected, and around of 16% of OOIP was produced between 0.2 and 5 pore volume injected. A slight increase (3.5% OOIP) in oil recovery was noted

after flooding the core at 1 $cm^3$/min. Compared to the results of S-2, there was a significant decrease in the oil recovery of more than 14% OOIP (**Figure 49**).

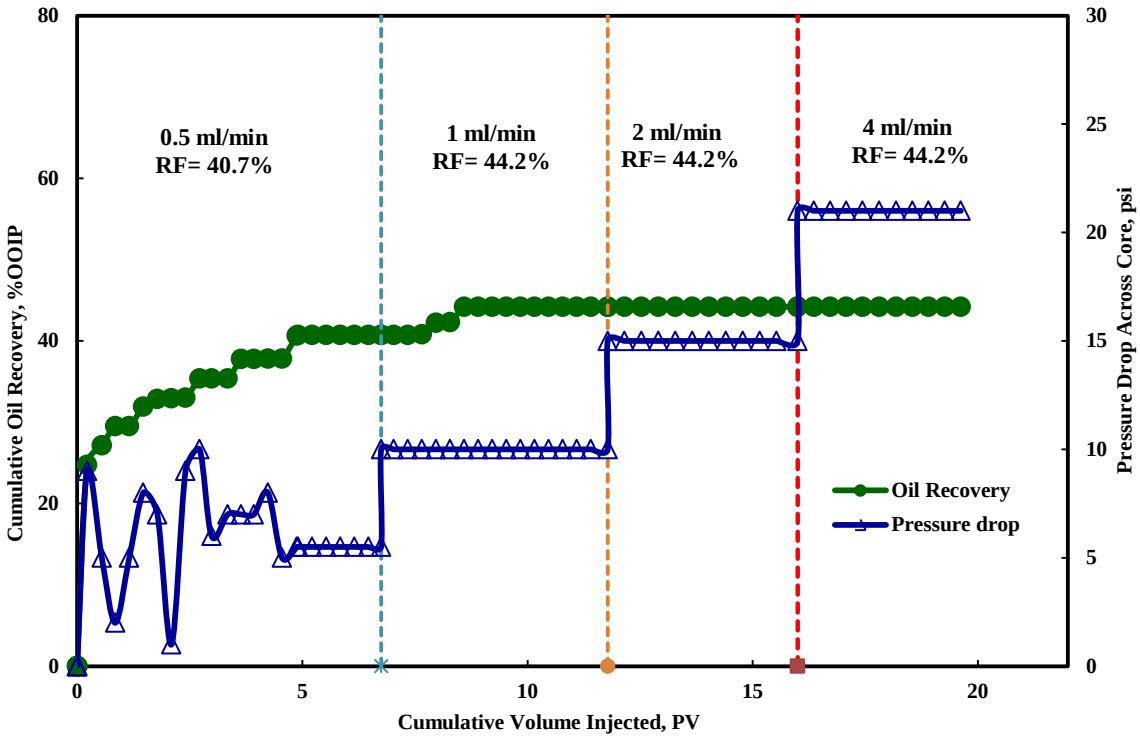


**Figure 49—Oil recovery for experiment S-4 at 160°F and $S_{wi}$ = 31.1%. The core was saturated with high salinity connate water CW (H-2). The injection was performed by NaCl brine (5,000 ppm) using injection rates of 0.5, 1, 2, and 4 $cm^3$/min. The vertical dashed lines separate the different injected brine stages.**

The main objective of the experiment S-20 was to test the efficiency of LSW for the core saturated initially with reservoir connate water containing only monovalent ions. The core was saturated with brine containing 54,400 ppm of $Na^+$ cations. NaCl brine of 5,000 ppm was passed through the core at a constant flow rate of 0.5 $cm^3$/min. About 19% OOIP was recovered after an injection of 0.3 pore volumes, and 12% OOIP between 0.3 and 1.4 pore volume injected. Brine injection rates were increased to 1, 2, and 4 $cm^3$/min to ensure that no oil was produced from the core in this stage and that the

remaining oil was the residual oil. Further injection gave a small increase in the oil production of 1.1% OOIP during 1 $cm^3$/min with no increase using 2 and 4 $cm^3$/min. **Figure 50** shows the oil recovery and the pressure drop across the core against the injected pore volume. Evidently, this result was considerably lower compared to the oil recovery obtained from Cores S-2 and S-4.

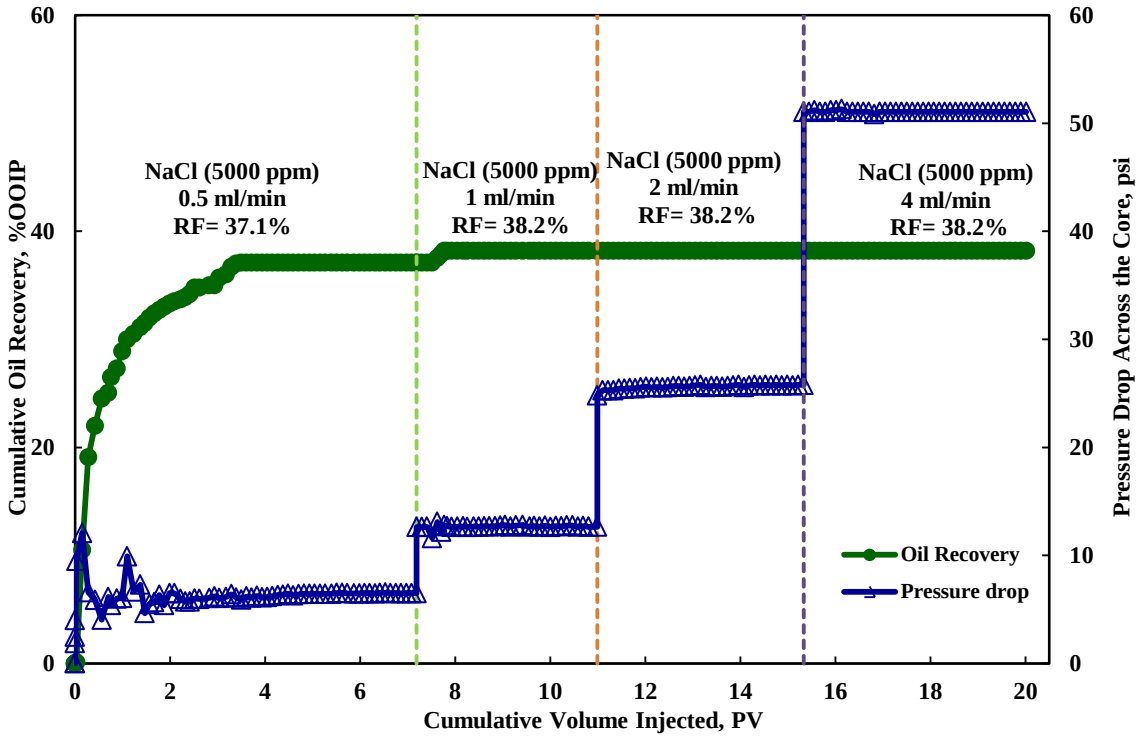


**Figure 50—Oil recovery for experiment S-20 at 160°F and $S_{wi}$ = 31.1%. The core was saturated with high salinity connate water CW (H-2). The injection was performed by NaCl brine (5,000 ppm) using injection rates of 0.5, 1, 2, and 4 $cm^3$/min. The vertical dashed lines separate the different injected brine stages.**

It was noticed that the cumulative oil recovery is highly dependent on the reservoir connate water composition ($Na^+$, $Ca^{2+}$, and $Mg^{2+}$). A higher oil recovery was obtained in the core saturated with divalent cations. Bassin and Ichiye (1977) showed that salinity is a prerequisite for interactions between oil and clay minerals. **Figure 51** shows oil

recovery comparisons for experiments S-2, S-4, and S-20 at 160°F during secondary recovery mode.

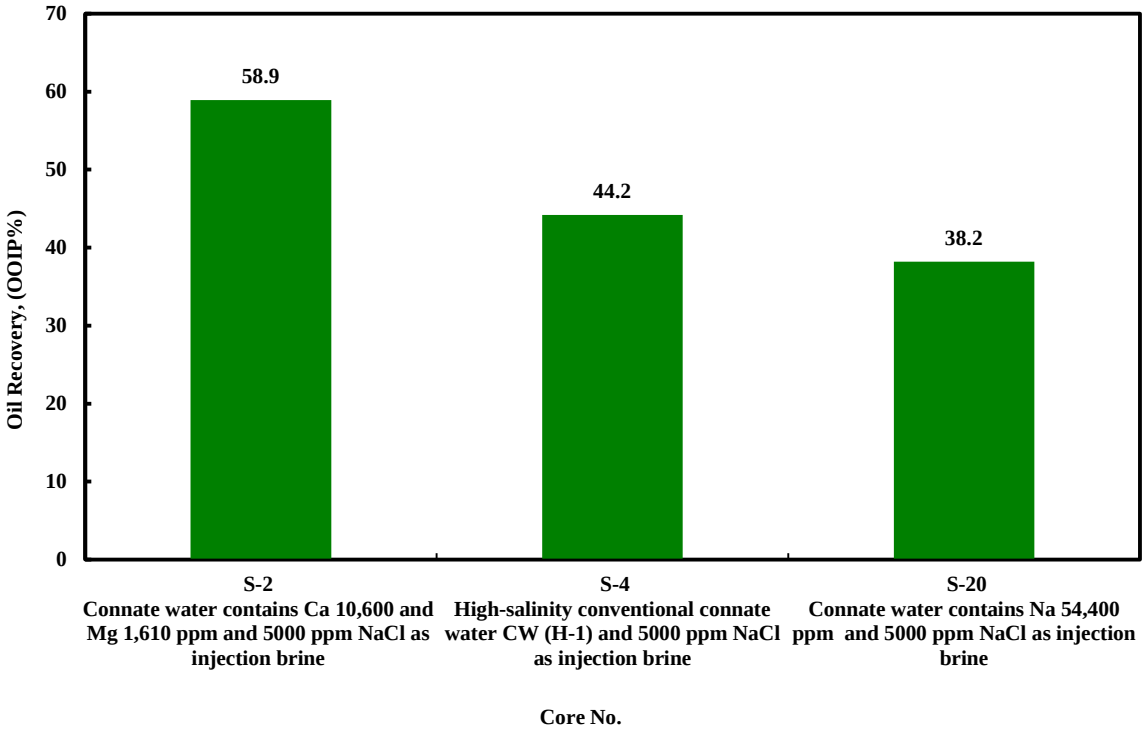


**Figure 51—Oil recovery comparison for coreflood experiments for Buff Berea sandstone cores at 160°F. The Cores were saturated with different connate water composition.**

Three coreflood experiments (S-1, S-5, and S-21) were designed to test the effect of the reservoir connate water salinity with lower TDS (4,633 ppm). NaCl brine with 500 ppm was used as the invading brine. In experiment S-1, the efficiency of LSW was tested for the core saturated initially with reservoir connate water with divalent cations. The concentrations of $Ca^{2+}$ and $Mg^{2+}$ in the connate water were 133 and 630 ppm, respectively. We observed 24% of OOIP was recovered during the first 0.2 pore volume injected. Then, another 14% of OOIP was recovered between 0.3 to 1.1 pore volume

injected. The continuous injection of NaCl (500 ppm) brine using 0.5 $cm^3$/min resulted in a total recovery of 51.9% of OOIP. There was no incremental increase in oil recovery due to the increase in the injection rate to 1, 2, and 4 $cm^3$/min (**Figure 52**).

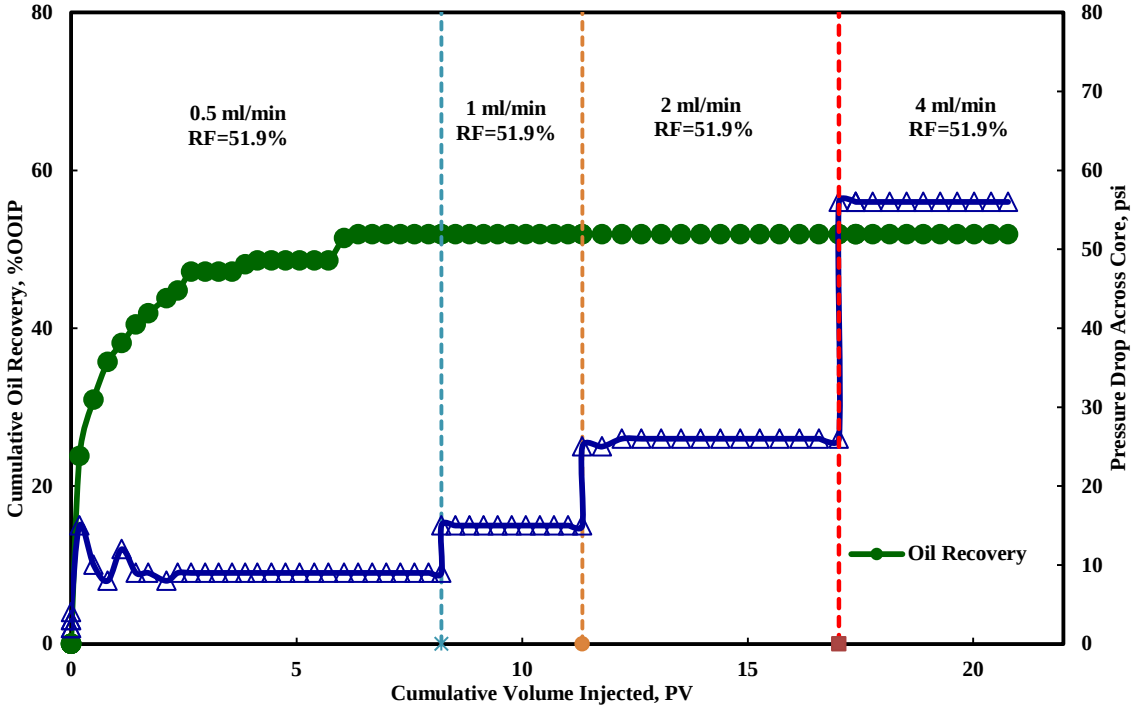


**Figure 52—Oil recovery for experiment S-1at 160°F and $S_{wi}$ = 31.1%. The core was saturated with high salinity connate water CW (H-2). The injection was performed by NaCl brine (5,000 ppm) using injection rates of 0.5, 1, 2, and 4 $cm^3$/min. The vertical dashed lines separate the different injected brine stages.**

In experiment S-5, the core was saturated with connate water containing only monovalent cations ($Na^+$). The concentration of $Na^+$ cations in the connate water was 610 ppm. A total of 7.5 pore volumes at 0.5 $cm^3$/min was injected. Then the rate was increased to 1, 2, and 4 $cm^3$/min to ensure that no oil was produced from the core. The oil volumes produced were monitored and recorded. 19.5% of OOIP was recovered during the first 0.25 pore volume injected and 12% OOIP was recovered between 0.25 to

1.3 pore volume injected. After 7 pore volumes, more than 35.4% of the oil recovery was achieved. Oil recovery increased slightly to 35.9% after increasing the rate to 1 $cm^3$/min. The total oil recovery for experiment S-1 was about 16% higher than the total oil recovery of experiment S-5.

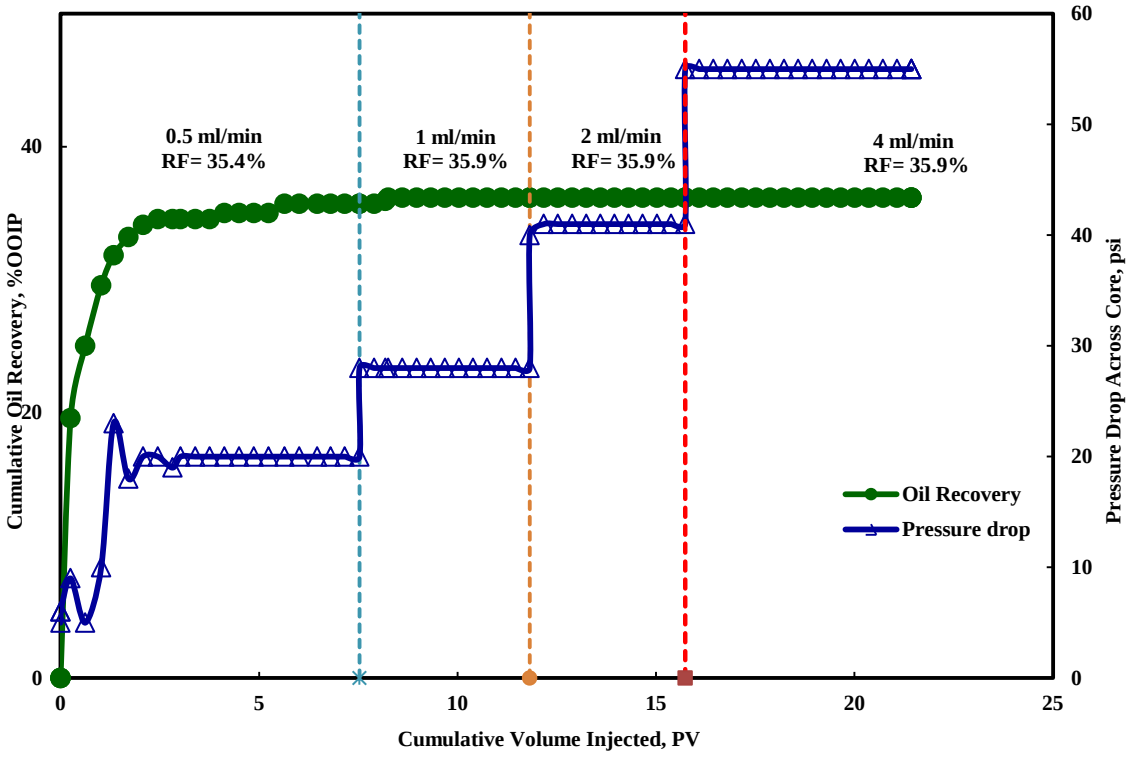


**Figure 53—Oil recovery for experiment S-5 at 160°F and $S_{wi}$ = 31.1%. The core was saturated with high salinity connate water CW (H-2). The injection was performed by NaCl brine (5,000 ppm) using injection rates of 0.5, 1, 2, and 4 $cm^3$/min. The vertical dashed lines separate the different injected brine stages.**

In the last test, the effect of low-salinity connate water was tested using Core S-21. Injection began at a rate of 0.5 $cm^3$/min. The oil recovery that was obtained when using the 500 ppm NaCl brine was about 42.1% of the OOIP. Then, the core was flooded at an injection rate of 1, 2, and 4 $cm^3$/min. 32.2% of OOIP was recovered during the first 0.5

pore volume injected and 10% OOIP was recovered between 0.5 to 1.7 pore volume injected.. The total oil recovery for experiment S-1 was about 9.8% higher than the total oil recovery of experiment S-21. The pH of the effluent samples was measured at room temperature and atmospheric pressure in order to study the effect of brine salinity. The measured pH values were in the range of 7 to 8.2. There is no clear relationship between the effluent pH and the oil recovery. Austad (2013) reported that the pH value at the effluent end could increase or decrease.

The production data from these experiments, showed similar behavior to the description of shock front and spreading wave by Jerauld et al. (2006). They stated that the low-salinity solution consist of two fronts; one corresponding to the transition between low and high salinity and the second corresponding to the transition between high water saturation and connate at high salinity. **Figure 54** shows oil recovery comparisons for experiments S-1, S-21, and S-5 at 160°F during secondary recovery mode.

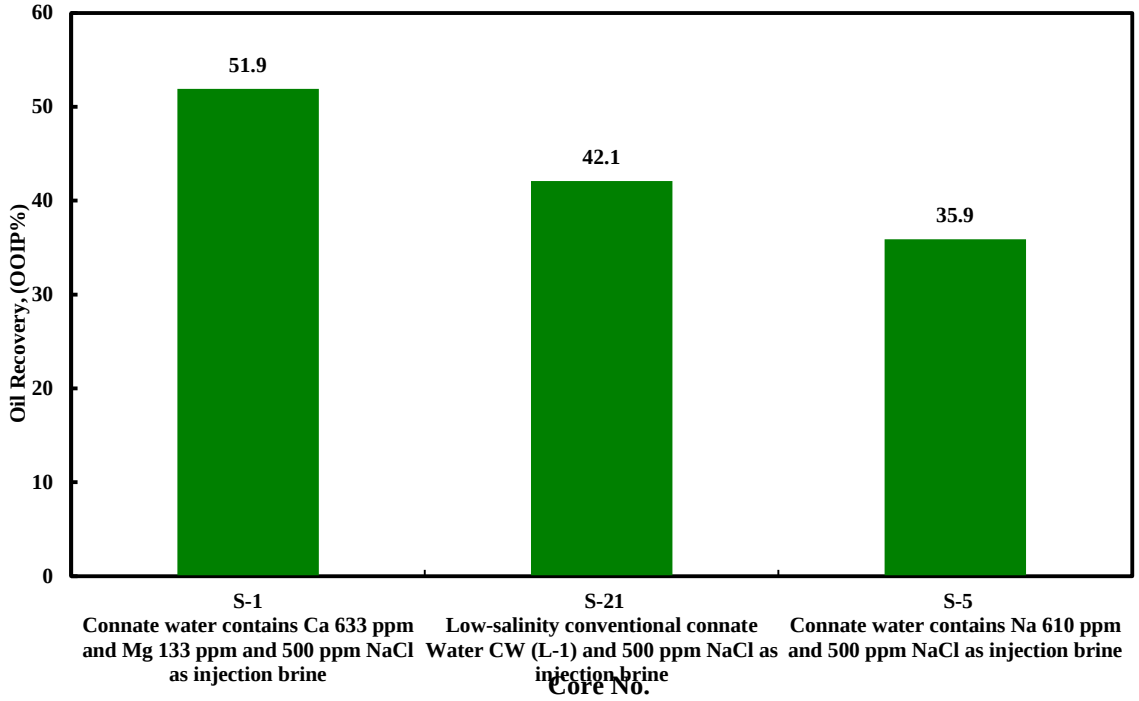


**Figure 54—Oil recovery comparison for coreflood experiments for Buff Berea sandstone cores at 160°F. The cores were saturated with different connate water composition.**

For the three experiments S-2, S-4, and S-20, an increase in the pressure drop was observed across the core in the beginning of the experiment. It was attributed to a two-phase flow. Then, a stable pressure profile was noticed at different injection rates. There was a major increase in the pressure profile induced by a change in the injection rate. No fine minerals or color changes were observed at the effluent samples by injecting brine of 5,000 ppm NaCl.

For experiment S-20, the average stabilized pressure was around 6.5 psi at a rate of 0.5 $cm^3$/min. A further increase in pressure from 6.5 to 12.6 psi was noticed by increasing the injection rate to 1 $cm^3$/min. The pressure drops were 25.6 and 51 psi at injection rates of 2 and 4 $cm^3$/min, respectively. However, the stabilized pressure across

the core was consistent for the different cores during the permeability measurements, and it was observed that the differential pressure values of the core flooded with 500 ppm NaCl were slightly higher than the core flooded with 5,000 ppm NaCl. The average stabilized pressure was around 9 psi at a rate of 0.5 $cm^3$/min for Core S-21. The pressure drops were 18.2, 36.1, and 72.4 psi at injection rates of 1, 2, and 4 $cm^3$/min, respectively. Also, no fine production or color changes were observed at the effluent samples.

It is believed that the increase in differential pressure across the core is due to the salinity reduction of the injected brines. Baptist and Sweeney (1955) reported that the water sensitivity of the reservoir sands is related to the salinity of the water, the permeability of the sand, and the type and amount of clays present. Tang et al (1999) stated that expansion of the electric double layer clay particles and other mixed-wet fines are removed from the rock surface at low-salinity conditions, leaving a water-wet spot. The migrating fines might block narrow pore throats and cause microscopic diversion of the injected water. Ashraf et al (2010) observed an increase in pressure drop and a decrease in effective permeability when reducing the salinity of injection brine. Cissokho et al (2010) observed that the pressure drop increase and fine release can also occur when brine concentration was reduced, even if no particles were produced in the effluent.

The results reflect the variation in oil recoveries obtained by LSW. For Buff Berea waterflood tests, oil recovery is highly dependent on the brine concentration of the connate water. The oil recovery using cores saturated with different reservoir connate water salinities was in the range of 35.9 to 58.9% of OOIP. The oil recovery decreased

as the salinity of reservoir connate water decreased. The coreflood experiments confirmed that the low-salinity brine had a significant positive effect on oil recovery for sandstone cores saturated with divalent cations ($Ca^{+2}$ and $Mg^{+2}$).

It can also be observed that the oil recovery decreased by injection of low-salinity brines for cores saturated with monovalent cations only. The magnitude of incremental oil recovery increased from 51.9 to 58.9% OOIP when the divalent cation concentration increased from 709 to 12,210 ppm. On the other hand, increasing the monovalent cations ($Na^{+}$) from 610 to 54,400 ppm showed a small improvement in oil recovery (1.2% OOIP).

**Table 26—Summary of the Coreflood Experiments Saturated With Different Connate Water Salinities.**

| Core # | Initial Water Composition | Injected Brine Composition | Injection Rate ($cm^3$/min) | Slug Size (PV) | Incremental Oil Recovery (% OOIP) | Total Oil Recovery (% OOIP) |
|---|---|---|---|---|---|---|
| S-2 | CW (H-3) $Ca^{2+}$ 10,600 ppm and $Mg^{2+}$ 1,610 ppm | NaCl (5,000 ppm) | 0.5 | 6.3 | 57.4 | 57.4 |
| | | | 1 | 4.4 | 1.46 | 58.9 |
| | | | 2 | 4.4 | 0 | 58.9 |
| | | | 4 | 4.9 | 0 | 58.9 |
| S-4 | CW (H-1) High-Salinity Connate Water | NaCl (5,000 ppm) | 0.5 | 6.8 | 40.7 | 40.7 |
| | | | 1 | 5.0 | 3.5 | 44.2 |
| | | | 2 | 4.2 | 0 | 44.2 |
| | | | 4 | 4.0 | 0 | 44.2 |
| S-20 | CW (H-2) $Na^{+}$ 54,400 ppm | NaCl (5,000 ppm) | 0.5 | 7.2 | 37.1 | 37.1 |
| | | | 1 | 3.8 | 1.1 | 38.2 |
| | | | 2 | 4.3 | 0 | 38.2 |
| | | | 4 | 5.8 | 0 | 38.2 |
| S-1 | CW (L-3) $Ca^{2+}$ 633 ppm and $Mg^{2+}$ 133 ppm | NaCl (500 ppm) | 0.5 | 8.2 | 51.9 | 51.9 |
| | | | 1 | 3.1 | 0 | 51.9 |
| | | | 2 | 5.7 | 0 | 51.9 |
| | | | 4 | 3.8 | 0 | 51.9 |
| S-5 | CW (L-2) $Na^{+}$ 610 ppm | NaCl (500 ppm) | 0.5 | 7.5 | 35.4 | 35.4 |
| | | | 1 | 4.2 | 0.5 | 35.9 |
| | | | 2 | 3.9 | 0 | 35.9 |
| | | | 4 | 5.7 | 0 | 35.9 |
| S-21 | CW (L-1) Low-Salinity Connate Water | NaCl (500 ppm) | 0.5 | 6.8 | 42.1 | 42.1 |
| | | | 1 | 4.2 | 0 | 42.1 |
| | | | 2 | 3.9 | 0 | 42.1 |
| | | | 4 | 5.2 | 0 | 42.1 |

### 6.3. Relative Permeability Measurements

Relative permeability and capillary pressure determine the macroscopic fluid flow behavior in hydrocarbon reservoirs over the scale of centimeters to kilometers (Bryant and Blunt 1992). Relative permeability, a dimensionless quantity, is the ratio of effective permeability to a base permeability. The base permeability can be absolute air permeability, absolute liquid permeability or effective oil permeability at irreducible water saturation. Relative permeability is a function of pore structure, saturation history and wettability. Several laboratory techniques are introduced to measure the relative permeability using steady-state and unsteady-state methods.

Ibrahim and Koederitz (2000) developed a prediction equation for water-oil, gas-oil, gas-water, and gas-condensate relative permeability from experimental data using a linear regression model approach. Twenty-four equations for the two-phase relative permeability have been developed for four different systems of strongly water-wet, water-wet, intermediate (or mixed-wet) and oil-wet conditions.

A few researchers have studied the changes in relative permeability in the presence of different levels of salinity (Webb et al. 2008; Rivet et al. 2010; Fjelde et al. 2012; Law et al. 2014; Shojaei et al. (2015)

In this study, the effective permeability to water was measured in the presence of remaining oil saturation ($S_{or}$) after waterflooding for the coreflood studies. Then, the relative permeability to water was calculated using the absolute liquid permeability as a base permeability. The summary of the relative permeability measurements are listed in

**Table 27**. The relative permeability to water appears sensitive to the salinity of the reservoir connate water and the injected brine. The relative permeability to water was relatively higher for the core saturated with high-salinity connate water than for the cores saturated with low-salinity connate water. This effect would be due to fines movement and clay swelling. The end-point relative permeability to water increased from 0.07 to 0.39 when the reservoir connate water salinity increased from 4,633 to 174,156 ppm for injected brine salinity of 500 and 5,000 ppm, respectively. The change in the relative permeability to water generally decreased with increasing the salinity of the reservoir connate water. The end-point relative permeability to water for Cores S-4, S-20, and S-2 were 0.391, 0.138, 0.148, while the remaining oil saturation was 39.6, 33.3, and 26.4, respectively. The end-point relative permeability to water for Core S-21, S-5, and S-1 were 0.07, 1.0, and 0.08, while the remixing oil saturation were 37.4, 44.9, 33.5, respectively.

**Table 27 —Summary of Experimental Results for the Relative Permeability Measurements for Buff Berea Sandstone.**

| Core # | Initial Water Composition | Initial Water Saturation, Swi | Residual Oil Saturation, Sor | Relative Permeability to water at $S_{or}$ |
|---|---|---|---|---|
| S-2 | CW (H-3) $Ca^{2+}$ 10,600 ppm and $Mg^{2+}$ 1,610 ppm | 35.9 | 26.4 | 0.15 |
| S-4 | CW (H-1) High-Salinity Connate Water | 29.0 | 39.61 | 0.39 |
| S-20 | CW (H-2) $Na^{+}$ 54,400 ppm | 31.1 | 33.3 | 0.14 |
| S-1 | CW (L-3) $Ca^{2+}$ 633 ppm and $Mg^{2+}$ 133 ppm | 30.6 | 33.5 | 0.08 |
| S-5 | CW (L-2) $Na^{+}$ 610 ppm | 29.9 | 44.9 | 0.10 |
| S-21 | CW (L-1) Low-Salinity Connate Water | 30.8 | 37.4 | 0.07 |

Finally, oil/water relative permeability measurements was performed using coreflood system for two Bandera sandstone samples (Cores K-2 and K-5). The two cores were saturated and the absolute permeability was measured with high-salinity connate water (174,156 ppm). Then, the brine-saturated cores were flooded with oil to establish the initial water saturation. The relative permeability to oil at connate water saturation was measured for both cores. Then, the 5,000 ppm NaCl brines and high-salinity connate water (174,156 ppm) were used as the injection brine for core K-5 and K-2, respectively. The high-salinity relative permeability compared to the low-salinity relative permeability. The summary of the end-point relative permeability measurements for the two cores are listed in **Table 28**. Comparison between the high-salinity relative

permeability and low-salinity relative permeability showed that the end-point water relative permeability decreased for the cores after using low-salinity brine as injected brine compared to the end-point water relative permeability after flooding with high-salinity brine.

**Table 28—Summary of Experimental Results for the Oil and Water Relative Permeability Measurements for Buff Berea Sandstone K-2 and K-5.**

| Core ID | Porosity (vol%) | Absolute Permeability (md) | Initial Water Saturation (%) | Oil relative permeability at connate water saturation | Remaining oil Saturation (%) | Water relative Permeability at residual oil saturation |
|---|---|---|---|---|---|---|
| K-5 | 22.13 | 27.17 | 0.41 | 0.07 | 0.30 | 0.16 |
| K-2 | 20.89 | 24.30 | 0.39 | 0.06 | 0.39 | 0.35 |

# CHAPTER VII

# CONCLUSIONS AND RECOMMENDATIONS

The main objectives of this work are to: (1) evaluate the potential of LSW on the performance of oil recovery improvement four outcrop sandstone rocks (Buff Berea, Grey Berea, Bandera, and Parker, (2) investigate the role of clay content, rock permeability, and average pore throat radius on the performance of low-salinity waterflooding, (3) examine the effect of the salinity of the reservoir connate water, (4) investigate the role of the composition ($Na^+$, $Ca^{2+}$, and $Mg^{2+}$) of reservoir connate water, (5) test the effect of temperature and rock quality on the performance of the LSW performance, and (6) evaluate the effects of mineral type, brine salinity, cation type, and pH on the zeta-potential measurements.

This study includes four types of sandstone cores with different permeabilities, rock qualities, and mineral compositions. Connate water compositions with wide ranges of salinity were used. Long outcrop sandstone cores (20 and 6 in.) were used to minimize uncertainty in oil and water saturations to reduce the impact of capillary end effects that are common in short plugs. X-ray powder diffraction (XRD), scanning electron microscopy (SEM), and X-ray fluorescence (XRF) were used to analyze the mineralogy composition of the sandstone cores. High-pressure mercury injection (MICP), nuclear magnetic resonance (NMR), and Winland's empirical equation were used to characterize the types of sandstone rocks. The zeta potential measurements were used to investigate the effect of brine salinity, composition, and pH on the surface charge.

Based on the obtained results, the following conclusions can be drawn:

1. The Parker, Bandera, Grey Berea, and Buff Berea sandstone cores showed additional oil recoveries of 4.3, 9.2, 13.3, and 17.1% OOIP, respectively, through the injection of low-salinity brine (5,000 ppm NaCl) as the secondary recovery mode. None of the three sandstone rock types (Buff Berea, Grey Berea, and Parker) showed a response in the tertiary recovery mode. Incremental oil recovery of 6.9% OOIP was recovered in the tertiary recovery mode for Bandera sandstone rock.
2. As the permeability increased from 6 to 167 md, an additional oil recovery of up to 32.9% of OOIP was observed with low-salinity waterflooding as a secondary recovery mode, while an additional oil recovery up to 18% of OOIP was observed with high-salinity waterflooding as a secondary recovery mode. The average pore–throat radius (rock quality) has a higher effect in the performance of low-salinity waterflooding than high-salinity waterflooding on the secondary recovery mode. The incremental oil recovery for the low-salinity waterflooding increased from 4.3 to 17% when the average pore-throat radius (R35) of the core increased from 1.4 to 8.5 microns.
3. The total clay content is not the main factor influencing the low-salinity waterflooding performance. However, the clay type and composition seem to be playing a significant role.
4. Monovalent cations ($Na^+$) are more efficient in increasing the absolute values of the zeta potential than the divalent cations at the same concentration at 25°C. Zeta potential become more negative while the salinity of the brine decreased.

5. Changing the pH of the solution causes a significant alteration in charge of Buff Berea and Bandera sandstone particles and subsequently, the zeta potential values. The zeta potential of Bandera is more negative than that of Buff Berea at pH values in the range of 5 and 10.
6. The measured zeta potential of kaolinite and montmorillonite particles in 5,000 ppm NaCl brine at 25°F and a pH of 7 were -26.5 and -29.4 mV, respectively. The zeta potential values indicated a stronger negative charge on muscovite and albite minerals of -33.8 and -31.5 mV, respectively. The zeta potential values indicated a less negative charge on the chlorite and illite particles than the other minerals. Results indicate that chlorite and illite have a smaller contribution to electrical-double layer expansion than kaolinite, feldspars, montmorillonite, and muscovite. On the other hand, the zeta potential values of calcite and dolomite particles are 1.0 and -4.5 mV, respectively. The effect of double layer expansion would decrease in the presence of dolomite and calcite minerals which affect on the performance of low-salinity waterflooding.
7. The spontaneous imbibition produced oil ranging from 38 to 69% OOIP for high permeability Buff Berea cores (164-207.7 md), while the produced oil of the low permeability Bandera cores (31.1-39.2 md) ranged from 20 to 51.5% OOIP at 77°F and 14.7 psia. The produced oil recovery decreased when the average pore-throat radius (rock quality) decreased.
8. As the temperature increased from 77 to 150°F, additional produced oil up to 15% of OOIP was observed by spontaneous imbibition for Buff Berea cores.

9. The reservoir connate water composition had a dominant influence on the oil recovery rate. The changes in the ion composition of reservoir connate water ($Ca^{2+}$, $Mg^{2+}$, and $Na^{+}$) showed a measurable change in the oil production trend. Reservoir cores saturated with connate water containing divalent cations of ($Ca^{+2}$ and $Mg^{+2}$) showed higher oil recovery than for cores saturated with monovalent cations ($Na^{+}$).
10. In all cases, a measurable ion exchange was observed, while there was no significant change in the pH of the imbibition brine during the experiment. The ion exchange effect was more pronounced than the pH effect in the low-salinity waterflooding performance for Buff Berea and Bandera sandstone.
11. The total oil recovery increased from 51.9 to 58.9% OOIP when the divalent cation ($Ca^{+2}$ and $Mg^{+2}$) concentration of the reservoir connate water increased from 709 to 12,210 ppm for injected brine salinity of 500 and 5,000 ppm, respectively. Furthermore, increasing the monovalent cation ($Na^{+}$) concentration from 610 to 54,400 ppm resulted in a slight increase in oil recovery (2.3% OOIP).

## REFERENCES


Anderson, W.G. 1986. Wettability Literature Survey—Part 1: Rock/Oil/Brine Interactions and the Effects of Core Handling on Wettability. *J. Pet Technol* **38** (10): 1125–1144. SPE-13932-PA. http://dx.doi.org/10.2118/13932-PA.

Alotaibi, M.B., Nasralla, R.A., and Nasr-El-Din, H.A. 2010. A Comprehensive EOR Study Using Low Salinity Water in Sandstone Reservoirs. Presented at the SPE Improved Oil Recovery Symposium held in Tulsa, Oklahoma, USA, 24–28 April. SPE 129976. http://dx.doi.org/10.2118/129976-MS.

Alotaibi, M.B. and Nasr-El-Din, H.A. 2011. Electrokinetics of Limestone Particles and Crude-Oil Droplets in Saline Solutions. *SPE Res Eval & Eng* **13** (5): 604-611. http://dx.doi.org/10.2118/151577-PA.

Alotaibi, M.B., Nasralla, R.A., and Nasr-El-Din, H.A. 2011. Wettability Studies Using Low-Salinity Water in Sandstone Reservoirs. *SPE Res Eval & Eng* **14** (6): 713–725. http://dx.doi.org/10.2118/149942-PA.

Alshehri, A.J. and Kovscek, R. 2015. Impact of Chemical Flood Mode on Oil Recovery in Fractured Carbonates. Presented at SPE Middle East Oil & Gas Show and Conference, Manama, Bahrain. 8-11 March. SPE-172809-MS. http://dx.doi.org/10.2118/172809-MS.

Archer, J.S. and Wall, C.G. 1986. *Petroleum Engineering: Principles and Practice*, first edition, Chap. 11, 173. London, United Kingdom: Graham and Trotman.

Ashraf, A., Hadia, N.J., and Torsaetar, O. 2010. Laboratory Investigation of Low Salinity Waterflooding as Secondary Recovery Process: Effect of Wettability. Presented at SPE Oil and Gas India Conference and Exhibition in Mumbai, India 20-22 January. SPE-129012-MS. http://dx.doi.org/10.2118/129012-MS.

Austad, T., Rezaeidoust, A., and Puntervold, T. 2010. Chemical Mechanism of Low-Salinity Water Flooding in Sandstone Reservoirs. Presented at the SPE IOR Symposium, Tulsa, USA, 24-28 April. SPE 129767-MS. http://dx.doi.org/10.2118/129767-MS.

Austad, T. 2013. Water-based EOR in carbonates and sandstones: New Chemical Understanding of the EOR Potential Using Smart Water. In *EOR Field Case Studies*, ed. Sheng, J.J., Chap. 13, 301–335. MA, USA: Gulf Professional Publishing.

Baptist, O. C. and Sweeney, S. A. 1955. Effects of Clays on the Permeability of Reservoir Sands to Various Saline Waters, Wyoming, U. S. Bur. Mines RI 5180: 23.

Bassin, N.J. and Ichiye, T. 1977. Flocculation of Suspended sediments and oil emulsions. *J. Sediment. Petrol.* **47** (2): 671-677.

Bataweel, M.A., Nasr-El-Din, H.A., and Schechter., D.S. 2011. Fluid Flow Characterization of Chemical EOR Flooding: A Computerized Tomography (CT) Scan Study. Presented at the SPE/DGS Saudi Arabia Section Technical Symposium and Exhibition, Al-Khobar, Saudi Arabia, 15-18 May. SPE-149066-MS. http://dx.doi.org/10.2118/149066-MS.

Bedrikovetsky, P., Zeinijahromi, A., Badalyan, A., et al. 2015. Fines-Migration-Assisted Low-Salinity Waterflooding: Field Case Analysis. Presented at the SPE Russian Petroleum Technology Conference, Moscow, Russia, 26-28 October. SPE-176721-MS. http://dx.doi.org/10.2118/176721-MS.

Bernard, G.G. 1967. Effect of Floodwater Salinity on Recovery of Oil from Cores Containing Clays. Presented at the 38th Annual California Regional Meeting, California, USA, 26-27 October. SPE 1725-MS. http://dx.doi.org/10.2118/1725-MS.

Bryant, S. and M. J. Blunt. 1992. Prediction of Relative Permeability in Simple Porous-Media, *Phys. Rev. A*, 46 (4): 2004-2011.

Borchardt, G. 1989. Smectites. In *Soil Mineralogy with Environmental Applications*, ed. J.B. Dixon and D.G. Schulze, Chap. 15, Soil Science Society of America, Inc.

Chilingarian, G.V. 1963. Relationship between Porosity, Permeability, and Grain Size Distribution of Sands and Sandstones. In *Deltaic and Shallow Marine Deposits*, ed. Van Straaten L.M.J.U., Chap. 8, 71-77. Amsterdam: Elsevier Science.

Cissokho, M., Boussour, S., Cordier, P. et al. 2010. Low Salinity Oil Recovery on Clayey Sandstone: Experimental Study. *Petrophysics* **51** (5): 305-313.

Coates, G., Xiao, L., and Prammer, M. 1999. NMR Logging: Principles and Applications. Chap. 3, 45-76. Gulf Publishing Company, Houston, Texas.

Civan, F. 2007. Reservoir Formation Damage: Fundamentals, Modeling, Assessment, and Mitigation, Second Edition, Chap. 2, 13–77: Gulf Professional Publishing, Burlington.

Cuiec, L.E. 1984. Rock/Crude Oil Interactions and Wettability: An Attempt to Understand their Interrelation. Presented at SPE Annual Technical Conference and Exhibition, Houston, USA, 16-19 September. SPE 13211. http://dx.doi.org/10.2118/13211-MS.

Diamond, S. and Kinter, E.B. 1956. Surface Area of Clay Minerals as Derived From Measurements on Glycerolretention. 1956. *Clay and Clay Minerals* **5** (01): 334-347.

Dixon, J.B. 1989. Kaolin and Serpentine Group Minerals. In *Mineral in Soil Environments*, ed. J.B. Dixon and S.B. Weed, Soil Science Society of America, Inc.

Emadi, A. and Sohrabi, M. 2013. Visual Investigation of Oil Recovery by Low Salinity Water Injection: Formation of Water Micro-Dispersions and Wettability Alteration. Presented at the SPE Annual Technology Conference and Exhibition, New Orleans, Louisiana, USA, 30 September-2 October. SPE 166435-MS. http://dx.doi.org/10.2118/166435-MS.

Farida, A., Hashem, S.H., Abdulraheem B. et al. 2013. First EOR Trial Using Low Salinity Water Injection in the Greater Burgan Field, Kuwait. Presented at the 18th Middle East Oil and Gas Show and Conference, Manama, Bahrain, 10–13 March. SPE 16434-MS. http:// dx.doi.org/10.2118/16434-MS.

Fjelde, I., Asen, S.M., and Omekeh, A. 2012. Low Salinity Water Flooding Experiments and Interpretation by Simulations. Presented at the Eighteenth SPE Improved Oil Recovery Symposium, Tulsa, Oklahoma, USA, 14-18 April. SPE-154142-MS. http://dx.doi.org/10.2118/154142-MS.

Fjelde, I., Polanska, A., Taghiyev, F. et al. 2013a. Low Salinity Water Flooding: Retention of Polar Oil Components in Sandstone Reservoirs. Presented at the IOR 2013-17th European Symposium on Improved Oil Recovery. Saint Petersburg, Russia, 16-18 April.

Fjelde, I., Asen, S.M., Omekeh, A. et al. 2013b. Secondary and Tertiary Low Salinity Water Floods: Experiments and Modelling. Presented at the EAGE Annual Conference & Exhibition incorporating SPE Europec, London, United Kingdom, 10-13 June. SPE-164920-MS. http://dx.doi.org.ezproxy.uis.no/10.2118/164920-MS.

Fjelde, I., Omekeh, A.V., and Sokama-Neuyam, Y.A. 2014. Low Salinity Water Flooding: Effect of Crude Oil Composition. Presented at SPE Improved Oil Recovery Symposium, Tulsa, Oklahoma, USA, 12-16 April. SPE-169090-MS. http://dx.doi.org/10.2118/169090-MS.

Guo, G., Diaz, M., Paz, F. et al. 2005. Rock Typing as an Effective Tool for Permeability and Water-Saturation Modeling: A Case Study in a Clastic Reservoir in the Orient Basin. Presented at the SPE Annual Technical Conference and Exhibition, Dallas, TX, USA, 9-12 October. SPE 97033-MS. http://dx.doi.org/10.2118/97033-MS.

Hoffman, B.T. and Kovscek, A.R. 2004. Efficiency and Oil Recovery Mechanisms of Steam Injection into Low Permeability, Hydraulically Fractured Reservoirs. *Pet Sci & Technol* **22** (5-6): 537-564. 10.1081/LFT-120034187.

Hughes, R.V. and Pfister, R.J. 1947. Advantages of Brines in Secondary Recovery of Petroleum by Waterflooding: Petroleum Development and Technology. *Transactions of the AIME* **170** (01): 187-201. SPE 947187-G. http://dx.doi.org/10.2118/947187-G.

Ibrahim, M.N.M. and Koederitz, L.F. 2000. Two-Phase Relative Permeability Prediction Using a Linear Regression Model. Proceedings of Eastern Regional Meeting of Society of Petroleum Engineers, 17-19 October, Morgantown, West Virginia, USA, SPE 65631. http://dx.doi.org/10.2118/65631-MS.

Jadhunandan, P.P. and Morrow, N.R. 1995. Effect of Wettability on Waterflood Recovery for Crude-Oil/Brine/Rock Systems. *SPE Res Eng* **10** (1): 40-46. http://dx.doi.org/doi:10.2118/22597-PA.

Jerauld, G.R., Webb, K.J., Lin, C., Seccombe, J.C. 2006. Modeling Low-Salinity Waterflooding. *SPE Res Eval & Eng* **11** (6): 1000-1012. http://dx.doi.org/10.2118/102239-PA.

Jia, D., Buckley, J.S., and Morrow, N.R. 1991. Control of Core Wettability with Crude Oil. Presented at the SPE International Symposium on Oilfield Chemistry, Anaheim, California, USA, 20-22 February. SPE-21041-MS. http://dx.doi.org/10.2118/21041-MS.

Júnior, J.A.A. and Baldo, J.B. 2014. The Behavior of Zeta Potential of Silica Suspensions. *New Journal of Glass and Ceramics* **4** (2): 29-37. http://dx.doi.org/10.4236/njgc.2014.42004.

Kaya, A. and Yukselen, Y. 2005. Zeta Potential of Clay Minerals and Quartz Contaminated by Heavy Metals. *Canadian Geotechnical Journal* **42**: 1280-1289. http://dx.doi.org/10.1139/t05-048.

Kolodzie, J. 1980. Analysis of Pore Throat Size and Use of the Waxman-Smits Equation to Determine OOIP in Spindle Field, Colorado. Presented at the Annual Technical Conference and Exhibition of the Society of Petroleum Engineers of AIME, Dallas, TX, USA, 21-24 September. SPE 9382-MS. http://dx.doi.org/10.2118/9382-MS.

Kohut, C.K. and Warren, C.J. 2002. Chlorites. In *Soil Mineralogy with Environmental Applications*, ed. J.B. Dixon and D.G. Schulze, Chap. 17, Soil Science Society of America, Inc.

Lager, A. Webb, K.J., and Black, C.J.J. 2006. Low Salinity Oil Recovery - An Experimental Investigation. Presented at the Society of Core Analysts meeting in Trondhiem, Norway.

Law, S., McDonald, A., Fellows, S. et al. 2015. Influence of Clay Content and Type on Oil Recovery Under Low Salinity Waterflooding in North Sea Reservoirs. Presented at the SPE Offshore Europe Conference and Exhibition, Aberdeen, Scotland, UK, 8-11 September. SPE-175506-MS. http://dx.doi.org/10.2118/175506-MS.

Lee, S.Y., Webb, K.J., Collins, I.R. et al. 2010. Low Salinity Oil Recovery – Increasing Understanding of the Underlying Mechanisms. Presented at the SPE IOR Symposium, Tulsa, Oklahoma, USA, 24-28 April. SPE 129722-MS. http://dx.doi.org/10.2118/129722-MS.

Ligthelm, D.J., Gronsveld, J.P., Hofman, N.J. et al. 2009. Novel Waterflooding Strategy by Manipulation of Injection Brine Composition. Presented at Europec/Eage Conference and Exhibition, Amsterdam, The Netherlands, 8-11 June. SPE 119835-MS. http://dx.doi.org/10.2118/119835-MS.

Lucia, F.J. 1995. Rock-Fabric/Petrophysical Classification of Carbonate Pore Space for Reservoir Characterization. *AAPG Bulletin* **79** (9): 1275-1300.

Mahani, H., Sorop, T.G., Ligthelm, D. et al. 2011. Analysis of Field Responses to Low-Salinity Waterflooding in Secondary and Tertiary Mode in Syria. Presented at the SPE Europec/Eage Annual Conference and Exhibition, Vienna, Austria, 23-26 May. SPE-142960-MS. http://dx.doi.org/10.2118/142960-MS.

Martin, A.J., Solomon, S.T., and Hartmann, D.J. 1997. Characterization of Flow Units in Carbonate Reservoirs. *AAPG Bulletin*. **81** (5): 734-759.

McGuire, P.L., Chatham, J.R., Paskvan, F.K. et al. 2005. Low Salinity Oil Recovery: An Exciting New EOR Opportunity for Alaska's North Slope. Presented at the SPE Western Regional Meeting, Irvine, California, USA, 30 March-1 April. SPE 93903-MS. http://dx.doi.org/10.2118/93903-MS.

Meyers, K.O. and Salter, S.J. 1984. Concepts Pertaining to Reservoir Pretreatment for Chemical Flooding. Presented at SPE Enhanced Oil Recovery Symposium, Tulsa, Oklahoma, 15-18 April. SPE-12696-MS. http://dx.doi.org/10.2118/12696-MS.

Morrow, N.R., Tang, G.Q., Valat, M. et al. 1998. Prospects of Improved Oil Recovery Related to Wettability and Brine Composition. *J. of Pet Sci & Eng* **20** (3): 267-276.

Nasralla, R. A. and Nasr-El-Din, H.A. 2011. Impact of Electrical Surface Charges and Cation Exchange on Oil Recovery by Low Salinity Water. Presented at the SPE Asia Pacific Oil and Gas Conference and Exhibition, Jakarta, Indonesia, 20-22 September. SPE 147937-MS. http://dx.doi.org/10.2118/147937-MS.

Nasralla, R.A., Alotaibi, M.B., and Nasr-El-Din, H.A. 2011. Efficiency of Oil Recovery by Low Salinity Water Flooding in Sandstone Reservoirs. Presented at the SPE Western North American Region Meeting, Anchorage, Alaska, USA, 7-11 May. SPE 144602-MS. http://dx.doi.org/10.2118/144602-MS.

Nasralla, R.A. and Nasr-El-Din, H.A. 2014. Double-Layer Expansion: Is It A Primary Mechanism of Improved Oil Recovery by Low-Salinity Waterflooding? *SPE Res Eval & Eng* **17** (1): 49-59. SPE 154334-PA. http://dx.doi.org/10.2118/154334-PA.

Nasr-El-Din, H.A., Samuel, M.M., and Kelkar, S.K. 2007. Investigation of a New Single-Stage Sandstone Acidizing Fluid for High-Temperature Formations. Presented at the European Formation Damage Conference, Scheveningen, The Netherlands, 30 May-1 June. SPE-107636-MS. http://dx.doi.org/10.2118/107636-MS.

Pittman, E.D. and Thomas, J. 1979. Some Applications of Scanning Electron Microscope to the Study of Reservoir Rock. *J Pet Technol* **31** (11):1375-1380. SPE 7550-PA. http://dx.doi.org/10.2118/7550-PA.

Pu, H., Xie, X., Yin, P. et al. 2010. Low-Salinity Waterflooding and Mineral Dissolution. Presented at SPE Annual Technical Conference and Exhibition,

Florence, Italy, 19-22 September, SPE-134042-MS. http://dx.doi.org/10.2118/134042-MS.

Robertson, E.P. 2007. Low-Salinity Waterflooding to Improve Oil Recovery-Historical Field Evidence. Presented at SPE Annual Technical Conference and Exhibition, Anaheim, California, U.S.A., 11-14 November. SPE-109965-MS. http://dx.doi.org/10.2118/109965-MS.

RezaeiDoust, A., Puntervold, T., and Austad, T. 2010. A Discussion of the Low Salinity EOR Potential for a North Sea Sandstone Field. Presented at the SPE Annual Technical Conference and Exhibition, Florence, Italy, 19-22 September. SPE 134459-MS. http://dx.doi.org/10.2118/134459-MS.

Rivet, S.M., Lake, L.W., and Pope, G.A. 2010. A Coreflood Investigation on Low-Salinity Enhanced Oil Recovery. Presented at the SPE Annual Technology Conference and Exhibition, Florence, Italy, 19-22 September. SPE 134297-MS. http://dx.doi.org/10.2118/134297-MS.

Robbana, E., Buikema, T.A., Mair, C. et al. 2012. Low Salinity Enhanced Oil Recovery - Laboratory to Day One Field Implementation - LoSal EOR into the Clair Ridge Project. Presented at the Abu Dhabi International Petroleum Exhibition & Conference, Abu Dhabi, UAE, 11-14 November. SPE 161750-MS. http://dx.doi.org/10.2118/161750-MS.

Schumacher, M.M. 1978. Enhanced Oil Recovery: Secondary and Tertiary Methods. Chap 2: 18-23: Noyes Data Corp, Park Ridge, New Jersey,.

Seccombe, J., Lager, A., Webb, K. et al. 2008. Improving Waterflood Recovery: LoSal™ EOR Field Evaluation. Presented at the SPE/DOE Symposium on Improved Oil Recovery, Tulsa, Oklahoma, USA, 20-23 April. SPE 113480-MS. http://dx.doi.org/10.2118/113480-MS.

Seccombe, J., Lager, A., Jerauld, G. et al. 2010. Demonstration of Low-Salinity EOR at Interwell Scale, Endicott Field, Alaska. Presented at the SPE Improved Oil Recovery Symposium in Tulsa, Oklahoma, USA, 24-28 April. SPE 129692-MS. http://dx.doi.org/10.2118/129692-MS.

Sharma, M.M. and Filico, P.R. 2000. Effect of Brine Salinity and Crude-Oil Properties on Oil Recovery and Residual Saturations. *SPE J.* **5** (03): 293 – 300. SPE-65402-PA. http://dx.doi.org/10.2118/65402-PA.

Shehata, A.M. and Nasr-El-Din, H.A. 2015a. Zeta Potential Measurements: Impact of Salinity on Sandstone Minerals. Presented at the 2015 SPE International Symposium on Oilfield Chemistry, The Woodlands, TX, USA. 13 - 15 April. SPE 173763. http://dx.doi.org/10.2118/173763-MS.

Shehata, A.M. and Nasr-El-Din, H.A. 2015b. Spontaneous Imbibition Study: Effect of Connate Water Composition on Low-Salinity Waterflooding in Sandstone Reservoirs. Presentation at the SPE Western Regional Meeting, Anaheim, California, USA, 27-30 April. SPE 171690-MS. http://dx.doi.org/10.2118/171690-MS.

Shehata, A.M. and Nasr-El-Din, H.A. 2015c. Role of Sandstone Mineral Compositions and Rock Quality on the Performance of Low-Salinity Waterflooding. Presented at

the International Petroleum Technology Conference, Kuala Lumpur, Malaysia, 10-12 December. IPTC-18176-MS. http://dx.doi.org/10.2523/18176-MS.

Sheng, J.J. 2014. Critical Review of Low-salinity Waterflooding. *J. Pet. Sci. Eng.* **120**: 216-224. http://dx.doi.org/10.1016/j.petrol.2014.05.026.

Shojaei, M., Ghazanfari, M.H., and Masihi, M. 2015. Relative Permeability and Capillary Pressure Curves for Low Salinity Waterflooding in Sandstone Rocks. *J. of Natural Gas Sci. Eng.* **25**: 30-38.

Skrettingland, K., Holt, T., Tweheyo, M.T. et al. 2011. Snorre Low-Salinity-Water Injection — Core Flooding Experiments And Single Well Field Pilot. *SPE Res Eval & Eng* **14** (02): 182-192. http://dx.doi.org/10.2118/129877-PA.

Sorop, T.G., Masalmeh, S.K., Suijkerbuijk, B.M.J.M. et al. 2015. Relative Permeability Measurements to Quantify the Low Salinity Flooding Effect at Field Scale. Presented at the Abu Dhabi International Petroleum Exhibition and Conference, Abu Dhabi, UAE, 9-12 November. SPE-177856-MS. http://dx.doi.org/10.2118/177856-MS.

Suijkerbuijk, B.M.J.M., Kuipers, H.P.C.E., Van Kruijsdijk, C.P.J.W., et al. 2013. The Development of a Workflow to Improve Predictive Capability of Low Salinity Response. Presented at the International Petroleum Technology Conference, Beijing, China, 26-28 March, IPTC 17157-MS. http://dx.doi.org/10.2523/IPTC-17157-MS.

Tang, G. and Morrow, N.R. 1997. Salinity, Temperature, Oil Composition, and Oil Recovery by Waterflooding. *SPE Res Eng* **12** (4): 269–276. SPE 36680-PA. http://dx.doi.org/10.2118/36680-PA.

Tang, G. and Morrow, N.R. 1999. Influence of Brine Composition and Fines Migration on Crude Oil/Brine/Rock Interactions and Oil Recovery. *J Pet Sci Eng* **24** (2-4): 99-111.

Tavassoli, Z., Zimmerman, R.W., and Blunt, M.J. 2005. Analytic Analysis for Oil Recovery During Counter-Current Imbibition in Strongly Water-Wet Systems. *Transport in Porous Media* **58** (4): 173-189.

Veldder, P., Fonseca, J.C., Wells, T. et al. 2010. Low Salinity Waterflooding: Proof of Wettability Alteration on A Field Wide Scale. Presented at the SPE Improved Oil Recovery Symposium, Tulsa, Oklahoma, USA, 24-28 April. SPE 129564-MS. http://dx.doi.org/10.2118/129564-MS.

Webb, K.J., Black, C.J.J., and Al-Ajeel, H. 2004. Low Salinity Oil Recovery - Log-Inject-Log. Presented at the SPE/DOE Symposium on Improved Oil Recovery, Tulsa, Oklahoma, USA, 7-21 April. SPE 89379-MS. http://dx.doi.org/10.2118/89379-MS.

Webb, K., Lager, A., and Black, C., 2008, Comparison of High/Low Salinity Water/Oil Relative Permeability. International Symposium of the Society of Core Analysis, SCA 2008-39.

Wickramathilaka, S., Howard, J.J., Morrow, N.R. et al. 2011. An Experimental Study of Low Salinity Waterflooding and Spontaneous Imbibition. Presented at the 16th European Symposium on Enhanced Oil Recovery, Cambridge, UK, 12-14 April.

Wilding, L.P., Smeck, N.E., and Drees, L.R. 1977. Silica in soils: Quartz and Disordered Silica Polymorphs. In *Minerals in Soil Environment*, ed. J.B. Dixon and S.B. Weed, Chap. 19, Soil Science Society of America, Inc.

Yildiz, H.O. and Morrow, N.R. 1996. Effect of Brine Composition on Recovery of Moutray Crude Oil by Waterflooding. *J Pet Sci Eng* **14** (3-4): 159–168.

Yildiz, H. O., Valat, M., and Morrow, N.R. 1999. Effect of Brine Composition on Wettability and Oil Recovery of a Prudhoe Bay Crude Oil. *J Can Pet Technol* **38** (1): 26-31. http://dx.doi.org/doi:10.2118/99-01-02.

Zhang, Y. and Morrow, N.R. 2006. Comparison of Secondary and Tertiary Recovery with Change in Injection Brine Composition for Crude Oil Sandstone Combinations. Presented at the SPE/DOE Symposium on Improved Oil Recovery, Tulsa, Oklahoma, USA, 22-26 April. SPE 99757. http://dx.doi.org/10.2118/99757-MS.

Zhao, H., Long, J., Masliyah, J. et al. 2006. Effect of Divalent Cations and Surfactants on Silica-Bitumen Interaction. *Ind Eng Chem Res* **45** (22):7482-7490.

Zhou, X., Morrow, N., and Ma, S. 2000. Interrelationship of Wettability, Initial Water Saturation, Aging Time, and Oil Recovery by Spontaneous Imbibition and Waterflooding. *SPE J* **5** (2): 21–24. http://dx.doi.org/doi:10.2118/62507-PA.